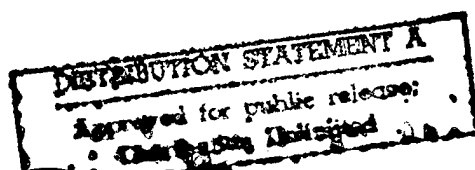




**FOREIGN
BROADCAST
INFORMATION
SERVICE**

JPRS Report



Science & Technology

Japan

POWDER METALLURGY TECHNOLOGY

19980612 029

REPRODUCED BY
U.S. DEPARTMENT OF COMMERCE
NATIONAL TECHNICAL INFORMATION SERVICE
SPRINGFIELD, VA. 22161

JPRS-JST-88-028

13 DECEMBER 1988

SCIENCE & TECHNOLOGY

JAPAN

POWDER METALLURGY TECHNOLOGY

43067591 Tokyo NIHON FUNMATSU FUNTAI YAKIN KYOKAI in Japanese
16-19 May 88 pp 12-67; 142-153; 194-215

[Selected articles form a special issue prepared for the Spring
1988 Advanced Materials Convention held 16-19 May 1988 in Tokyo,
sponsored by the Japan Society of Powder and Powder Metallurgy]

CONTENTS

Structure of High-Temperature Superconducting Oxides.....	1
YBCO Single Crystal Thin Films by Reactive Deposition.....	4
Synthesizing High-Temperature Superconductors by Sol Gel Method.....	7
Single Crystal, Fine Tissue Growth.....	11
Synthesis, Properties of Bismuth Superconducting Oxides.....	16
Superconducting Oxide Materials Manufacture, Properties.....	20
Wire Production From Superconducting Oxides.....	24
Wire Production by Drawing-Rolling Process.....	27
ICB Deposition of High-Temperature Superconducting Oxide Thin Films.....	30
Phase Diagram of Ba-Y-Cu Oxide System Ceramics.....	34

Phase Equilibrium of Y-Ba-Sr-Cu-O System.....	36
Reaction Process of Superconducting Ceramic Materials by Differential Thermal Balance.....	38
Preparation of Oxide Superconductors by Wet Coprecipitation Preparation.....	40
Preparation of Oxide Superconductors by Sol-Gel Method.....	43
Preparation of Orientative $\text{YBa}_2\text{Cu}_3\text{O}_y$ Sintered Material.....	46
Synthesis of Superconducting Oxides Under High-Pressure Oxygen.....	48
Superconductivity of Hot-Pressed $\text{YBa}_2\text{Cu}_3\text{O}_x$ Ceramics.....	50
Sintering Process of $\text{YBa}_2\text{Cu}_3\text{O}_x$ by Oxalate Method.....	53
Effect of Lengthy Sintering of $\text{YBa}_2\text{Cu}_3\text{O}_y$ on Superconducting Characteristics.....	55
Pore Structure Effect on Superconducting $\text{YBa}_2\text{Cu}_3\text{O}_x$ Ceramics.....	57
Superconducting Ceramics Reaction, Atmospheric Gas.....	60
Electron Microscope Observation of $\text{Ba}_2\text{YCu}_3\text{O}_{7-\delta}$	62
Electrical Resistance, Thermoelectromotive Force in High Temperature of $\text{YBa}_2\text{Cu}_3\text{O}_y$	64
Critical Current Density of $\text{GdBa}_2\text{Cu}_3\text{O}_{7-\delta}$ Ceramics.....	66
Crystal Structure, Superconductivity Characteristics of $\text{YBa}_{2-x}\text{K}_x\text{Cu}_3\text{O}_{7-\delta}$ System.....	68
Copper Site Substitution, Oxygen Content of $\text{YBa}_2\text{Cu}_3\text{O}_{7-\delta}$	70
Electrical, Magnetic Properties of $\text{YBa}_2(\text{Cu}_{1-x}\text{M}_x)_3\text{O}_{7-y}$	72
Cu-Fe Substitution Effect on Superconductivity.....	74
Y-La Substitution Effect on Superconductivity of $\text{YBa}_2\text{Cu}_3\text{O}_y$	76
Effect of Sn Addition to $\text{YBa}_2\text{Cu}_3\text{O}_y$ Superconducting Oxides.....	78
Composition Control of Bipolar RF Sputtering Y-Ba-Cu-O High-Temperature Superconducting Thin Film	80
High-Temperature Superconducting Multi Hetero Epitaxial Growth.....	82

Preparation of High-Temperature Superconducting $\text{Ba}_2\text{Y}_1\text{Cu}_3\text{O}_{7-\delta}$ Thick Film.....	84
Pt/ AlO_y / $\text{YBa}_2\text{Cu}_3\text{O}_{7-x}$ / SrTiO_3 Single Crystal Thin Film Tunnel Junction.....	86
High-Temperature Superconductivity Generating Mechanism Proposed by New System Physics.....	88
Superconducting Oxides With New Structure--Bi-Sr-Cu-O System.....	91
Phase Equilibrium of Bi_2O_3 -SrO-CuO System.....	93
Crystal Phase of Bi_2O_3 -SrO-CaO-CuO System.....	95
Superconductors With Bi-Sr-Cu System Oxides as Base.....	97
Complex Magnetization Rate of Bi System Superconductors.....	99
Preparation of $\text{BiSrCaCu}_2\text{O}_{5.5\pm\delta}$, Superconducting Characteristics.....	101
Bi System Oxide Superconductors by Oxalate Method, I.....	103
Bi System Oxide Superconductors by Oxalate Method, II.....	105
Superconducting Characteristics of Bi-Sr-Ca-Cu-O System Single Crystal.....	107
Superconducting Characteristics of Ti-Ba-Ca-Cu-O System Superconductors.....	109
Crystal Structure, Superconductivity of $\text{YBa}_2\text{Cu}_3\text{O}_{7-\delta}$	111
Crystal Structure, Superconductivity of $\text{Sm}_x\text{Ba}_{1-x}\text{CuO}_y$ System.....	113
Powder Metallurgy Composite Products Using HIP Method.....	115
Superplasticity Behavior, Mechanical Properties of Superalloy Composites.....	118
Mechanical Properties of Superalloy Compound Disk.....	121
Molding Tool Steel Powder by Hydraulic Pressure HIP.....	124
Sintering/Forging of Steel Copper Alloy Powder.....	127
Relationship Between Processing, Mechanical Properties.....	131
WC Content in Cemented Carbide.....	135
Joint of Cemented Carbide by Ni-Group Amorphous Materials.....	138

Relationship Between Strength, Matrix Organization of CVD Coated Cemented Carbide.....	141
Low Ni Layer Produced on TiC-TiN-Mo ₂ C-Ni Cermet Surface.....	144
Ni, Carbon Effect on Sintering Mechanism of Mo ₂ FeB ₂ Hard Alloys.....	147
Enhancing Toughness of TiB ₂ Sintered Body.....	151
Reactivity of Al ₂ O ₃ -SiC Ceramics With Ni.....	155
Mechanical Properties of SiC Whisker Reinforced Al ₂ O ₃ Ceramics.....	158
Preparation of Composite Ceramics.....	162
Seed Effect on c-BN Reaction Sintering.....	166
Ceramic Particle Dispersed Alloy Powder.....	170

Structure of High-Temperature Superconducting Oxides

43067591 Tokyo NIHON FUNMATSU FUNTAI YAKIN KYOKAI in Japanese 16-19 May 88
pp 12-13

[Report by Hajime Asano, Institute of Materials Science, Tsukuba University]

[Text] Since the discovery of $\text{La}_{2-x}\text{Ba}_x\text{CuO}_4$ by Bednorz and Muller, high-temperature superconducting oxides including Cu have been found one after another. $\text{BaPb}_{1-x}\text{Bi}_x\text{O}_3$ ($T_c = 12\text{K}$) in the zero generation has a perovskite structure, $\text{YBa}_2\text{Cu}_3\text{O}_{7-\delta}$ has an oxygen-free triple perovskite structure, and $\text{La}_{2-x}\text{Ba}_x\text{CuO}_4$ and Bi-Sr-Ca-Cu-O have a stratified structure based on a perovskite structure. In this report I will describe the crystallographic characteristics commonly visible in the four kinds of superconducting oxides.

1. $\text{BaPb}_{1-x}\text{Bi}_x\text{O}_3$

Figure 1 shows an ABO_3 perovskite structure. Metal atoms A and B are at the center and vertex of a cube, respectively. Oxygen atoms form an octahedron surrounding atom B, and the octahedra, each sharing a vertex with another, are three-dimensionally connected with one another. $\text{BaPb}_{1-x}\text{Bi}_x\text{O}_3$ is a crystal consisting of BaPbO_3 mixed with BaBiO_3 . Superconductivity occurs in a component region of $x = 0.1-0.4$. As can be seen from Figure 1, the oxygen octahedra can turn around the three crystallographic axes of the perovskite structure. Figure 2 shows the way in which the oxygen octahedra turn around in the case of $\text{BaPb}_{0.75}\text{Bi}_{0.25}\text{O}_3$. This structure can be obtained by turning the oxygen octahedra by about 7 degrees around an axis which is perpendicular to the sheet of paper.

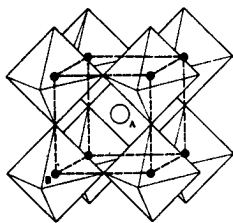


Figure 1

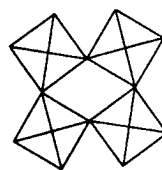


Figure 2

2. $\text{La}_{2-x}\text{Ba}_x\text{CuO}_4$

A 40K-level superconductor $\text{La}_{2-x}\text{A}_x\text{CuO}_4$, produced by partially replacing the La in La_2CuO_4 with an alkaline earth metal, has a K_2NiF_4 structure. As seen in Figure 3, the K_2NiF_4 structure is tetragonal, and the length of the base agrees with that of one side a_p of the perovskite structure. Each oxygen octahedron surrounding Cu is two-dimensionally connected with another within the $Z = 0$ and $Z = 1/2$ planes. The K_2NiF_4 structure is characteristically a stratified structure consisting of (La,A) planes parallel with the base, and CuO_6 octahedra, with each (La,A) plane as one unit, and having no interlayer Cu atomic plane such as exists in a perovskite structure. Moreover, the $Z = 1/2$ layer shifts in parallel with the $Z = 0$ layer only in the $(1/2, 1/2, 0)$ position.

3. $\text{YBa}_2\text{Cu}_3\text{O}_{7-\delta}$

The crystal structure of a 90K-level superconductor $\text{YBa}_2\text{Cu}_3\text{O}_{7-\delta}$ is given in Figure 4. This substance has a period three times that of a perovskite structure in the c-axis direction, with Y (●) and Ba (⊖) regularly arranged in a Ba-Y-Ba order. Among the oxygen atoms (○ and ⊖) in the octahedra each surrounding Cu (●), there is no oxygen on the $Z = 1/2$ plane containing Y, and the oxygen atoms (⊖) on the base selectively occupy only the $(1/2, 0, 0)$ positions.

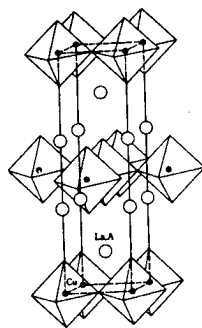


Figure 3

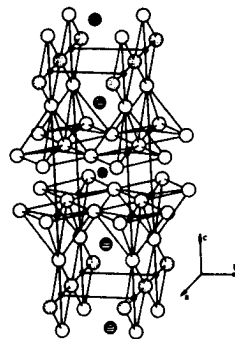


Figure 4

4. Rare Earth Element Substitutes

$\text{RBa}_2\text{Cu}_3\text{O}_{7-\delta}$, a compound produced by replacing Y in $\text{YBa}_2\text{Cu}_3\text{O}_{7-\delta}$ with a rare earth element, also shows 90K-level superconductivity. The crystal structures of substances of this kind have been examined by X-ray and neutron diffraction, and they are shown to have the same form as orthorhombic $\text{YBa}_2\text{Cu}_3\text{O}_{7-\delta}$.

These groups of substances were thought to exist only in 1-2-3 ratio composition. Recently, however, it has become clear that there exists $\text{R}_{1+x}\text{Ba}_{2-x}\text{Cu}_3\text{O}_{7-\delta}$, an R (La, Nd, Sm, Eu) compound consisting of R and a Ba solid solution. Figure 5 shows a result of examination of an Nd- system.

With x as 0.2, the crystal structure changes from an orthorhombic to a tetragonal phase, on the one hand, while on the other, T_c drops at a steady pace along with x , and the structure becomes superconductive in the neighborhood of $x = 0.4$. Similar phenomena are recognized in the case of La-, Sm-, and Eu- compounds as well. In regard to tetragonal structures, neutron diffraction experiments were conducted on Nd- compounds ($x = 0.2$) and La- compounds ($x = 0.5$), and it was ascertained that their crystal structures were the same in form as a tetragonal $\text{YBa}_2\text{Cu}_3\text{O}_{7-\delta}$, and that surplus R atoms had supplemented the Ba position.

5. Bi-Sr-Ca-Cu-O System

$\text{BiSrCaCu}_2\text{O}_y$, a new superconducting compound, has been found recently. This substance contains two superconducting phases, each exhibiting 105K and 70K in T_c . In a Bi- compound based on a perovskite structure, there is a group of substances represented by the chemical formula $(\text{Bi}_2\text{O}_2)(\text{M}_{n-1}\text{R}_n\text{O}_{3n+1})$. The substances have a structure in which perovskite layers in an n number are inserted between Bi_2O_2 layers. The $T_c = 70\text{K}$ phase has a $\text{Bi}_4\text{Ti}_3\text{O}_{12}$ structure, with $n = 3$ (Figure 6). The laminate of the atomic plane of the perovskite structure consists of $(\text{Sr,Ca})\text{O}$, CuO_2 , $(\text{Sr,Ca})\text{O}$, CuO_2 , and $(\text{Sr,Ca})\text{O}$, and its chemical composition is $\text{Bi}_2\text{Sr}_{1.5}\text{Ca}_{1.5}\text{Cu}_2\text{O}_y$. This substance has a 4.8-fold nonintegral long-period modulated structure in the (110) direction of the perovskite structure, but the details of its crystal structure have not been clarified. It has been pointed out that $n = 2$ and $n = 4$ phases exist in this system, and further investigation is required.

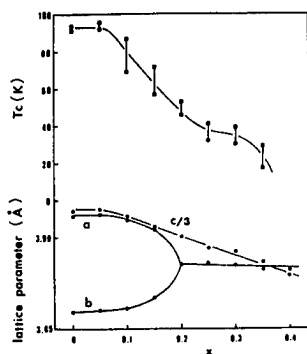


Figure 5

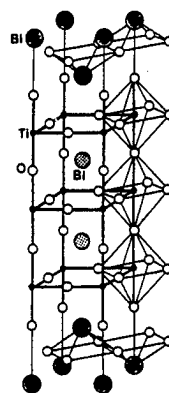


Figure 6

YBCO Single Crystal Thin Films by Reactive Deposition

43067591 Tokyo NIHON FUNMATSU FUNTAI YAKIN KYOKAI in Japanese 16-19 May 88
pp 14-15

[Report by Yoshichika Bando, Kyoto University Chemical Research Laboratory:
"Production of YBCO Single Crystal Thin Films by the Reactive Deposition
Method"]

[Text] 1. Introduction

The superconducting properties of YBCO ($\text{YBa}_2\text{Cu}_3\text{O}_{7-\delta}$) are characterized by great anisotropy, and basic research on its single crystals is regarded as important. Because bulk single crystals involve such problems as control of oxygen content and crystal quality arising from the occurrence of twins, there is the possibility that thin-film single crystals of good quality will become a decisive factor for the measurement of physical properties. Furthermore, it is necessary to produce single crystal thin films of good quality from the viewpoint of their application to the field of electronics. Here I will report on methods for the manufacture of YBCO single crystals which are currently considered to be the best in quality, and on the properties of their thin films.

2. Production of YBCO Single Crystals by the Reactive Deposition Method

The reactive deposition method is used to grow crystals while applying oxygen gas and metal atoms to substrates. The amount of film oxidation and crystal quality are determined by the kind of substrate crystal, oxygen pressure, speed of metal deposition, and substrate temperature. As YBCO contains Cu that is not readily oxidized, oxygen pressure to the extent of 10^{-4} Torr, which is used for conventional reactive deposition, is not sufficient. For this reason, it is necessary to achieve higher oxygen pressure, but this cannot be accomplished when evaporation is a problem. Therefore, a plan has been elaborated to raise the pressure only in the vicinity of the substrate. To make each metal evaporate on a stable basis, Y and Ba are heated by electron beams and Cu is subjected to resistance heating. Thus they are adjusted by controlling their respective evaporation speeds so that they can constitute stoichiometric ratios. SrTiO_3 (100) and (110) planes are used for the substrate, and the substrate temperature is kept constant within the limit of $500^\circ\text{--}650^\circ\text{C}$. The evaporation speed is in a 4~6 A/s range.

Figure 1 shows X-ray diffraction patterns for an as-grown YBCO deposited on the (100) plane. Diffraction patterns for (00 l) alone are obtained where $c = 11.749\text{\AA}$, with the c axis somewhat long. RHEED shows that it is a single crystal film, with the c axis extending at right angles to the substrate plane, and that the surface is fairly flat. The T_c of the film is 45K where the resistance is zero, and the amount of oxygen is found to be insufficient. Figure 2 shows measurements of resistance of a film which oxidized at 500°C in which $c_0 = 11.686\text{\AA}$. The straight line showing changes in resistance due to temperature above T_c passes through the starting point, indicating that the film is a single crystal of good quality. Also, the Meissner effect ($-x'$) measured by complex magnetic susceptibility rose rapidly at less than T_c , as shown in Figure 3, at the same time exhibiting a sharp energy dispersion (x''). These results indicate that the superconducting phases are uniform.

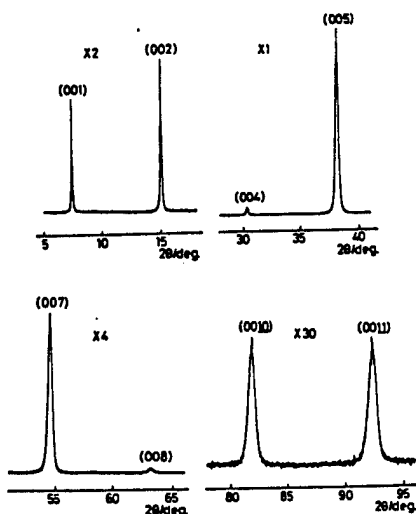


Figure 1. X-ray diffraction patterns for the as-grown (001)YBCO film (2000A)

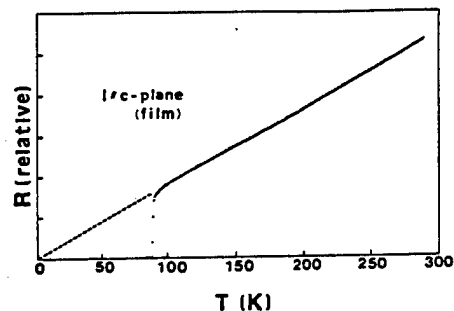


Figure 2. Resistance vs temperature for the oxidation-treated YBCO thin films (1000A)

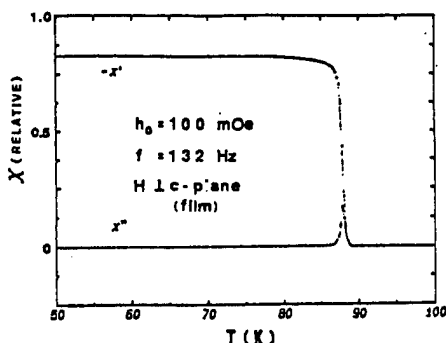


Figure 3. Real and imaginary components of complex susceptibility for oxidation-treated YBCO film (1000A). The onset temperatures of x' and x'' are the same, 88.9K

3. Growth to (110) SrTiO₃ Plane and Anisotropy

A (001) plane of YBCO grows on the (100) plane, but two kinds of crystal planes--(110) and (103)--attain epitaxial growth on the (110) plane. The (110) plane of YBCO grows in parallel with the substrate plane at a substrate temperature of less than 540°C, and a (105) plane grows at a higher temperature. The YBCO growing on the (110) plane is a single crystal, and this is convenient for looking into its properties in the c-axis and c-plane directions. It has become clear for the first time that even in the c-axis direction, its electric resistance undergoes much the same metallic temperature change as within the c plane, as shown in Figure 4. The measurements conducted to date make evident its anisotropy and indicate that changes in resistivity due to temperature in the c-axis direction are of a semiconductive nature. The possibility is strong that this has something to do with the problem of superfine structures of crystals.

4. Superconductivity and Critical Current Density (J_c) of Ultrathin Films and Energy Gap (Δ)

With the reactive deposition method, it is easy to produce thin films below 2000Å, and high-temperature superconducting films can be obtained even with a thickness of 100Å, for example. This means that no reaction is caused to the substrate and that flat and smooth films are obtained by stratified growth. Figure 5 shows changes in electric resistance due to temperature. On the other hand, we measured the J_c of 1000Å films growing on the c plane, and found that in the case of a film 100 μ m wide, electric current at a maximum of 0.4A had flowed at the liquid nitrogen temperature. We also obtained a current density of 4×10^6 A/cm².

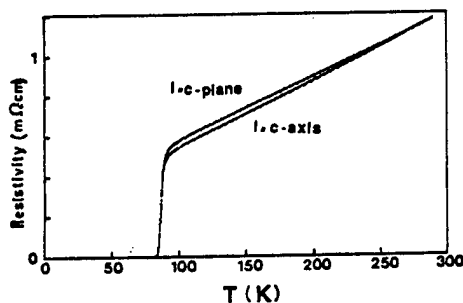


Figure 4. Resistivity vs temperature for YBCO (110) thin film (1000Å)

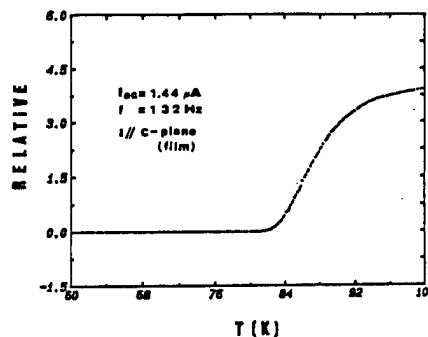


Figure 5. Resistance vs temperature for oxidation-treated YBCO ultra-thin film (100Å)

It was found that there was anisotropy in the energy gap, but no reliable data has yet been obtained. Recently, Tsai et al. examined the anisotropy of the energy gap by bringing a thin film plane cleaved at a low temperature into contact with Pb, obtaining a value of $2\Delta(0)/kT=6$ in the tunnel in the c-plane direction and 3.6 in the c-axis direction. When we created an NIS (normal conductor/insulator/superconductor) junction and measured the energy gap in a similar way, we obtained a value of $2\Delta(0)/kT=3.2$, close to the above-mentioned value, in the c-axis direction. As to the c-plane direction, study is under way at present.

Synthesizing High-Temperature Superconductors by Sol Gel Method

43067591 Tokyo NIHON FUNMATSU FUNTAI YAKIN KYOKAI in Japanese 16-19 May 88
pp 16-17

[Report by Shinichi Hirano, Suguru Hayashi, Masatsugu Miura, and Hiroyuki Tomonaga, Nagoya University Engineering Department: "Process of Synthesizing High-Temperature Superconductors by the Sol Gel Method"]

[Text] 1. Introduction

Superconducting oxide $\text{Ba}_2\text{YCu}_3\text{O}_{7-\delta}$ has so far been synthesized by such methods as the solid state reaction of BaCO_3 , Y_2O_3 , CuO powder; the thermal cracking of Y-, Ba-, and Cu- system organic oxacid solutions; the citric acid method, with citric acid added to a nitrate aqueous solution; the freezing and drying of an acetate solution; and the emulsion method. In this report, we will introduce the results of our research on chemical synthesis methods using organic metal compounds as raw materials for the purpose of synthesizing superconducting oxides with uniform chemical composition, formed by preparing homogeneous compound solutions and adjusting their viscosity.

2. Processing From Organic Metal Compounds

As to a starting raw material, we examined a solution reaction system which is considered to make it possible to create an intermediately coordinated compound in a solvent and to control composition and crystallization. We used $\text{Y}(\text{O}-i\text{Pr})_3$ or $\text{Y}(\text{acac})_3$ as the Y source and a Ba metal as the Ba source. As for Cu sources, we examined $\text{Cu}(\text{OEt})_2$, $\text{Cu}(\text{OC}_2\text{H}_4\text{OC}_2\text{H}_5)_2$, $\text{Cu}(\text{acac})_2$, and Cu-organic oxacid. $\text{Cu}(\text{OEt})_2$ hardly melts in solvents other than amines and acetylacetone. Cu-stearate melts well in toluene, pyridine and acetylacetone, but Y- and Ba- compounds do not melt in these solvents. As Cu sources, therefore, we chose $\text{Cu}(\text{acac})_2$ and $\text{Cu}(\text{OC}_2\text{H}_4\text{OC}_2\text{H}_5)_2$ which dissolve in a solvent system common with Y and Ba sources and produce intermediately coordinated compounds. As to solvents, we found that 2- methoxyethanol or 2- ethoxyethanol, which melts and coordinates these compounds, is the most effective common solvent. Figure 1 is a flow chart showing the processing of superconducting oxide $\text{Ba}_2\text{YCu}_3\text{O}_{7-\delta}$. Ba, $\text{Y}(\text{O}-i\text{Pr})_3$ or $\text{Y}(\text{acac})_3$ and $\text{Cu}(\text{OC}_2\text{H}_4\text{OC}_2\text{H}_5)_2$ or $\text{Cu}(\text{acac})_2$ are melted in dehydrated 2- ethoxyethanol at a stoichiometric ratio of 2:1:3, and they are heated in a dry nitrogen gas

flow up to 40°C so they will show reactions. Hydrolysis is effected by gradually adding water that is diluted with a solvent, as necessary, and thus a polycondensation reaction is obtained. It is possible to increase the metal ion density of this solvent by concentrating it and adjusting its viscosity. We found that a polycondensation reaction by partial hydrolysis is important for the coordination of metal ions in the homogeneous solution created, and that this reaction influences the process of synthesizing $\text{Ba}_2\text{YCu}_3\text{O}_{7-\delta}$ superconductors through the thermal cracking of precursors of fine particles and films created.

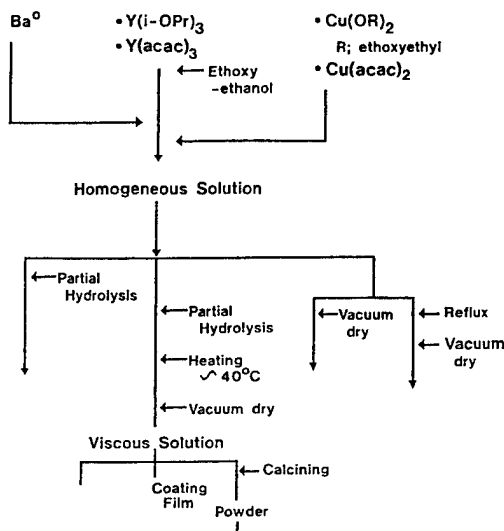


Figure 1. Flow chart showing processing of superconducting oxides

Figure 2 shows X-ray diffraction patterns of products created through thermal cracking of precursors. From a condensed, intermediately coordinated compound produced by partial hydrolysis, orthorhombic $\text{Ba}_2\text{YCu}_3\text{O}_{7-\delta}$ can be synthesized in a single phase. Also under fully controlled calcining conditions, $\text{Ba}_2\text{YCu}_3\text{O}_{7-\delta}$ is created at 650°C--a fairly low temperature compared with the solid phase method. This process makes it possible to synthesize a superconducting oxide fine particle (Figure 3) with a uniform diameter of less than 0.5 μm . By sintering this particle it is possible to synthesize a sintered body consisting of uniform tissues (2~3 μm) with a particle diameter of 2~3 μm . The superconducting transition temperature T_c (end) of this body was about 80K.

We checked also into the creation of $\text{Ba}_2\text{YCu}_3\text{O}_{7-\delta}$ films on Al_2O_3 , SrTiO_3 , and PSZ substrates by a dip coating or dripping method from a solution whose viscosity was appropriately controlled. On the Al_2O_3 substrate, a reaction to the Ba compound took place above 800°C, and BaAl_2O_4 was created easily. On the SrTiO_3 substrate, we were able to create a uniform, smooth, thin film consisting of $\text{Ba}_2\text{YCu}_3\text{O}_{7-\delta}$ through sintering at a temperature of more than 650°C (Figure 4). Also, we found that use of active oxygen gas in the course of sintering expedites the dissolution of organic constituents, holds down the growth of barium carbonate, and makes it possible to synthesize $\text{Ba}_2\text{YCu}_3\text{O}_{7-\delta}$ at low temperature.

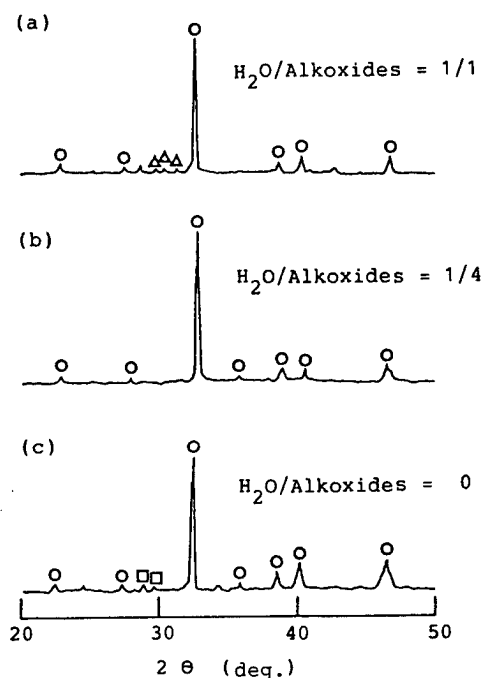


Figure 2. X-ray diffraction patterns of calcined powder of hydrolytic products of metal alkoxide--effects of partial hydrolysis of solutions upon the homogeneity of products

○: $\text{Ba}_2\text{YCu}_3\text{O}_{7-\delta}$
 △: Y_2BaCuO_5
 □: BaCuO_2

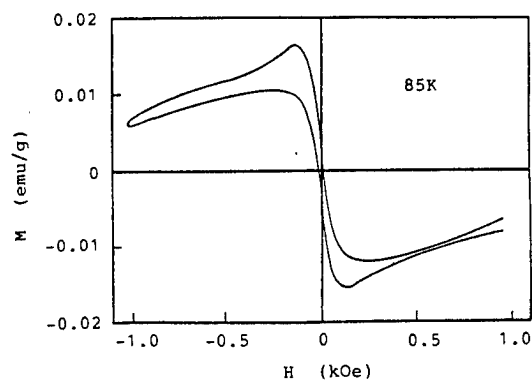


Figure 3. Magnetization curves of $\text{Ba}_2\text{YCu}_3\text{O}_{7-\delta}$ particle

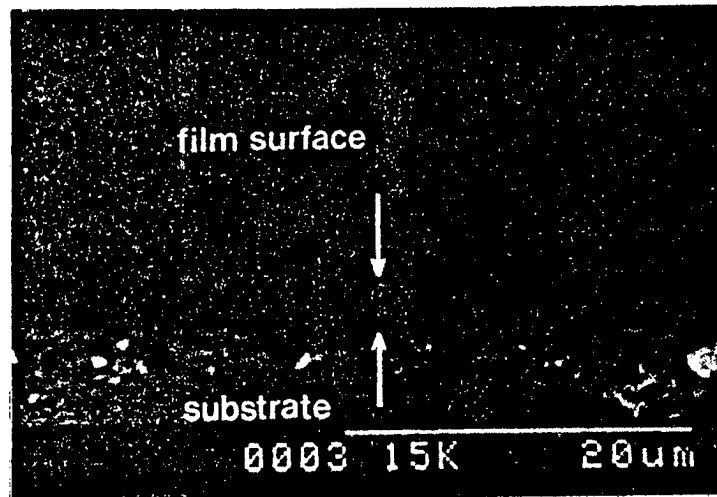


Figure 4. Tissue of film produced

Single Crystal, Fine Tissue Growth

43067591 Tokyo NIHON FUNMATSU FUNTAI YAKIN KYOKAI in Japanese 16-19 May 88
pp 18-19

[Report by Hiroshi Komatsu, Shigeyuki Hayashi, and Tetsuo Inoue, Institute
for Materials Research, Tohoku University]

[Text] 1. Research Objective

The purpose of our research was to grow mainly $\text{RBa}_2\text{Cu}_3\text{O}_{7-\delta}$ ($\text{R} = \text{Y}, \text{Eu}, \text{Er}, \text{Dy}, \text{Ho}$ and Yb) high-temperature superconducting single crystals from a high-temperature solution; to examine their crystal forms, growth patterns, twins, and fine structures and tissues including cleavage; and to ascertain the correlation between the crystal growth mechanism and the superconducting properties.

2. Methods and Conditions of Single Crystal Growth

Because of the resolving and dissolving nature of the crystals on which we conducted research, we added CuO or $\text{CuO} + \text{BaO}$ three times as large in composition in order to use it as flux, in an attempt to grow crystals from a high-temperature solution. Using 99.9 percent R_2O_3 , CuO , and BaCO_3 as reagents, we pulverized and mixed them in a mortar and thereafter calcined press-formed pellets at 900°C for 20 hours. Then we melted them in a platinum or high-purity aluminum crucible.

The simplest method of growing single crystals is to cool the high-temperature solution gradually and to grow crystals from spontaneous nuclei. However, this method has the disadvantages that 1) many small crystals come into being because the number of nuclei cannot be controlled, and 2) it is difficult to remove the crystals from the crucible after they are solidified. What must be done in growing crystals is to put the solution into the crucible to no more than 70 percent of the crucible's capacity. Otherwise, the liquid will come out of the crucible because the liquid readily travels upward alongside the inside wall of the crucible.

With the configuration given in Figure 1, the solution was gradually cooled by $2^\circ\sim 3^\circ\text{C}$ per hour after dissolution. Heating was stopped at $1,000^\circ\text{C}$, and the solution was left to cool spontaneously. The test sample was cut

crosswise together with the crucible, and they were immediately annealed at 900°C for 24 hours. The crystals were picked up mechanically out of the test sample, and they were annealed at a temperature between 900°C and 700°C for more than 10 hours. All this was carried out in air.

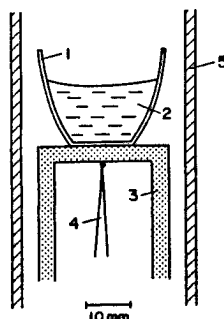


Figure 1. Gradual cooling method

1--aluminum crucible; 2--solution; 3--aluminum stand; 4--thermo-couple; 5--Siliconit furnace

The top-seeding method (or cold-finger method) shown in Figure 2 is a superior means of controlling the number of nuclei and taking crystals out of the liquid. However, this method takes time before the most appropriate growing conditions are found, and effort is also required to keep the growing conditions stabilized for a long time.

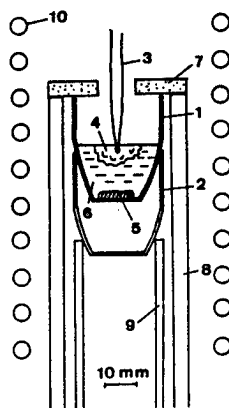


Figure 2. Top-seeding method or cold-finger method

1--platinum crucible; 2--platinum crucible for adjusting temperature gradients; 3--thermocouple; 4--crystals formed; 5--sintering raw material; 6--flux; 7--lid; 8--adiabatic wall; 9--support stand; 10--high-frequency induction coil

The component rates of each crystal obtained are analyzed by EDX, while its form is examined by SEM. After they are confirmed by the combined result

of X-ray diffraction, it is possible to remove the crystals under a stereomicroscope while ascertaining the crystal characteristics and fine surface structures. The biggest single crystal obtained by the gradual cooling method had the shape of a flat board, with one side measuring 5 mm in length.

3. Results of Experiments

The crystals obtained were all thin-plate crystals with (001) planes developed widely, and the fine tissues of their surfaces had the following characteristics: 1) the steps followed chiefly a (100) direction, with some parts extending in a (110) direction; 2) innumerable twin boundaries in a (110) direction were found (no twin was found in the single crystals showing no superconductivity); 3) there was conspicuous (100) cleavage; and 4) there were many cases where volute growth patterns were well developed. Examples of these characteristics are given in Figures 3, 4, and 5, respectively.



Figure 3. Growth plane of $\text{YBa}_2\text{Cu}_3\text{O}_{7-\delta}$

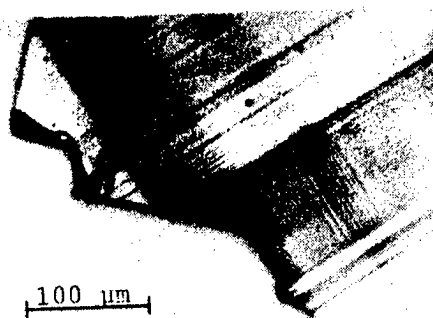


Figure 4. Twin of $\text{YbBa}_2\text{Cu}_3\text{O}_{7-\delta}$ and an edge due to cleavage



Figure 5. Volute growth pattern of $\text{EuBa}_2\text{Cu}_3\text{O}_{7-\delta}$

It is well known that twins arise because of the easing of distortions at the time of transformation from a tetragonal to an orthorhombic system. In

research on this fine surface tissue, using a reflection phase-contrast microscope is the best way to detect growth layers and dissolution patterns (Figure 6). A reflection-polarization microscope makes twins visible, reflecting their anisotropy. Under the reflection differential interference microscope that is often used, optical anisotropy overlaps infinitesimal surface forms, and this makes it difficult to separate them, because polarized light is used for this microscope. It is necessary to take measures to estimate the infinitesimal surface forms, while comparing the polarized pattern in Figure 7 with the differential interference pattern in Figure 8. The phase-contrast pattern shown in Figure 6 is useful in avoiding such measures. Anisotropy as high as $H_{c21}/H_{c2//} = 4.39$ was also obtained in a 6-tesla magnetic field. Its correspondent relationship with the optical anisotropy is a matter of interest.

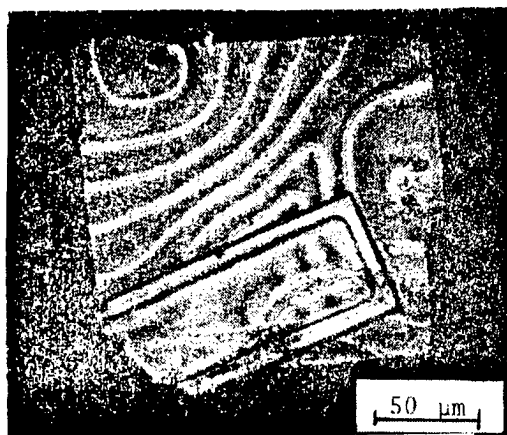


Figure 6. $\text{ErBa}_2\text{Cu}_3\text{O}_{7-\delta}$ (phase difference)



Figure 7. $\text{ErBa}_2\text{Cu}_3\text{O}_{7-\delta}$ (polarized)

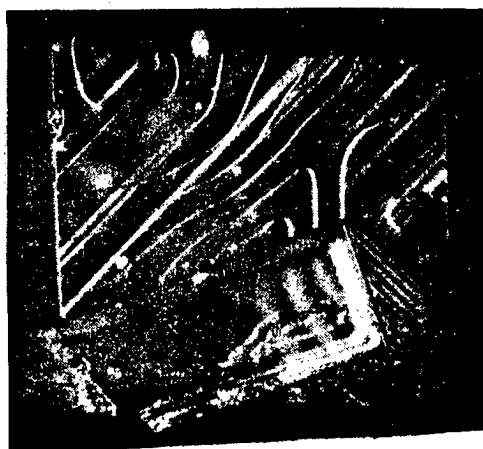


Figure 8. $\text{ErBa}_2\text{Cu}_3\text{O}_{7-\delta}$ (differential interference)

References

1. T. Inoue, S. Hayashi, H. Komatsu: Jpn. J. Appl. Phys., 26, L 732, 1987.
2. H. Hayashi, H. Komatsu, T. Inoue, T. Ohno, K. Sasaki, Y. Koike, T. Fukase: *ibid.*, L 1197.
3. Hiroshi Komatsu, Shigeyuki Hayashi, Tetsuo Inoue: "Boundary" magazine, July 1987 issue, pp 8-13.
4. Hiroshi Komatsu: "Kogaku" (published by the Optics Division, Japan Society of Applied Physics), Vol 12, No 3, pp 154-159, 1983.

Synthesis, Properties of Bismuth Superconducting Oxides

43067591 Tokyo NIHON FUNMATSU FUNTAI YAKIN KYOKAI in Japanese 16-19 May 88
pp 20-21

[Report by Hiroshi Maeda, National Research Institute for Metals: "Synthesis and Properties of Bismuth High-Temperature Superconducting Oxides"]

[Text] 1. Objective

The discovery of La-Ba-Cu-O high-temperature superconductors by Bednorz and Muller was followed by the discovery of 90K-level Y-Ba-Cu-O oxides that can be used with liquid nitrogen. This has triggered keen development competition both at home and abroad, and at the same time, the search for superconductors of higher T_c has continued. Recently, Bi-Sr-Ca-Cu-O high-temperature superconductors with a T_c in excess of 100K have been discovered, followed by a confirmation of 125K superconductivity in a Tl-Ba-Ca-Cu-O system. Thus, research and development have also taken on new aspects. In this report I will dwell on Bi-Sr-Ca-Cu-O high-temperature superconductors.

2. Methods

Powdered Bi_2O_3 , SrCO_3 , CaCO_3 and CuO of high purity were combined and mixed to become $\text{Bi}_1\text{Sr}_u\text{Ca}_v\text{Cu}_w\text{O}_x$ ($0 \leq u \leq 3$, $0 \leq v \leq 3$, $1 \leq w$). Thereafter, the mixture was calcined in air at $800^\circ\text{--}850^\circ\text{C}$ for several hours. This was pulverized, compressed and formed into a disk-shaped pellet 0.5~mm thick and 20 mm across under $2\text{--}6\text{t/cm}^2$ pressure. The pellet was sintered in air at $800^\circ\text{--}880^\circ\text{C}$ for 10 hours or more, and then cooled at a speed of about 100°C/h . The superconducting properties of the test sample were measured by the electric resistance method (four-terminal DC method) and the induction method (AC magnetic susceptibility and DC magnetic susceptibility). Its structure and composition were examined by such means as X-ray diffraction, EDAX, and high resolving power TEM.

3. Results

Figure 1 shows transition of the electric resistance of an oxide initially composed of $\text{Bi}_1\text{Sr}_1\text{Ca}_1\text{Cu}_2$ and O_x . When this oxide is sintered at a comparatively low temperature, below 850°C , there appears a superconducting phase (low T_c phase) showing a transition where electric resistance becomes

completely nonexistent (end T_c) at about 75K, as in the case of sample B. On the other hand, when it is sintered at a temperature above 870°C, close to melting point, there appears a phase (high T_c phase) showing a transition where the electric resistance begins to fall rapidly from 120K, as in the case of sample A. However, as a low T_c phase coexists in this sample, the transition curve bends sharply at 107K and reveals a complete loss of electric resistance at about 80K after leaving a slight trail. The end T_c in a high T_c phase, obtained by extending the transition curve to the point of zero resistance, is 105K. Figure 2 shows the dependence of A's magnetization on temperature. A decline in magnetization (complete diamagnetism) due to the Meissner effect, which is peculiar to superconductivity, can be recognized here. The two transition temperatures, indicated by arrows, are in agreement with those obtained by measuring the electric resistance given in Figure 1. The cubic ratio of the coexisting high T_c phases, obtained from these magnetism measurements, is about 20 percent. To produce a high T_c phase, it is important to effect sintering within an extremely narrow temperature range above 870°C. Now it is possible to produce a sample causing resistivity to become completely zero at 103K by means of precise temperature controls in that range. But even in the case of this sample, the cubic ratio of a high T_c phase is 25 percent or so, and no sample has yet been produced for a layer consisting of a high T_c phase alone.

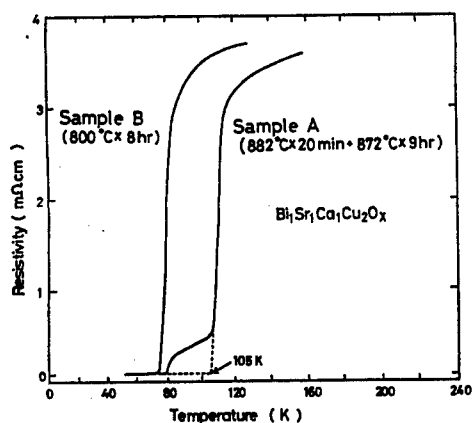


Figure 1. Resistivity-temperature curves of $\text{Bi}_1\text{Sr}_1\text{Ca}_1\text{Cu}_2\text{O}_x$

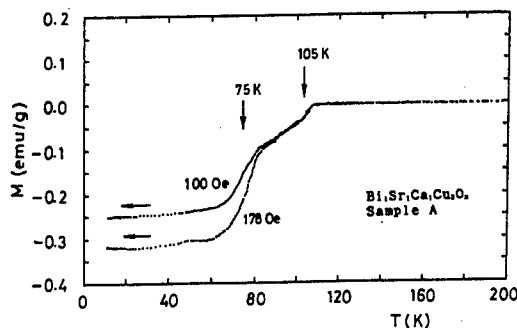


Figure 2. Magnetization-temperature curves of sample A

Figure 3 shows the T_c values of an oxide initially composed of Bi_1 , Sr_u , Ca_v , Cu_2 and O_x , produced by changing the amounts of Sr and Ca and sintering them at a temperature of more than 870°C. In this illustration, the Cu/Bi quantitative rate is fixed at 2 and is shown in terms of a component rate to Bi, Sr, and Cu. The high T_c phases (black marks) appear on the side of large-amount Ca, centered on the Bi/Sr/Ca ratio of 1:1:1, but the amount is the largest in the case of 111 composition. With their separation from the 111 composition, only low T_c phases appear regardless of the temperature for heat treatment.

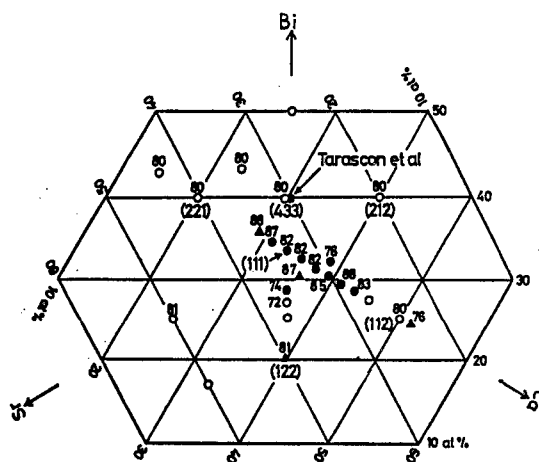


Figure 3. Tc's of $\text{Bi}_1\text{Sr}_u\text{Ca}_v\text{Cu}_2\text{O}_x$. (●▲ represent Tc's where high Tc phases are revealed, and ○ shows those where only low Tc phases are revealed. The numerical figures represent temperatures showing zero resistivity. The bracketed figures represent integral ratios among Bi, Sr and Ca.)

Through X-ray diffraction, EDAX and electron microscope observations, the low Tc phases are presumed to cover $\text{Bi}_2\text{Sr}_2\text{Ca}_1\text{Cu}_2\text{O}_x$ having an orthorhombic structure, with lattice constant $a = 5.4$, $b = 27$ and $c = 30.8\text{\AA}$. As for the high Tc phase, it is presumed that although the structure is the same as in the case of the low Tc phase, the c axis is as long as 36\AA , and that it covers $\text{Bi}_2\text{Sr}_2\text{Ca}_2\text{Cu}_3\text{O}_y$ where the amounts of Ca and Cu are larger than in the low Tc phase. Figure 4 shows a pattern of high resolving power in the case of sample A, observed by electron microscope. From this pattern it is found that phases of $C = 30\text{\AA}$ (S_3), $C = 36\text{\AA}$ (S_2), and $C = 42\text{\AA}$ are distributed in this sample in the form of a belt. Minute analysis reveals that in the $C = 30\text{\AA}$ structure, a five-layer pseudo-perovskite layer, where an SrO or Ca(Sr)O layer and a CuO layer are alternately arranged in the form of a $[\text{Sr}-\text{Cu}-\text{Ca}-(\text{Sr})-\text{Cu}-\text{Sr}]$ layer, is inserted between double Ba_2O_2 layers. In the $C = 36\text{\AA}$ structure, one CaO layer and one CuO layer are further added to the five-layer structure. A modulated structure accompanied by very large lattice distortions in six axial directions has also been observed among Bi oxides. So they are a substance which is of great interest from a structural point of view as well.

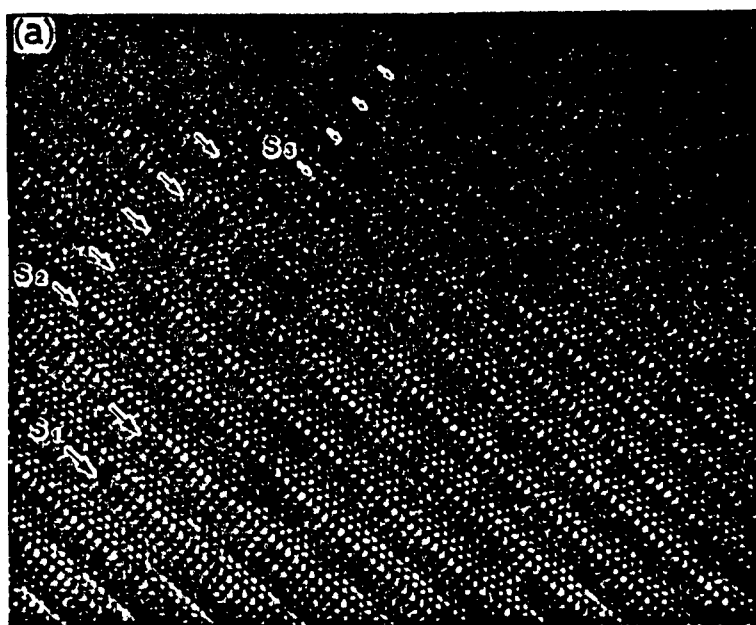


Figure 4. [510] directions of beams incident upon high resolving power pattern of sample A, observed by an electron microscope

Superconducting Oxide Materials Manufacture, Properties

43067591 Tokyo NIHON FUNMATSU FUNTAI YAKIN KYOKAI in Japanese 16-19 May 88
pp 22-23

[Report by Shoichi Matsuda, R&D Laboratory 1, Nippon Steel Corporation:
"Manufacture of Superconducting Oxide Materials and Their Physical
Properties"]

[Text] 1. Introduction

In regard to superconducting oxide materials represented by $\text{YBa}_2\text{Cu}_3\text{O}_x$, quite a number of points concerning their physical properties have become clear during the past year. It has been found that their critical current density (J_c) is extremely low, and that this is the biggest obstacle to putting them to practical use.

Here I will introduce ways of improving the J_c value by a sintering method, also briefly describing such matters as the relationship between critical temperature (T_c) and oxygen content, results of dynamic observations of twins by an electron microscope, measurement of specific heat, and the state of Cu valence estimated by XANES (X-ray absorption near edge structure).

2. J_c

The J_c of a sintered body is influenced by the heating temperature at the time of sintering (Figure 1). The J_c rises with the increase in heating temperature, but it shows the highest value between 920° and 930°C and falls rapidly when the temperature rises further. This trend is generally the same under both the coprecipitation method and the process of mechanical mixture, wherein the highest values of J_c are $1130\sim 1190\text{A}/\text{cm}^2$ and $1038\sim 1050\text{A}/\text{cm}^2$, respectively.

When the tissue of a high-temperature sintered sample is observed with an optical microscope, cracks and the second phase are observed in the grain boundary. From two-dimensional EPMA mapping, wave-front EDX, etc., it is conceivable that the second phase consists of such Y-free low-melting point oxides as BaCuO and CuO .

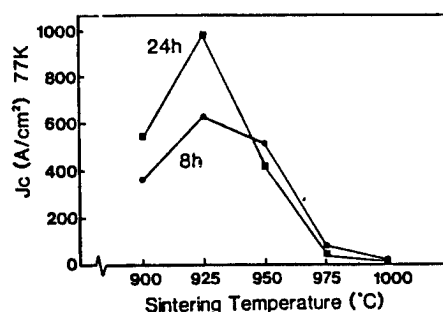


Figure 1. Relationship between sintering conditions and J_c

3. T_c and Oxygen Content

It is known that the T_c of $\text{YBa}_2\text{Cu}_3\text{O}_x$ is extremely sensitive to oxygen content¹. Figure 2 shows the relationship between the lattice constant and the oxygen content of a test sample where the oxygen content is controlled by changing annealing temperature and cooling speed. In the neighborhood of $x = 6.65$, the orthorhombic structure coexists with the tetragonal one, and in this case the difference between a and b is smaller than in the case of a single orthorhombic structure. It has already been reported that the orthorhombic structure is of two types--ortho-I and ortho-II--but it is conceivable that the lattice constant of the orthorhombic structure undergoes a generally continuous change. Incidentally, the T_c of a sample where orthorhombic structures coexist with tetragonal ones was 38K.

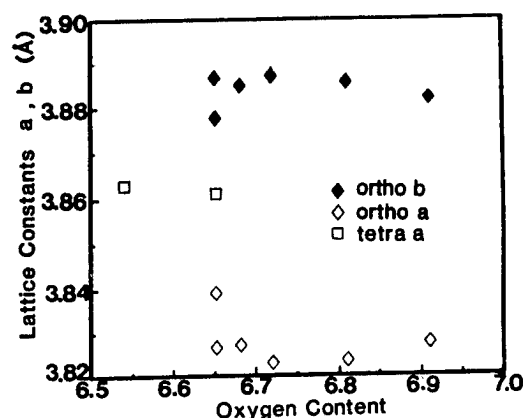


Figure 2. Relationship between oxygen content and lattice constants

4. Structure and Physical Properties of $\text{YBa}_2\text{Cu}_3\text{O}_x$

The crystal structure and internal tissue of $\text{YBa}_2\text{Cu}_3\text{O}_x$ have been clarified to a considerable extent through use of X-rays, electron microscopes, etc.^{2,3}. The results of spot observations of heating in an electron microscope concerning the appearance of a twin structure (Photo 1) show that the contrast gradually becomes weak when the twin disappears, and that it appears in an instant when it arises, while accompanied by discontinuous

jumps. The temperature for structural change was 520K, lower than in the case of transition from an orthorhombic to a tetragonal structure.

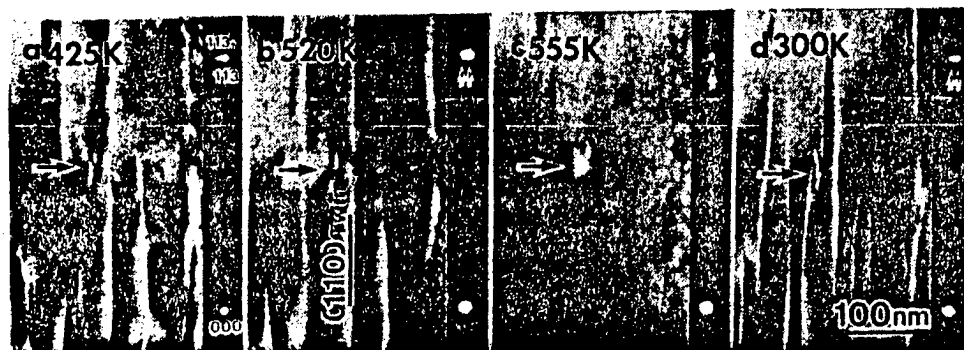


Photo 1. Results of spot observations of twins by a heated electron microscope

5. Measurement of Specific Heat

There have been many reports on data concerning specific heat⁴. The modulus (r) of electron specific heat and electronic-state density $[N(o)]$ in the vicinity of the Fermi surface can be estimated from a jump ΔC_p of specific heat at T_c . Figure 3 shows that $(\Delta C_p/T_c)$ is 52 mJ/mole K^2 . When a BCS model is presumed to materialize (it is said that a mechanism other than BCS is also connected), r and $N(o)$ are 36 mJ/mole K^2 and 5.1 states/eVCu-atom, respectively. The same values can be obtained when Y is replaced by another rare earth element.

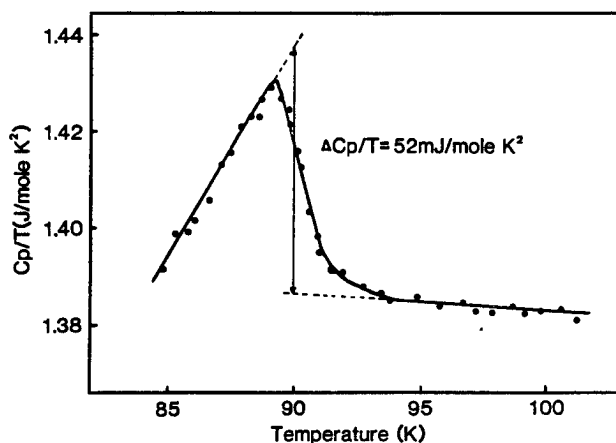


Figure 3. Specific heat curves

6. XANES

It is said that a state of Cu valence is important for $\text{YBa}_2\text{Cu}_3\text{O}_x$ superconductivity. The position of an absorption terminal is basically close to CuO [$\text{Cu}(+2)$]. However, from an analysis of the peak seen in the 8975 eV~8990 eV region, which is most characteristic among fine structures, $\text{Cu}(+1)$ is considered to increase when the system becomes tetragonal. As a result of XPS observations, it is said that there is $\text{Cu}(+2)$ in both orthorhombic and tetragonal systems. It is necessary to clarify such points further in the future.

References

1. Shinichi Uchida: Nontraditional Science and Technology, No 10, 21 (1987).
2. M.A. Beno et al.: Appl. Phys. Lett., 51, 57, 1987.
3. F. Izumi et al.: Jpn. J. Appl. Phys., 26 L694, 1987.
4. Masayasu Ishikawa: Verity, No 2, 49, 1988.

Wire Production From Superconducting Oxides

43067591 Tokyo NIHON FUNMATSU FUNTAI YAKIN KYOKAI in Japanese 16-19 May 88
pp 24-25

[Report by Osamu Kono, Fujikura Ltd.]

[Text] 1. Introduction

Following Y-Ba-Cu oxides, which are 90K-level high-temperature superconducting materials, 100K-level Bi-Sr-Ca-Cu oxides and 120K-level Tl-Ba-Ca-Cu oxides have been discovered since the beginning of this year, and high-temperature superconducting materials have reached a new level of development. Thus, there is an increasing number of research tasks, including searching for high-T_c materials, analyzing their physical properties and structures by turning them into single crystals, and raising the T_c value of wires.

It can be said that the issue of whether high-temperature superconducting materials can be applied to power application techniques for the future depends upon whether they can be turned into coils. To turn them into coils, long and uniform wires are necessary, as well as securing higher J_c values in high magnetic fields. Therefore, there are many difficult tasks facing the ceramic materials that are being developed at present. Here I will report on the measures for turning mainly Y-system superconducting oxides into wires.

2. Methods of Wire Production

As methods of producing wires and conductors from these materials, various studies are being conducted in terms of solid phase, liquid phase and vapor phase processes, as shown in Figure 1. The methods mentioned here have already been checked into, but especially the powder-sheath processing method and the sputtering process under the vapor phase method are being studied most.

The powder-sheath processing method is performed by filling a metal sheath with mixed powder, shortening its diameter by processing it, and heat-treating it in the final process to produce Y-Ba-Cu oxide superconducting phase inside it. This is closest to the conventional methods for the

manufacture of metal superconducting materials, and now it is being studied in many ways. With this method, however, it is impossible to obtain a high J_c value; it is limited to 10^3 – 4 A/cm² (77K, OT) at the highest. On the other hand, a J_c value of 3.5×10^6 A/cm² is reported to have been obtained in a Ho-Ba-Cu thin film by the sputtering process under the vapor phase method, and a 10^6 A/cm² level has already been reported by many research organizations. Thus, this process has produced very high properties in regard to J_c in comparison with the powder method. This is due to such factors as single crystallization and orientation; properties that cannot readily be achieved by the powder method are well utilized. Furthermore, various studies are being conducted to see whether the technique of obtaining a high J_c value under this thin film method can be applied to the production of conductors.

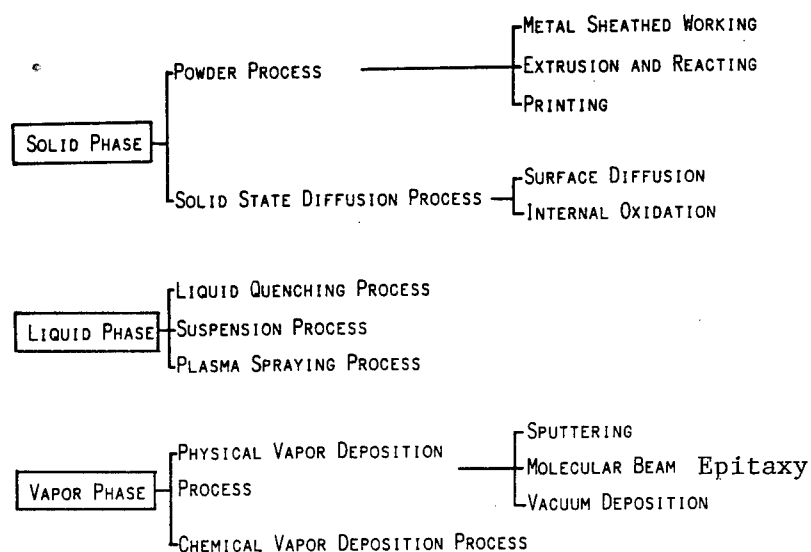


Figure 1. Wire/conductor process for superconducting oxide

3. Examples of the Powder-Sheath Method

One of the characteristics of our company's powder-sheath processing method is that a process of removing the sheath is adopted between wire processing and final heat treatment. The process of removing the sheath before heat treatment has been adopted because it has been ascertained that the difference in the rate of expansion between the surrounding sheath material (silver) and the internal oxide causes tension in the oxide and results in cracking on the oxide surface. A big crack in the direction of the oxide diameter causes the current path to be cut off and brings about a considerable loss in the value of J_c . In our view, we have been able to achieve a high J_c value by preventing this result. In addition, we are trying to produce wires of higher J_c value by introducing unique ideas to our research organizations. These ideas include putting the sheathed powder into the form of very thin tape by a rolling process to obtain a high J_c value, or adding a binder to the mixed powder before the final heat treatment and matching them with a

coil frame by an extrusion process. This is designed to be followed by heat treatment and creation of coils.

4. Conclusion

Turning high-temperature superconducting materials into wires is essential for application to electric power, and we think that research will be continued in the future chiefly for the purpose of improving the J_c value. Studies will be carried out with the immediate target set at improving the J_c value by one digit, as shown in Figure 2. At the same time, studies on such matters as securing higher J_c value in the magnetic field, and deposition on continuous substrates (metals, etc.) to apply size-lengthening and thin film producing techniques to the production of conductors, will be taken up as major tasks. Furthermore, studies must be conducted on the production of wires from Bi and Tl systems which are high- T_c materials.

POWDER PROCESS

$$J_c = 10^3 - 10^4 \longrightarrow \begin{array}{l} 10^4 - 10^5 \text{ A/cm}^2 \text{ (0T)} \\ 10^3 - 10^4 \text{ A/cm}^2 \text{ (1T)} \end{array}$$

LONG LENGTH, UNIFORM PROPERTIES AND REPRODUCIBILITY

VAPOR PROCESS

$$J_c = 10^4 - 10^6 \longrightarrow \begin{array}{l} 10^6 - 10^7 \text{ A/cm}^2 \text{ (0T)} \\ 10^5 - 10^6 \text{ A/cm}^2 \text{ (1T)} \end{array}$$

LONG CONDUCTOR, METAL SUBSTRATE AND NO ANNEALING
FOR APPLYING TO WIRE

OTHER PROCESS (MELT, ALLOY, ETC)

HIGH J_c AND LONG CONDUCTOR

Figure 2. Targets of SC oxide wire

Wire Production by Drawing-Rolling Process

43067591 Tokyo NIHON FUNMATSU FUNTAI YAKIN KYOKAI in Japanese 16-19 May 88
pp 26-27

[Report by Katsuzo Aihara, Hitachi Research Laboratory, Hitachi: "Turning Superconducting Oxides Into Wires by a Drawing-Rolling Process"]

[Text] 1. Introduction

Superconducting oxides having a high critical temperature (T_c) have been discovered successively since 1986, and expectations are being placed in many quarters upon their practical use at the temperature of liquid nitrogen. To apply them to high-power machinery and equipment consisting mainly of superconducting magnets, wires of high critical current density (J_c) are indispensable, and studies are being conducted to turn them into wires by such methods as a powdering process, a method of rapidly cooling a melted state, a dissolving-spraying method, a CVD method, and a sputtering method. In an attempt to turn them into wires by powdering $\text{YBa}_2\text{Cu}_3\text{O}_7$ (YBCO) having a 90K-level T_c , we first manufactured Ag-sheathed tape wire by a drawing-rolling process, and obtained a J_c value of $3330\text{A}/\text{cm}^2$ with the liquid nitrogen temperature. In this report I will describe ways of turning superconducting oxides into wires by the drawing-rolling process, focusing on the YBCO system.

2. Methods of Wire Production

The YBCO powder was produced by calcining $\text{Y}_2\text{O}_3\text{-BaCO}_3\text{-CuO}$ mixed powder ($950^\circ\text{C} \times 5\text{h}$), molding the powder by pressing and solidifying it, sintering the mold on a full scale ($950^\circ\text{C} \times 5\text{h}$ in an O_2 flow at a cooling speed of $200^\circ\text{C}/\text{h}$), and pulverizing it.

Figure 1 shows an outline of the process of manufacturing tape wire. We filled the YBCO powder in an Ag pipe with an outer diameter of 6 mm and a wall thickness of 0.5 mm, reduced its size to $\phi 2.8$ mm by drawing the wire through dies, and then processed it in the shape of a tape 0.05 mm thick by a rolling process. We sintered this wire in an O_2 flow at $850^\circ\text{--}910^\circ\text{C}$ for 5~50 hours, and cooled it to room temperature at a rate of $6^\circ\text{--}200^\circ\text{C}/\text{h}$.

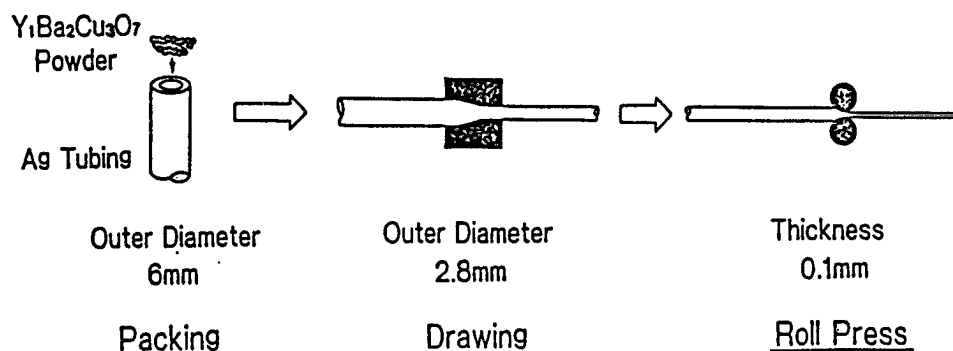


Figure 1. Process of manufacturing tape wire by the drawing-rolling method

Figure 2 shows an optical microscope photo of the tape wire cross-section after heat treatment, with a thickness of 0.1 mm. Both the YBCO core and the Ag sheath are processed uniformly, and the adhesion between the core and the sheath is also satisfactory.

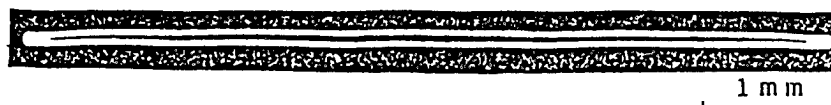


Figure 2. Photo of a tape wire cross-section

The J_c was measured in liquid helium and liquid nitrogen by making four terminals on the Ag sheath and using a superconducting magnet. As for the definition of J_c , we regarded the occurrence of $1 \mu\text{V/cm}$ voltage as a standard.

3. Results and Examination

Figure 3 shows changes in the J_c value (at liquid nitrogen temperature in a zero magnetic field) of tape wires when their thickness is changed. The value undergoes hardly any change up to 0.3 mm or so, but it shows a rapid rise when the thickness is reduced to less than 0.2 mm. When it is below 0.2 mm, some wires show low J_c values, but most of them show more than 1000A/cm^2 . At present, the value has reached a maximum of 3330A/cm^2 .

The J_c value of a round-section sample produced by the drawing method alone was about 500A/cm^2 , but in the case of a tape-shaped sample produced by adding the rolling process, a value several times that was achieved. As reasons for this, the following points can be considered: 1) the YBCO core was made more compact (density: $5.7\sim 5.9\text{g/cc}$); 2) O_2 diffusion terms were improved by reducing the wall thickness of the Ag sheath; 3) the adhesion between the YBCO core and Ag sheath was improved; etc.

Figure 4 shows the J_c characteristics in the magnetic field of a sample 0.1 mm thick. At 4.2K the J_c value in a zero magnetic field was 5700A/cm^2 , but at 1T it dropped to 600A/cm^2 , one digit lower, and to 200A/cm^2 at 7T.

At 77K, the effect of the magnetic field was more conspicuous, with the J_c value in the zero magnetic field standing at 1410 A/cm^2 and dropping by nearly two digits with the application of a very low magnetic field of 20mT.

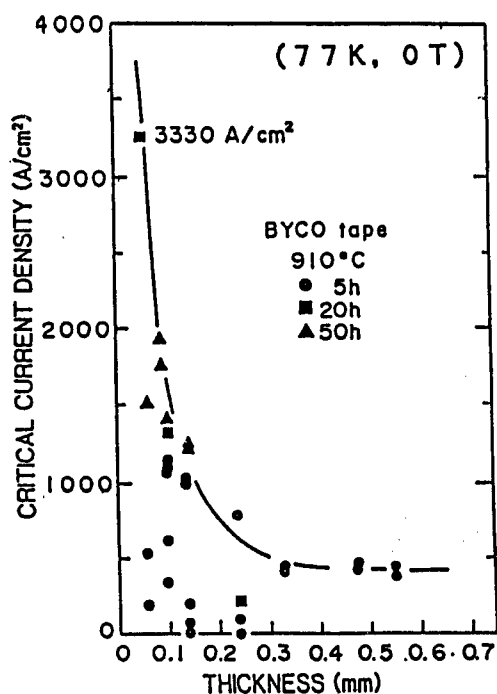


Figure 3. Relationship between tape-plate thickness and critical current density

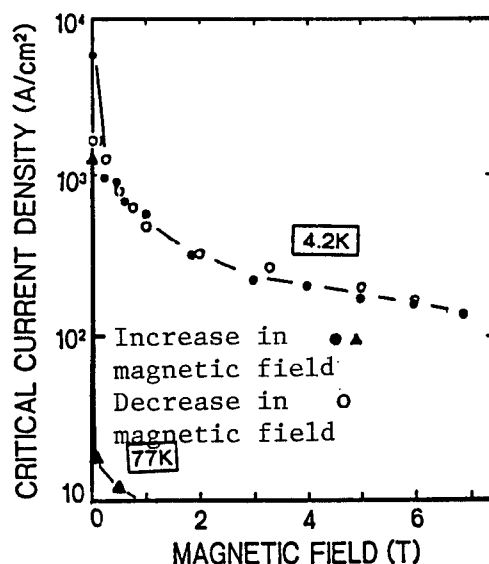


Figure 4. Dependence of critical current density upon magnetic field

As mentioned above, it has become possible to obtain a J_c value exceeding 3000 A/cm^2 in the case of a tape wire produced by the drawing-rolling method. However, the rapid fall in J_c value due to the impressed magnetic field is a big problem for the generation of a strong magnetic field, which is a pattern for the application of superconductivity. In the case of YBCO oxides, the J_c anisotropy due to their crystal structures is conspicuous, and a grain-connecting layer sensitive to a magnetic field tends to arise in a grain boundary. To raise J_c value in a magnetic field, therefore, it will be necessary to develop a new manufacturing process focusing on the control of grain orientation.

References

1. M. Okada, et al., Jpn. J. Appl. Phys. 27 L185, 1988.
2. S. Matsuda, et al., MRS 1987 fall meeting, AA7 21, Boston, USA.
3. Kiyofuji, et al., Hitachi Cable, 7, 7, 1987.

ICB Deposition of High-Temperature Superconducting Oxide Thin Films

43067591 Tokyo NIHON FUNMATSU FUNTAI YAKIN KYOKAI in Japanese 16-19 May 88
pp 28-29

[Report by Katsuhiro Imada and Ken Sato, Materials Research Laboratory, Mitsubishi Electric Corp.; and Yasuyuki Kawagoe and Kenichiro Yamanishi, Applied Products Research Laboratory, Mitsubishi Electric Corp.: "High-Temperature Superconducting Oxide Thin Films Produced by ICB Deposition Method"]

[Text] 1. Introduction

Turning high-temperature superconducting materials into thin films is indispensable for applying them to devices. Many reports have already been made on films formed by such methods as sputtering, electron beam deposition, laser deposition, and CVD. Besides these, however, our company is attempting to form thin films by the ion cluster beam (ICB) method. The ICB method makes it possible to form films of high density and adhesive power by means of the strong kinetic energy imparted by chemical reactivity with high cluster ions and by accelerating voltage. Thus it is possible to control the crystal state of films even at a comparatively low temperature. In the case of Au, for example, high density, high adhesive power, and flatness of the surface are achieved by applying accelerating voltage, and this is put to practical use for high-reflectance laser mirrors, X-ray mirrors, etc., which are difficult to obtain by other methods. As to Al on Si substrates, this method makes it possible to obtain unparalleled single crystal thin films by epitaxial growth.

With this background, we are conducting studies aimed at effecting low-temperature formation of superconducting oxide thin films of high quality, to make the most of the strong points of the ICB deposition method. Our report here is focused on the properties of superconducting thin films formed by three-element simultaneous ICB deposition in a high vacuum. At present, we are also attempting to use a reactive ICB method, introducing oxygen gas during deposition. Finally, we are planning to adopt a four-element ICB method, adding an excited oxygen source.

2. Methods

Using the metals Y, Ba, and Cu as deposition materials, we burst forth three-element cluster ions simultaneously in an approximately 5×10^{-4} Pa vacuum, as shown in Figure 1, and deposited them on an MgO (100) substrate at a speed of about 10 nm/min. The component ratio of the film to be produced was controlled by adjusting the crucible heating so that the speed of evaporation from each ICB source would constitute a given ratio. The accelerating voltage was 0~2 KV. To eliminate the influence of thermal energy in the case of film formation, the substrate was not heated, but the temperature rose to about 220°C because of the heat radiating from the ICB source. The as-depo. film was brown, the color tended to change in air, and there was no superconducting phase in an X-ray diffraction pattern. Therefore, we added the process of cooling the film gradually after heat-treating it in oxygen at about 900°C.

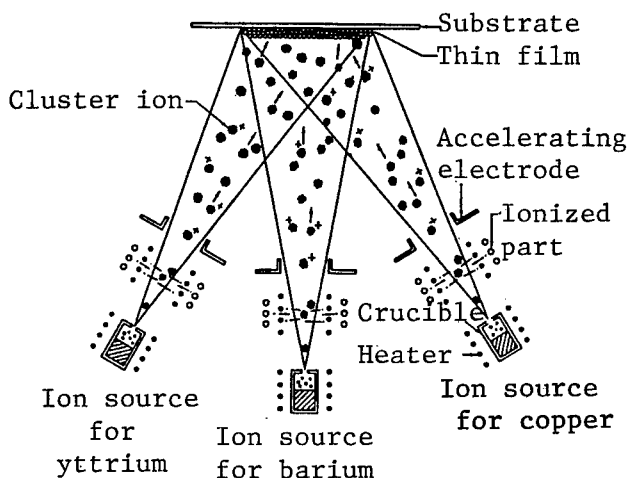


Figure 1. Conception of three-element simultaneous ICB deposition

3. Results

To evaluate the effect of accelerating voltage, we compared a case where there was no accelerating voltage for ordinary thermal deposition with a case where 500V accelerating voltage was applied (Figure 2). As a result, we saw many cracks in the film in the former case and hardly any crack in the film in the latter. Also, a test conducted by tearing off the tape (adhesive strength: about 200 kg/cm²) revealed that the latter film had high adhesive power, not permitting the tape to scale off. According to SEM observation, the film impressed with accelerating voltage was compact and showed large crystal growth. This is considered due to the fact that the kinetic energy of cluster ions under accelerating voltage contributes to higher density and higher adhesive power.

In regard to heat-treatment temperature, resistivity became zero between 870° and 930°C, and the range of transition temperature tended to narrow

slightly with a rise in temperature. In regard to composition, the drop in T_c value was slight even when the Y/Ba/Cu ratio shifted to the BaCu-rich side from 1:2:3, but the value tended to drop markedly when the ratio shifted to the YCu-rich side.

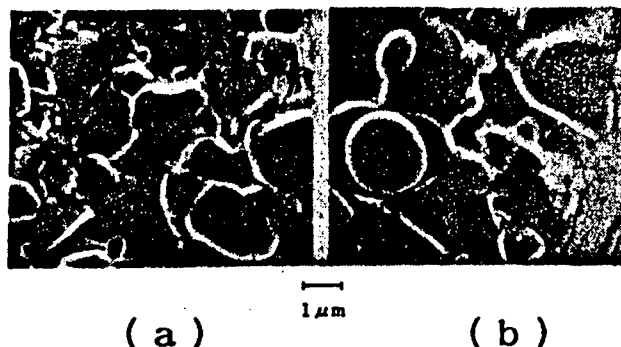


Figure 2. SEM photos representing the surfaces of superconducting thin films produced by the ICB method
 (a) No accelerating voltage is applied.
 (b) 500V accelerating voltage is applied.

In regard to film thickness, the range of superconducting transition temperature narrowed in the case of a thicker film, and the zero-resistivity temperature rose, too. When the component distribution in the direction of the thicker film was examined by Auger analysis, after heat treatment Mg diffusion was seen in the film near the substrate interface. Such a reaction to the substrate causes a drop in T_c value. However, this effect does not reach the vicinity of the film surface when the film grows thicker, and the T_c value is considered to come close to a bulk value as a consequence.

Within the scope of our studies up to now, the most appropriate conditions are 500V in accelerating voltage, 930°C in heat treatment temperature, and 2 μm in film thickness. At this time, films are obtained at 89K in zero resistivity temperature and 3K in the range of transition temperature.

In our studies using the reactive ICB method we introduced oxygen gas into air up to 1×10^{-2} Pa, but this did not lead to as-depo. superconductivity. For this, it appears to be necessary to raise oxygen pressure further or to use reactive oxygen.

4. Conclusion

Under the above-mentioned method, the T_c value is above the liquid nitrogen temperature, and, moreover, a film superior in adhesion to the substrate can be formed even without particularly heating the substrate, showing the characteristics of the ICB method. To obtain films of good properties, however, a temperature of about 900°C is necessary, as in the case of the coating method going through heat treatment in oxygen. In this case, the surface becomes uneven because of grain growth accompanying high-temperature

processing, and the properties tend to deteriorate, too, because of its reaction to the substrate. Therefore, it is necessary to form films at low temperature, and we think it is possible to achieve as-depo. crystallization by the four-element ICB method using kinetic energy with high cluster ions while taking reactive oxygen into the films.

Phase Diagram of Ba-Y-Cu Oxide System Ceramics

43067591 Tokyo NIHON FUNMATSU FUNTAI YAKIN KYOKAI in Japanese 16-19 May 88
p 30

[Report by Kozo Osamura and Shojiro Ochiai, Faculty of Technology, Kyoto University; and Cho I and Takashi Yamashita, graduate students of Kyoto University]

[Text] Objective

Ba-Y-Cu-O system ceramics are attracting attention as high T_c superconducting materials, and knowledge of phase diagrams is important for developing materials of further high performance. Therefore, a detailed explanation will be made in this report of isothermal cross-section diagrams at temperatures of 1173K and 1223K and with a composition in the neighborhood of the superconducting phase in air as part of the phase diagrams, and a report will be made on the nonvariant system reaction existing in the temperature range.

Experiment Method

$BaCO_3$, Y_2O_3 and CuO powders were weighed in an optional composition, and after pulverizing and mixing, a sample made into pellet form was sintered at 1173K and 1223K in air for 72 hours. Phase identification was carried out by the powder X-ray diffraction method and EPMA, and structure observation was accomplished by SEM and optical microscope on the sample quenched after sintering. Moreover, the following were used in the phases appearing in this research: T1: $Ba_2YCu_3O_x$, T2: BaY_2CuO_5 , T3: $Ba_8YCu_4O_{13.5}$, YC: $Y_2Cu_2O_5$, BC: $BaCuO_2$ and C: CuO .

Experiment Results

Isothermal cross-section diagrams with a composition in the neighborhood of the superconducting phase at temperatures of 1173K and 1223K are shown in Figures 1 and 2. The presence of the three-phase triangles T3 + T2 + BC and T2 + T1 + BC were confirmed at a temperature of 1173K. A liquid phase exists in the range surrounded by the three phases of T1, BC and C at this temperature. The approximate correlation was estimated by phase identification and structure observation, as shown in Figure 1. The liquid phase

exists in a fairly wide range at a temperature of 1223K. The monophasic range of the liquid phase reaches up to 15 mol% of $YO_{1.5}$, as shown in Figure 2. The two-phase and three-phase ranges of the liquid phase have been ascertained as shown in Figure 2. Moreover, the presence of the three-phase triangles $T1 + T2 + T3$ and $T1 + T3 + BC$, as shown in the diagram, have been confirmed. As seen here, the liquid phase changes greatly at two points in the phase diagrams at temperatures of 1173K and 1223K. Coping with this change, the presence of a covering eutecoid reaction expressed by $T1 + T3 \rightleftharpoons T2 + BC$ could be expected in the range surrounded by $T2$, $T1$, BC and $T3$, and it has been confirmed that it occurred in the temperature range of 1193K to 1173K. Moreover, it has been confirmed that the covering eutecoid reaction becoming $T2 + L \rightleftharpoons T1 + C$ brought about by the phase change related to the liquid phase occurred in the neighborhood of 1208K.

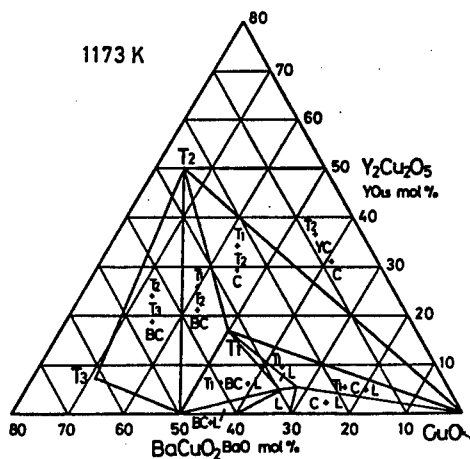


Figure 1. Isothermal cross-section phase diagram at 1173K

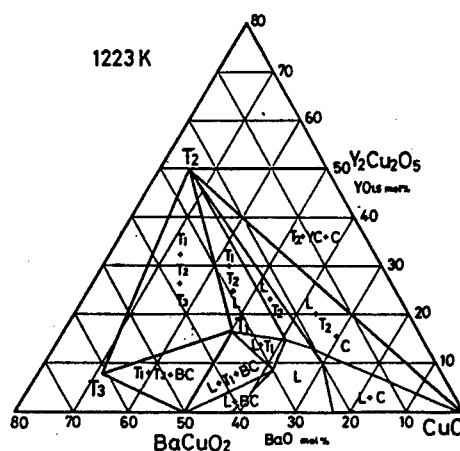


Figure 2. Isothermal cross-section phase diagram at 1223K

Phase Equilibrium of Y-Ba-Sr-Cu-O System

43067591 Tokyo NIHON FUNMATSU FUNTAI YAKIN KYOKAI in Japanese 16-19 May 88
p 31

[Report by Yasunori Ikeda, Yasushi Ooue, Kazuhisa Inaba and Yoshichika Bando, Institute for Chemical Research, Kyoto University; Yasuo Takeda and Ryoji Kanno, Faculty of Technology, Mie University; and Hitoshi Kitaguchi and Jun Takada, Faculty of Technology, Okayama University]

[Text] We took up the challenge of searching for a new superconducting phase as a process of equilibrium phase diagram preparation in the Y-Ba-Cu-O system, including the 90K-level oxide superconductor $\text{YBa}_2\text{Cu}_3\text{O}_x$ ("123"), and we have confirmed that there is no other superconducting phase than the "123." However, various reports on superconductivity, including a report on Y-Sr-Cu-O without Ba^{1,2}, have been made on the Y-Ba-Sr-Cu-O system that includes Sr.

We have studied the phase equilibrium of the Y-Ba-Sr-Cu-O system at various heating temperatures under the ordinary ceramics method using Y_2O_3 , BaCO_3 , SrCO_3 and CuO as materials. The result at a temperature of 900°C in air is shown in Figure 1.

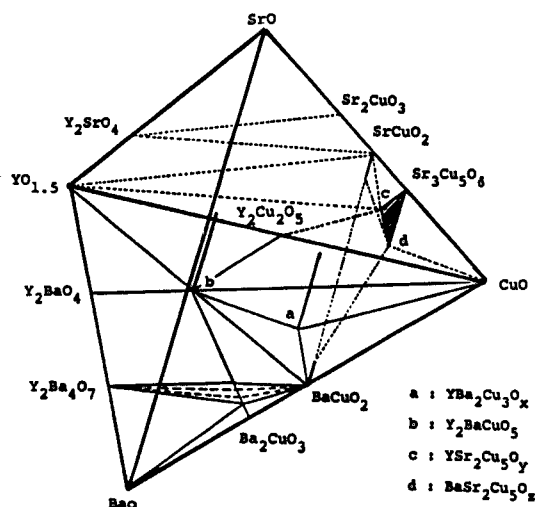


Figure 1. $\text{YO}_{1.5}$ -BaO-SrO-CuO system phase diagram

The result on "123" coincides with the many reports made, and Sr in practice becomes a solution up to 75 percent. Replacement of 80 percent by Sr is possible on the "211." The solution limit of Sr to BaCuO_2 and Ba to SrCuO_2 is about 15 percent.

The presence of $\text{Sr}_3\text{Cu}_5\text{O}_8$ has been confirmed as a new compound of this system; it is possible to replace about one-third of the Sr with Ba and Y in this phase, and a wide solution range exists, as shown in Figure 1. Moreover, the tie line of $\text{YO}_{1.5}\text{-SrCuO}_2$ in Figure 1 disappears at more than 950°C , and a tie line can be drawn between C; $\text{YSr}_2\text{Cu}_5\text{O}_z$ and Y_2SrO_4 .

Although the structure of $\text{Sr}_3\text{Cu}_5\text{O}_8$ has not been established, the X-ray diffraction diagram (Figure 2) is explainable by the orthorhombic. A resistance characteristic such as that in a semiconductor was shown electrically in the entire solution range.

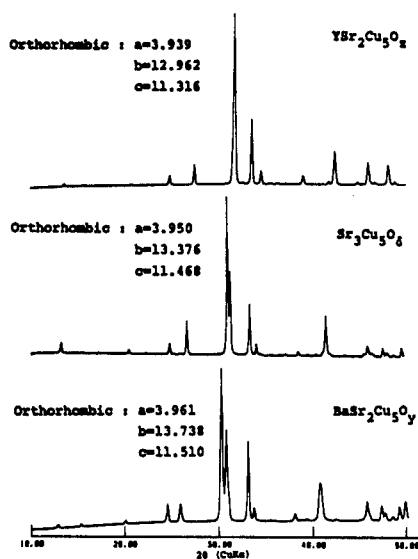


Figure 2. X-ray diffraction diagram of $\text{YSr}_2\text{Cu}_5\text{O}_z$, $\text{Sr}_3\text{Cu}_5\text{O}_8$, $\text{BaSr}_2\text{Cu}_5\text{O}_y$

It has been found that a solid solution of "123" exists only as a superconducting phase in the Y-Ba-Sr-Cu-O system and that T_c drops as the amount of Sr added is increased.

References

1. M. Oda, et al., Jpn. J. Phys., 26, L804, 1987.
2. Z. Qi-rui, et al., Solid State Commun., 63, 535, 1987.

Reaction Process of Superconducting Ceramic Materials by Differential Thermal Balance

43067591 Tokyo NIHON FUNMATSU FUNTAI YAKIN KYOKAI in Japanese 16-19 May 88
p 32

[Report by Tadahiko Azumi, Kiyoko Takahasi, Akira Kishi, and Masahiko Ichihashi, Shinku Riko Co., Ltd.: "Study of Reaction Process of Superconducting Ceramic Materials by Means of Differential Thermal Balance and High-Temperature Heating Observation Devices"]

[Text] Objective

A differential thermal balance (TG-DTA) is used in the preparation of a superconducting ceramic bulk sample for determining the reaction temperature, reaction conditions, etc., of the material powder mixture. However, it is not easy in a complicated plural system such as the Bi system to determine accurately what sort of reactions are occurring in regard to each respective peak by TG-DTA measurement alone. Therefore, microscopic observation at high temperature was also conducted in addition to the TG-DTA measurement in order to ascertain more concretely what sort of reactions occurred at which temperature and to what extent they had progressed.

Experiment Method

A differential thermal balance of type TGD7000RH made by Shinku Riko was used for the TG-DTA measurement. The Bi_2O_3 , SrCO_3 , CaCO_3 and CuO powders were mixed in the ratio $\text{Bi}:\text{Sr}:\text{Ca}:\text{Cu} = 1:1:1:2$; about 130 mg was inserted in a platinum cell and this was heated at $10^\circ\text{C}/\text{min}$ in oxygen flow. The image heating high-temperature observation device MS-EIR made by Shinku Riko was used for the high-temperature microscopic observation. A material mixture of about 50 mg with the same composition as that mentioned above was put into a platinum container and heated by a small infrared image furnace in oxygen flow; the change in appearance of the sample was continuously monitored by a CCD color camera, and the reactions were followed while VTR recording was carried out.

Measured Results

The TG-DTA measured results are shown in Figure 1. A weight reduction brought about by reaction starts in the neighborhood of 600°C and is approximately completed in the neighborhood of 960°C. Seven small and large endothermic peaks appear in the DTA in the temperature range 650°C-1020°C. Photos A to D in Figure 2 were taken from the VTR image of the high-temperature microscopic observation.

- Photo A 622°C: The entire sample is of a yellow color, becoming red in places
- Photo B 846°C: The reaction has progressed, and the black areas have increased
- Photo C 881°C: Melting of particles is progressing, one after another
- Photo D 942°C: The melted areas are expanding over the entire sample

As seen here, the state is one in which reactions, partial melting and phase transition of materials and reaction products are occurring continuously. We are conducting further studies on the correspondence between the DTA peaks and high-temperature microscopic observation results.

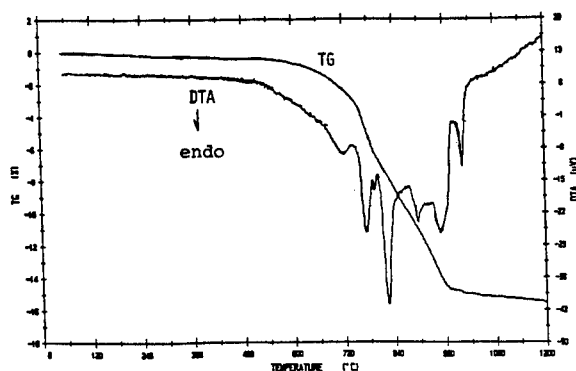


Figure 1. TG-DTA measurement results

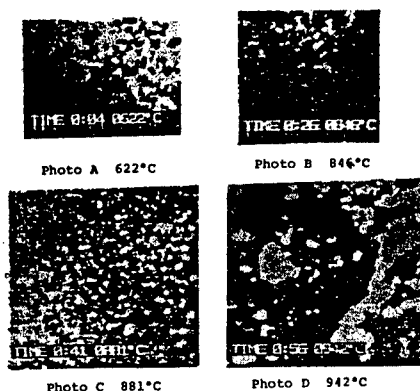


Figure 2. Photos (A-D) taken from VTR image of high-temperature observation

Preparation of Oxide Superconductors by Wet Coprecipitation Preparation

43067591 Tokyo NIHON FUNMATSU FUNTAI YAKIN KYOKAI in Japanese 16-19 May 88
p 33

[Report by Tatsuya Yamamoto and Takayuki Furusawa, Mitsui Mining and Smelting Co., Ltd.; Hideaki Seto and Boku Kyonbo, Fujitsu, Ltd.; and Shinsaku Kobe, Kazuyuki Kuwahara, Tetsuya Hasegawa, Koji Kishio, Koichi Kitazawa and Kazuo Fueki, Faculty of Technology, Tokyo University: "Preparation of Oxide Superconductors by Wet Coprecipitation Method"]

[Text] 1. Introduction

The method of preparing oxide superconducting powders is presently centered around the solid phase reaction method. However, the composition of powders obtained by this method lacks homogeneity and the particles are coarse, so it is difficult to obtain a fine sintered material when sintering is conducted using this powder. Whereas the high densification of oxide superconductors in relation to 1) improvement of critical current density, 2) improvement of mechanical characteristics and 3) prevention of deterioration of superconducting characteristics brought about by moisture, etc., is an important problem in regard to practical use, the decline of the superconducting characteristics with fining is a problem in the case of $\text{Ba}_2\text{YCu}_3\text{O}_{7-\delta}$ (BYCO). In our research, we prepared a high-density oxide superconductor using powder synthesized by the ethanol oxalate method, which is a coprecipitation method.

2. Experiment Method

Coprecipitation is conducted by adding ethanol oxalate solution in an amount equivalent to four times by volume fraction to the nitric acid solution containing the prescribed amount of metallic cation. After filtering and drying, synthesis of the BYCO is possible by heating it to a temperature of $800^\circ\text{--}850^\circ\text{C}$, and the fining of the powder for synthesis can be achieved at a comparatively low temperature for this material. The submicron size powder obtained by this method was cold pressed at a pressure of 8 MPa, and a high density sintered material was obtained by heating it to a temperature of $1000^\circ\text{--}1040^\circ\text{C}$ in oxygen flow.

3. Results and Considerations

The results of investigating the relationship between the sintering temperature and the sintered material density are shown in Figure 1. The sintered density is 6.05 g/cm^3 (~95 percent) when sintered at a temperature of 960°C ; however, it becomes 6.2 to 6.3 g/cm^3 at a temperature of 1000°C – 1040°C , reaching about 98 percent of the theoretical density, 6.39 g/cm^3 . The optimum temperature is in the neighborhood of 1020°C . Moreover, BYCO has a large nonstoichiometry according to the oxygen content, and it is necessary to allow the sample to absorb sufficient oxygen for the manifestation of superior superconducting characteristics. It is generally considered in the case of this oxide superconductor that the superconducting characteristics decline when subjected to fining. This is because the open pores in the interior of the sintered material practically disappear with fining, and the chemical dispersion of the bulk oxygen is therefore the rate-determining condition. The results of investigating the oxygen annealing effect at zero resistance temperature of BYCO sintered at 1020°C are shown in Figure 2. The T_{c0} was still 82K after 8 hours' annealing at 500°C in oxygen flow, it became 88K after 72 hours, and it finally became a superconductor 90K after 504 hours' (3 weeks') annealing. Moreover, the ΔT_c declined as the annealing time became longer, and this high density BYCO became a superior oxide superconductor generating a sharp superconducting transition, registering $\Delta T_c = 0.5\text{K}$ after 504 hours of annealing.

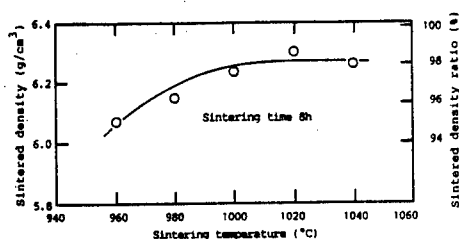


Figure 1. Relationship between sintering temperature and sintered material density

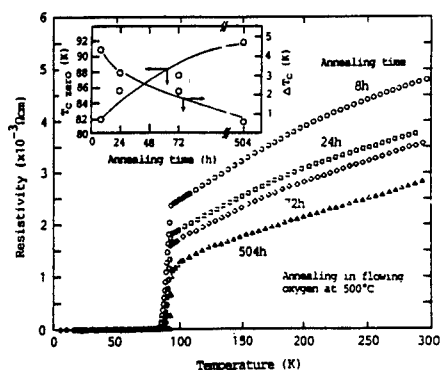


Figure 2. Oxygen annealing effect at zero resistance temperature

Upon investigating the temperature dependency of the resistivity on the surface and in the core of the sample that had been oxygen annealed for 504 hours, almost no difference was recognized between the two samples, as shown in Figure 3; the zero resistance temperature for each was about 91K to 92K. This result demonstrates that the oxygen has dispersed sufficiently into the core of the bulk by means of oxygen annealing for 504 hours and that the entire bulk has become an oxide superconductor of 90K. The I-V characteristic at liquid nitrogen temperature is shown in Figure 4. The J_c reached about 350 A/cm^2 as estimated on the basis of a sectional area of the sample. The J_c value obtained is not necessarily large as a bulk value. Since there are

still many unclear points concerning the relationship of the superconducting characteristics and the microstructure, etc., of the sintered materials, we intend to investigate them further in the future.

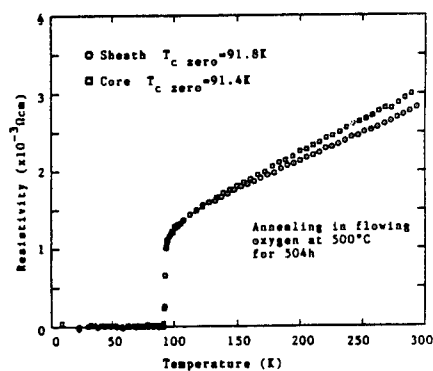


Figure 3. Temperature dependency of resistivity on the surface and in the core

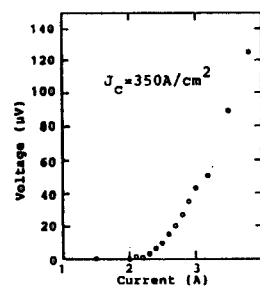


Figure 4. I-V characteristic at liquid nitrogen temperature

Preparation of Oxide Superconductors by Sol-Gel Method

43067591 Tokyo NIHON FUNMATSU FUNTAI YAKIN KYOKAI in Japanese 16-19 May 88
p 34

[Report by Sumio Sakka, Hiromitsu Kozuka, Tetsu Umeda, Takashi Monde and Kin Sokin, Institute for Chemical Research, Kyoto University: "Preparation of Oxide Superconductors by Sol-Gel Method"]

[Text] 1. Introduction

Coating films and fibers can be prepared by utilizing sol, which is the precursor of sol-gel, and it is possible to obtain a ceramic precursor with high homogeneity utilizing a sol-gel method that uses metallic alkoxide and metallic salt as starting material. In this research, an effort was made to prepare oxide superconductor $\text{YBa}_2\text{Cu}_3\text{O}_{7-x}$ fiber and coating film by making the most of the characteristics of the sol-gel method.

2. Experiment Method

2.1. Preparation of Fiber

A 100 ml acetate aqueous solution of a concentration equivalent to 38g/ $\text{YBa}_2\text{Cu}_3\text{O}_7/1$ was prepared, aqueous ammonia was dropped in it, and the pH was adjusted to 6. The gel fiber was spun from the high viscosity sol obtained by concentrating this solution at 60°C. Moreover, a heat treatment was performed on the transparent gel piece generated as a result of concentration.

2.2. Preparation of Coating Film

A $\text{Ba}(\text{OCH}_3)_2 \cdot \text{Y}(\text{OC}_4\text{H}_9\text{O})_3 \cdot \text{Cu}(\text{OCH}_3)_2$ system solution was prepared for which methanol, triethanolamine and xylene are the solvents, dropped on a YSZ substrate, and after drying on a hot plate, it was baked at 800°C for 5 minutes. After the operation from the dropping of the solution to baking was repeated 5 to 10 times, it was annealed at 800°C for 60 hours in oxygen flow and then cooled down in the furnace.

3. Results

Figure 1 is an X-ray diffraction diagram of the compact sample of the mixture of Y_2O_3 , BaCO_3 and CuO powders and the gel piece prepared from the acetate aqueous solution wherein the temperature was raised in air up to 750°C at a rate of $5^\circ\text{C}/\text{min}$ and then cooled to room temperature in the furnace after sintering for 19 hours at 750°C . It can be confirmed from this that the deposition of $\text{YBa}_2\text{Cu}_3\text{O}_{7-x}$ phase occurs more easily from a gel piece than from a powder compact. A gel piece that was cooled in the furnace after undergoing heat treatment for 5 hours at 910°C in air is a superconductor of $T_c(\text{end}) = 93\text{K}$; it was ascertained that the transition from gel to the superconducting phase occurs extremely easily.

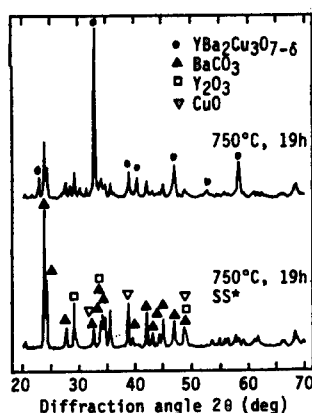


Figure 1. X-ray diffraction pattern for the gel-derived products heated at a rate of $5^\circ\text{C}/\text{min}$ to 750° , 800° and 910°C , kept there for 19 hours, and cooled down in the furnace.

*SS: prepared through the conventional solid-state reaction.

A SEM photo of gel fibers is shown in Figure 2. The spinning of a gel fiber having a diameter of $5\text{ }\mu\text{m}$ - 2 mm is possible by this method, and a fiber of a maximum length of 50 cm can be drawn. A deposition of the $\text{YBa}_2\text{Cu}_3\text{O}_{7-x}$ phase was recognized in the baked fiber, and a fiber of $T_c(\text{end}) = 62\text{K}$ was available.

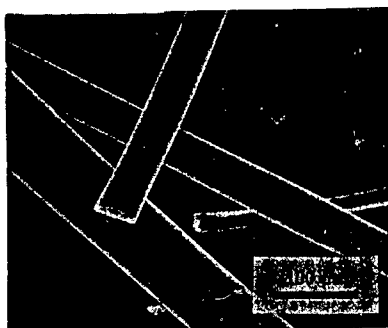


Figure 2. Scanning electron micrograph of the gel fibers

It was ascertained by SEM observation that the coating film prepared from the alkoxide solution had a thickness of about 7 μm and it consisted of particles with a diameter of 1-2 μm . The temperature change of the electric resistance was the same as that of a metal, and the superconducting transitions of $T_c(\text{onset}) = 98\text{K}$ and $T_c(\text{end}) = 56\text{K}$ were seen.

Preparation of Orientative $\text{YBa}_2\text{Cu}_3\text{O}_y$ Sintered Material

43067591 Tokyo NIHON FUNMATSU FUNTAI YAKIN KYOKAI in Japanese 16-19 May 88
p 35

[Report by Toshihiko Nishida, Takeshi Shiono, Hideaki Fujioka and Tomozo Nishikawa, Kyoto Institute of Technology: "Preparation of Orientative $\text{YBa}_2\text{Cu}_3\text{O}_y$ Sintered Material"]

[Text] Introduction

Sintered material (orientative sintered material) in which the crystallographic axis direction of the individual crystal particles is arrayed so that the polycrystal lies in a specific direction can be obtained by emphasizing the crystallographic axis anisotropy inherent in the crystal particle itself. Since the superconductivity of $\text{YBa}_2\text{Cu}_3\text{O}_y$ ceramics is generated in the (00 ℓ) surface of a crystal, it is considered that a high current density can be achieved by preparing a sintered material with the (00 ℓ) surface arrayed in one direction. We will report on the results we obtained when we used $\text{YBa}_2\text{Cu}_3\text{O}_y$ material powder prepared on the basis of the usual solid phase reaction, inserted this powder in a mold made of metal, and after a short period of heating, we immediately obtained an orientative sintered material by providing an unconfined compressive deformation.

Experiment and Results

$\text{YBa}_2\text{Cu}_3\text{O}_y$ powder of the orthorhombic phase synthesized by a solid phase reaction was sealed in a stainless (SUS 304) cylinder with an outer diameter of 22 mm, an inner diameter of 10 mm and a length of 30 mm. After being inserted into an electric heater maintained at 950°C and preheated for about 8 minutes, it was promptly taken out of the electric furnace and compression deformed by a press in a uniaxial direction. The deforming speed was 5 mm/sec and the rate of deformation ((mold height before deformation - height after deformation)/height before deformation) was about 30 percent. After taking the sintered material out of the mold after deformation, the orientation degree of the sintered material particles was examined by X-ray analysis of the sintered material abrasion surfaces vertical and parallel to the compression axis together with observing the structure by SEM. The starting substance of the material was of an orthorhombic single phase, whereas the presence of a tetragonal phase was recognized in the sintered

material after compression treatment. Figure 1 provides an example of the X-ray analysis result when the sintered material was processed by heat treatment in air at 950°C for 2 hours, and then at 550°C for 10 hours, and then made into an almost perfect orthorhombic single phase for computing the orientation degree more quantitatively. An X-ray diffraction diagram shows that the (00 ℓ) reflection becomes strong and the particle orientation has progressed from the sintered material surface that is vertical to the compression axis. These X-ray analysis results were rearranged by the Lotgering method¹ and the method used by Yanagida et al.² However, both methods proved to be inconvenient, so finally, it was ascertained that a stable evaluation could be made of the orientation degree of YBa₂Cu₃O_y sintered material when the results were rearranged on the basis of a (113) reflection in which the diffraction strength did not change much as a result of the orientation.

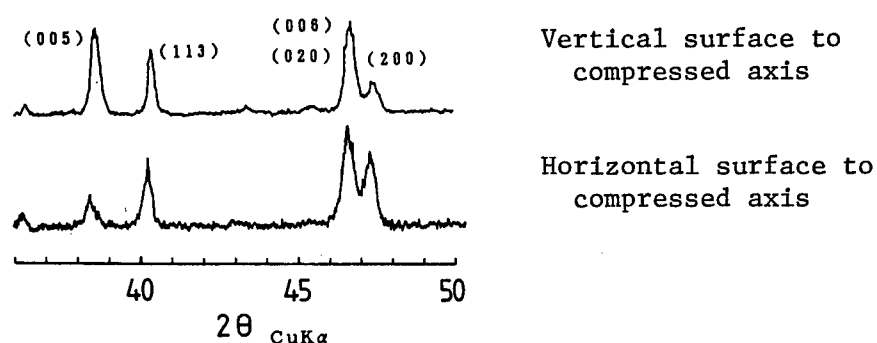


Figure 1. X-ray diffraction diagram of orientative YBa₂Cu₃O_y sintered material

References

1. F.K. Logtering, J. Inorg. Necl. Chem., 9, 113, 1959.
2. Chuta Cho, Kunihiro Kawamoto and Hiroaki Yanagida, Ceramics Industry Association, 90, 710, 1980.

Synthesis of Superconducting Oxides Under High-Pressure Oxygen

43067591 Tokyo NIHON FUNMATSU FUNTAI YAKIN KYOKAI in Japanese 16-19 May 88
p 36

[Report by Yasuo Takeda, Ryoji Kanno, Tomomi Ishigaki and Osamu Yamamoto, Faculty of Technology, Mie University; and Mikio Takano, Hiromasa Mazaki, Zenji Hiroi and Toshichika Bando, Institute for Chemical Research, Kyoto University: "Synthesis of Superconducting Oxides Under High-Pressure Oxygen"]

[Text] 1. High-temperature superconducting oxides are compounds that have a multifarious nonstoichiometry on oxygen and contain copper in which the valency number changes. The formal trivalent content of copper changes according to the oxygen partial pressure, and the superconducting characteristics change as a result. We wanted to ascertain what sort of properties would be exhibited by a sample synthesized under high oxygen pressure (more than 1 atmospheric pressure).

2. The value of y in $\text{YBa}_2\text{Cu}_3\text{O}_y$ did not become more than 6.9, which was obtained by treating it in oxygen flow at a temperature of $200^\circ\text{--}700^\circ\text{C}$ up to $\text{Po}_2 = 600$ atmospheres. Moreover, there were no changes on the structure, and the transition point did not change.

3. When the position of Cu was replaced by Fe and Co, changes were observed in the structure and also in the system, and the superconducting transition point was lowered. The occlusion of oxygen content was seen and the lowering of the transition point could be checked when synthesis was achieved under oxygen pressure. The explanation for this will be given another time.

4. A remarkable oxygen pressure dependency was seen in $\text{YBaSrCu}_3\text{O}_y$ in which half of the Ba was replaced with Sr. Similar to $\text{YBa}_2\text{Cu}_3\text{O}_y$, it is tetragonal at a high temperature (more than 700°C) in oxygen flow of 1 atmospheric pressure and it is orthorhombic ($a = 3.792$, $b = 3.852$ and $c = 11.556\text{\AA}$ at 400°C) at a low temperature in the same oxygen flow. However, when this orthorhombic $\text{YBaSrCu}_3\text{O}_y$ ($y = 6.85$) is treated under $\text{Po}_2 = 100\text{--}600$ atm at 300°C , it exhibits an X-ray pattern that again has a tetragonal index, as shown in Figure 1. The value of y also exceeds 7. The oxygen content and lattice constant changes are shown in Figure 2. The superconducting transition point, as in the orthorhombic structure, was 80-83K. It is interesting

to learn in what form the increased oxygen exists. Although it can be considered that the tetragonal structure in the range with a high oxygen content was due to the irregular array of Cu site oxygen deficiency, a complicated micro-domain structure was observed under electron microscope, and further studies are necessary.

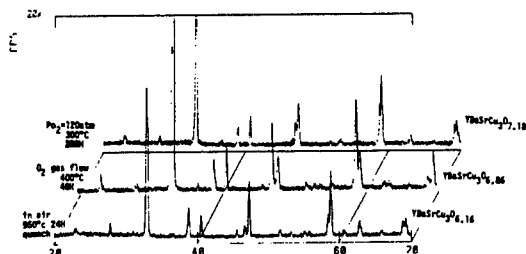


Figure 1. X-ray diffraction diagram of YBaSrCu₃O_y

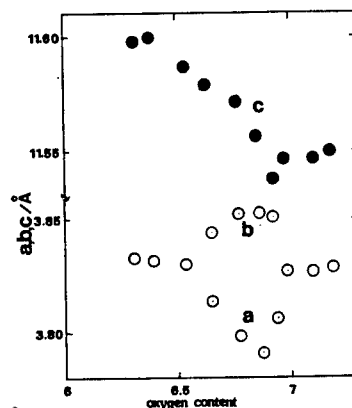


Figure 2. Oxygen content and lattice constant of YBaSrCu₃O_y

5. Synthesis under oxygen pressure was also performed on Bi system superconductors such as Bi₂Sr₂CaCu₂O_y, Bi₂Sr₂Ca₂Cu₃O_y, etc. Decomposition occurred at high temperature (more than 500°C), but no great change has been ascertained as yet under treatment of less than 500°C.

Superconductivity of Hot-Pressed $\text{YBa}_2\text{Cu}_3\text{O}_x$ Ceramics

43067591 Tokyo NIHON FUNMATSU FUNTAI YAKIN KYOKAI in Japanese 16-19 May 88
p 37

[Report by Kunihiro Nagata, Takahiko Iwai and Kiyoshi Okazaki, National Defense Academy; and Tatsuya Kiyota, Tamura Seisakusho Co., Ltd.: "Superconducting Characteristics and Oxygen Diffusion of Hot-Pressed $\text{YBa}_2\text{Cu}_3\text{O}_x$ Ceramics"]

[Text] 1. Introduction

$\text{YBa}_2\text{Cu}_3\text{O}_x$ superconducting ceramics do not exhibit superconductivity at about 90K when made finer by the ordinary hot pressing (HP) method. However, samples that have added an oxide such as Ag_2O and that undergo HP in oxygen of 1.5-2 atmospheric pressures become superconductors at 93K. This difference may be due to the differing crystal structure resulting from the intake content of oxygen. In this research, we studied the superconducting characteristics of ceramics prepared both by the HP method and by the atmospheric sintering method, as well as the diffusion effect of oxygen.

2. Sample Preparation Method

More than 99.9 percent of the Y_2O_3 , BaCO_3 and CuO powders used were made by the Furuuchi Chemical Co., Ltd. These powders were compounded in a composition of $\text{YBa}_2\text{Cu}_3\text{O}_{6.5}$ and mixed for 30 minutes by an electrically driven mixing machine. After preliminary sintering at 900°C in air for 20 hours, an oxide such as Ag_2O were mixed in, and the mixture was pulverized by a ball mill for 16 hours. Then a binder was added and the mixture was press molded into a disk shape 20 mm in diameter and 4-10 mm thick under pressure of 1 ton/cm^2 . The molded sample, after atmospheric sintering in air and HP processing in air, was subjected to annealing in oxygen and HP processing in oxygen. The sintering conditions were $930^\circ\text{--}950^\circ\text{C}$ for 10-20 hours under pressure of 200 kg/cm^2 . The temperature rise and cooling rates were 100°C/h . The density of the sample was $5.50\text{--}5.55 \text{ g/cm}^3$ in atmospheric sintered materials and $6.10\text{--}6.15 \text{ g/cm}^3$ for samples processed by HP in air and in oxygen.

3. Experiment Results and Considerations

The resistivity-temperature characteristics of samples sintered by various methods are shown in Figure 1. The nonaddition ordinary sintered and the Ag_2O addition oxygen atmosphere HP samples exhibited superconductivity at 92K, and the resistivity of the nonaddition HP samples in air dropped suddenly in the neighborhood of about 95K, but it did not become zero even at a temperature of 77K. Also, the resistivity of the sample that had been subjected to annealing at 930°C for 20 hours in oxygen atmosphere dropped considerably more than that of the sample before annealing, but it did not become zero at 77K. In checking the X-ray diffraction of these samples, it was found that the ordinary-sintered and HP samples in oxygen that became superconductors were of the orthorhombic system, and the HP samples in air that did not become superconductors were of the tetragonal system.

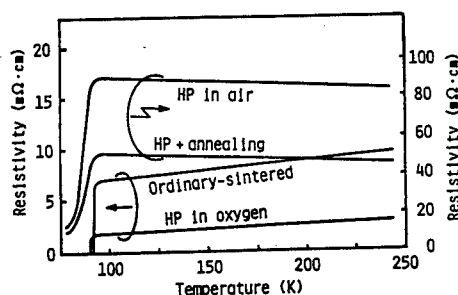


Figure 1. Resistivity temperature characteristic of various samples

The oxygen emission and absorption characteristics of various samples were measured by TGA. TGA was measured at 10°C/min for both the temperature rise and temperature drop in air. Figure 2 shows the TGA characteristics of (A) an ordinary-sintered example, (B) an annealed sample after HP in air and (C) an HP in oxygen Ag_2O added sample in solid and powdered conditions. The weight reduction at temperature rise from room temperature up to 800°C was about 1.2 percent for both solid and powdered conditions in the case of ordinary-sintered samples. Moreover, there was the same amount of weight increase at temperature drop and the emitted oxygen was absorbed by about the same content at temperature drop.

The weight reduction in the solid was only about 0.5 percent in the case of the HP in air sample, but it was about 0.8 percent in the powdered condition--about 1.6 times that of the solid condition sample. Moreover, while the temperature was dropping, both solid and powdered samples regained the weight back to where they were before the weight loss. In other words, the entry and exit of oxygen were promptly attained into the sample interior in ordinary-sintered samples but about only 40 percent of the oxygen that can enter into the ordinary-sintered samples could enter and exit in the solid condition HP samples and it was found that oxygen of only about 75 percent could enter and exit even when made into a coarse powder condition. On the other hand, the hot-pressed sample in oxygen atmosphere showed a weight

reduction of about 0.8 percent at temperature rise, but it only absorbed oxygen of about 0.5 percent at temperature drop, and it did not return to its weight before the temperature rise. This is considered to mean that the oxygen taken in during HP can be emitted at temperature rise (at high temperature), but oxygen cannot be absorbed sufficiently in the oxygen atmosphere at the rate of temperature drop in the TGA measurement.

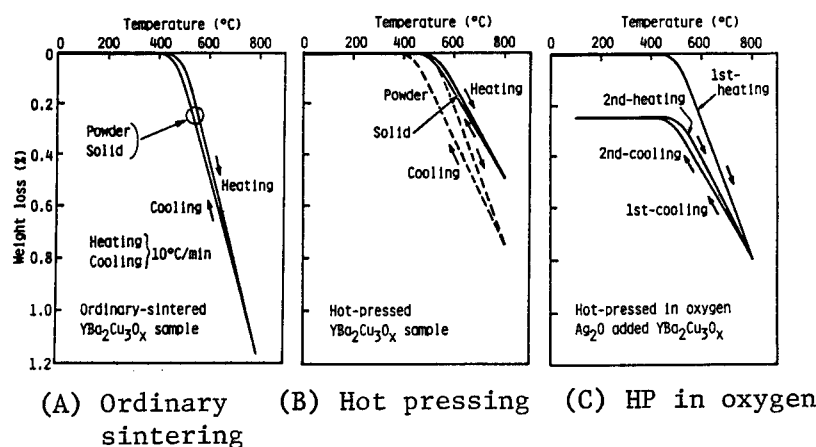


Figure 2. TGA characteristics of various samples

Based on the above results, suppose the oxygen content (x) of the pressure-less sintered specimen equals 6.9 by using the $\text{YBa}_2\text{Cu}_3\text{O}_x$ formula, then the oxygen content (x) of the nonaddition atmospheric HP specimen must equal 6.68. Therefore, we conclude that the atmospheric HP sample did not become a superconductor even at 77K.

Sintering Process of $\text{YBa}_2\text{Cu}_3\text{O}_x$ by Oxalate Method

43067591 Tokyo NIHON FUNMATSU FUNTAI YAKIN KYOKAI in Japanese 16-19 May 88
p 38

[Report by Teruyoshi Unesaki and Yoichi Tomii, Faculty of Technology, Kyoto University; Hitoshi Kitaguchi, Jun Takada and Yoshinari Muira, Faculty of Technology, Okayama University; Nooichi Yamamoto and Yoshio Oka, Faculty of Liberal Arts, Kyoto University; and Yasunori Ikeda, Mikio Takano and Yoshichika Bando, Institute of Chemical Research, Kyoto University:
"Observation of Changes Due to Sintering of $\text{YBa}_2\text{Cu}_3\text{O}_x$ by Oxalate Method"]

[Text] Introduction

Sintering of $\text{YBa}_2\text{Cu}_3\text{O}_x$ oxide high-temperature superconductors (YBCO) is an important process for producing a remarkable effect on the superconducting characteristics of this material. We observed in detail the surface change in the sintering process of YBCO using a scanning electron microscope (SEM), and we will explain systematically the configuration of the various changes we found.

Experiment

Sample adjustments were made by the oxalate method. After predrying of the compound obtained by this method, it was pulverized after temporary sintering at 500°C in air, press molded into $10\text{mm}\phi \times 1.5\text{t}$ pellets, and these pellets were made the starting material. The pellets were sintered mainly at 920°C in air, taken out of the furnace after a fixed period, and after being cooled down in air, they were immediately subjected to SEM observation; then, the sintering process was promptly repeated after the SEM observation. Measures were taken so that another SEM observation could be made with the same field of view of the same sample, and in elucidating the sintering process special attention was given to the microscopic configuration and system changes.

Experiment Results and Considerations

The powders after preliminary sintering by the oxalate method were extremely fine particles of less than the μm size seen in the SEM observation. After sintering in air for some 2-3 minutes at 920°C , the surface of the pellets

began to change, and in 10 minutes a superconducting phase in which $\text{Ya}:\text{Ba}:\text{Cu}$ was 1:2:3 (hereinafter called 123) appeared, with an average particle diameter of 0.6-1 μm and an extremely smooth surface. No conspicuous fluctuation (segregation) of the microstructure was observed under energy dispersion X-ray (EDX) in this case. The growth of the 123 phase was observed from the period of 10 minutes up to about 48 hours; a characteristic 123 phase with a rectangular tie shape 5-15 μm long and 2-4 μm wide was observed. However, it has been observed that in about 10 to 25 hours the BCO compound containing little Y appeared (Figure 1) [photo not reproduced] the 123 phase grain boundary and later disappeared when it was kept at high temperature. When the sample, on which sintering was considered as almost completed, was sintered again after being retained in air for 12-48 hours at room temperature, the configurational change of the neighboring 123 phase was not apparent, and oxidized compound crystals of Ba and Cu appeared on the surface, as shown in Figure 2 [photo not reproduced]. The sintering process used for YBCO, as seen here, characteristically differs considerably from the conventional sintering process used for single materials. The explanation of the sintering process given here takes into consideration the phase diagram.

Effect of Lengthy Sintering of $\text{YBa}_2\text{Cu}_3\text{O}_y$ on Superconducting Characteristics

43067591 Tokyo NIHON FUNMATSU FUNTAI YAKIN KYOKAI in Japanese 16-19 May 88
p 39

[Report by Kazuhiko Majima, Masaru Yokoyama and Hiroshi Nagai, Faculty of Technology, Osaka University; Ken Obayashi, graduate student, Osaka University; and Toshikatsu Kashiwaya, student at Osaka University: "Effect of Lengthy Sintering of $\text{YBa}_2\text{Cu}_3\text{O}_y$ on Superconducting Characteristics"]

[Text] I. Objective

Lengthy sintering of $\text{YBa}_2\text{Cu}_3\text{O}_y$ was conducted in this experiment, and studies were made of the change in structure resulting from the difference in sintering temperature and of the relationship of this change with the superconducting characteristics.

II. Experiment Method

The BaCO_3 , Y_2O_3 and CuO powders used in this experiment were precisely the same as those used in the experiment described in a previous report. Alcohol was added to these material powders, and after being pulverized, mixed and dried sufficiently, the powders were reacted by heating at 1173K in air for 86.4 ks, pulverized again and subjected to compression molding. In the compression molding, dies measuring 6 x 20 mm were filled with the powders and molding was performed at a compressive pressure of 98 MPa. A 2 x 6 x 20 mm green compact was prepared for T_c measurement, and 5 x 6 x 20 mm green compacts were prepared for measurement of sintering density and structural observation. Sintering was conducted at 1173-1223K for 86.4-1036.8 ks using these green compacts, and the density measurement of the obtained sintered material was in conformity with the method stipulated in JIS Z 2505. A JAS-733 type X-ray microanalyzer made by Nippon Denshi Co., Ltd. and an X-650 type scanning electron microscope made by Hitachi, Ltd. were used for surface and structural observation of the sintered materials, and an XD-5A X-ray diffraction device made by Shimadzu Corp. was used for the X-ray analysis.

III. Results

The temperature dependency of electrical resistivity for samples that were sintered at temperatures of 1173K and 1223K for 759.6 ks is shown in Figure 1. The T_{on} was about 92K for both samples, almost the same as that in case of sintering for 86.4 ks previously mentioned. The T_{off} became 83.3K in the case of 1223K sintering, in contrast to 90.5K in the case of 1173K sintering, and it was found that the superconductivity had deteriorated greatly.

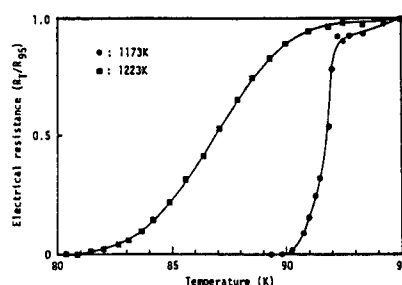


Figure 1. Resistivity vs. temperature curves for $YBa_2Cu_3O_y$ sample sintered at various temperatures for 759.6 ks

The surface structure of the sample sintered at 1223K for 759.6 ks is shown in Figure 2 [photo not reproduced]. It is clear from photo (a) of Figure 2 that a fusion liquid has been generated along the intergranular. It is confirmed that the liquid phase part has a layer structure, as is clear from photo (b), which is an enlargement of photo (a).

Pore Structure Effect on Superconducting $\text{YBa}_2\text{Cu}_3\text{O}_x$ Ceramics

43067591 Tokyo NIHON FUNMATSU FUNTAI YAKIN KYOKAI in Japanese 16-19 May 88
p 40

[Report by Kunihiro Nagata, Takahiko Iwai and Kiyoshi Okazaki, National Defense Agency: "Various Characteristics and Pore Structure of Superconducting $\text{YBa}_2\text{Cu}_3\text{O}_x$ Ceramics"]

[Text] 1. Introduction

When Y-Ba-Cu-O system superconducting ceramics absorb oxygen in the cooling process after sintering, the crystal structure changes from the tetragonal system to the orthorhombic system. When oxygen is not able to disperse into the sample interior in this way, the internal crystal structure remains in the tetragonal system. An orthorhombic system crystal with a small oxygen deficiency becomes a superconductor at about 95K, but a crystal of either the tetragonal or the orthorhombic system with a large oxygen deficiency becomes a superconductor only at a temperature of less than 70K. Therefore, it has been considered necessary to use a porous sample in which the oxygen is easily diffused in order to obtain a superconductor at liquid nitrogen temperature. In this research, we used $\text{YBa}_2\text{Cu}_3\text{O}_x$ ceramics in which the density was controlled by selecting the preliminary sintering condition, the pulverizing condition and the sintering condition, and we studied the relationship between the superconducting characteristics and the amount and size of pores.

2. Preparation Method of Sample

First of all, the Y_2O_3 , BaCO_3 and CuO powders used, of which more than 99.9 percent were made by the Furuuchi Chemical Co., Ltd., were prepared in the composition $\text{YBa}_2\text{Cu}_3\text{O}_{6.5}$, and they were mixed for 30 minutes by an electrically driven mixing machine. This mixture underwent preliminary sintering under the following conditions. After preliminary sintering at (A) 900°C for 20 hours, (B) 920°C for 60 hours and (C) 940°C for 60 hours, the mixture was pulverized by (a) an electrically driven mixing machine for 30 minutes and (b) a ball mill for 16 minutes. Then, a binder was added and press molding into a disk-shaped sample 20 mm in diameter and 4 mm thick was carried out at a pressure of 1 ton/cm^2 . The sintering condition was 900°C - 1000°C for a period of 10-60 hours. The rate of temperature rise and temperature drop was set at 100°C/h .

3. Experiment Results and Considerations

Figure 1 shows the resistivity-temperature characteristic of samples in which the powders underwent preliminary sintering at various temperatures (B, C) using pulverizing methods (a, b) and then were sintered at 950°C for 20 hours. The density in this case changed in the range of 5.28–6.04 g/cm². In samples (S-Ca and S-Ba) with a density of 5.28–5.63 g/cm², the resistivity was reduced as the density increased, and the critical temperature was fixed at 90–91K. However, in samples (S-Bb and S-Cb) with a density of more than 5.89 g/cm², the resistivity increased as the density increased and the critical temperature was low, 85–89K. The critical temperature and 300K resistivity of representative samples with different density are shown in Table 1. The critical temperature of samples with a density of more than 6.00 shifted to the low temperature side.

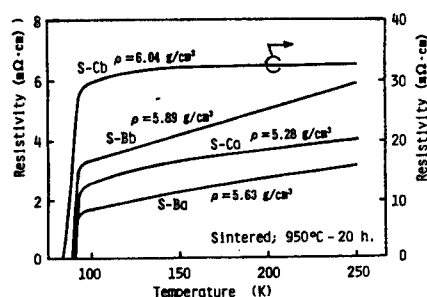


Figure 1. Resistivity temperature characteristics of various samples

Table 1. Density and Superconducting Characteristics of Various Samples

Density g/cm ³	Sintering °C	Presintering °C	Pulverization	T _c K	ρ _{300K} mΩ·cm
4.80	910	920	Mixing	91	22
5.15	910	900	Mill	91	10
5.21	930	940	Mill	90	6
* 5.28	950	940	Mixing	91	5
5.39	930	940	Mixing	91	3
* 5.63	950	920	Mixing	90	3
5.77	930	920	Mixing	91	4
* 5.89	950	920	Mill	89	7
5.98	950	940	Mill	86	32
* 6.04	950	940	Mill	85	33
6.07	980	940	Mill	86	21
6.17	1000	940	Mill	87	19

The pore distribution of representative samples is shown in Figure 2. The pore structure was measured using the "pore sizer type 9310" porosimeter made by Shimadzu Corp. The pores measured in this case were very nearly cylindrical in shape. The samples used were powders produced by different

preliminary sintering temperatures and pulverizing methods that were sintered at 950°C for 20 hours. With the high preliminary sintering temperature of 940°C, the pore diameter of most of the specimen (S-Ca), which was pulverized in the mixing machine, was about 5 μm and the pore rate was great, about 0.03 cc/g. At the same preliminary sintering temperature, the pore diameter of most of the specimen (S-Cb), which was powdered in the ball mill, was about 0.05 μm and the pore rate was extremely low, about 0.004 cc/g. On the other hand, when the preliminary sintering temperature was low, 920°C, the mixing machine pulverized sample (S-Ba) in comparison had pores of large size in comparison with that of the ball mill pulverized sample (S-Bb), and the pore rate was also higher. From the results shown in Figures 1 and 2, it was ascertained that the smaller the pore ratio, the lower the resistivity. However, it was also found that resistivity became very high when the pore rate became very low, a temperature characteristic similar to that of a semiconductor was exhibited, and the critical temperature tended to drop.

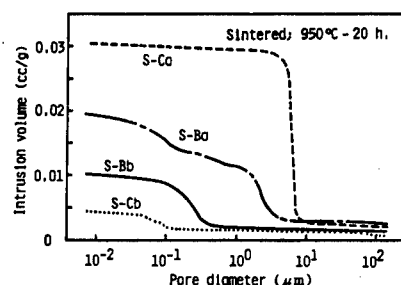


Figure 2. Pore distribution of various samples

The current density characteristic of these samples is shown in Figure 3. The critical current density has no correlation with the amount of density, but it does have a correlation with the resistivity-temperature characteristic shown in Figure 1. In other words, it was found that the lower the resistivity of samples before reaching superconducting state together with the fewer pores in the samples, the greater the critical current density.

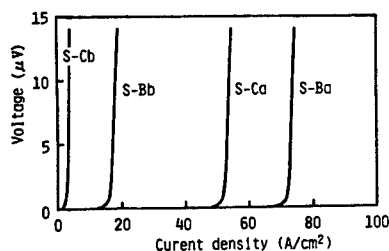


Figure 3. Current density characteristics of various samples

Superconducting Ceramics Reaction, Atmospheric Gas

43067591 Tokyo NIHON FUNMATSU FUNTAI YAKIN KYOKAI in Japanese 16-19 May 88
p 41

[Report by Masahiro Yoshimura, Seiji Inoue and Shigeyuki Somiya, Industrial Materials Laboratory, Tokyo Institute of Technology; and Yasuro Ikuma, Kanagawa Institute of Technology]

[Text] Elution of Ba^{2+} occurs when $YBa_2Cu_3O_{7-x}$ contacts water in a liquid state and decomposes into $Y(OH)_3$ and CuO . In this case, $BaCO_3$ precipitates and deposits when CO_2 exists in the atmosphere. At above $90^\circ C$, $Ba_2Cu(OH)_6$ was also formed. Since the droplet undergoes condensation when the steam partial pressure in the atmosphere, though lower than the saturated steam pressure of water, is higher than the steam pressure of $Ba(OH)_2$ aqueous solution, a similar decomposition occurs. On the other hand, the reaction between the $YBa_2Cu_3O_{7-x}$ and water in a gaseous state (steam) has not been made clear as yet. It has also been reported that $YBa_2Cu_3O_{7-x}$ absorbs gases such as F_2 , H_2 , N_2 and He as well as O_2 . Therefore, in our research, $YBa_2Cu_3O_{7-x}$ was treated in fleon gas (CF_4), H_2O and H_2 gas, and studies were conducted on the reaction with the atmospheric gas. Y_2O_3 , $Ba(NO_3)_2$ and CuO were used for the starting materials, and they were synthesized by the ordinary solid phase method.

1. Fleon Gas (CF_4) Treatment

The temperature of $YBa_2Cu_3O_{7-x}$ was raised in fleon gas from room temperature up to a prescribed temperature ($350^\circ-800^\circ C$) and maintained in this condition for 1 hour. Then, it was slowly cooled down to $400^\circ C$ after changing over to a dry oxygen flow, annealed at that temperature for 1 hour, and then it was slowly cooled down continuously to $100^\circ C$. The oxygen treatment at $400^\circ C$ was omitted when the fleon treatment was less than $400^\circ C$. The T_c rose by about 2K under $350^\circ-400^\circ C$ treatment. However, when left in air for a day, it returned to the same level as an untreated sample.

2. H_2 , H_2O Gas Treatment

After treating 0.124 g of the $YBa_2Cu_3O_{7-x}$ powder in O_2 that had been dehydrated with liquid nitrogen, it was further treated in H_2 , in H_2 and H_2O at room temperature and at $142^\circ C$, and the weight changes were measured.

(1) Weight changes were not observed in the treatment conducted in H_2 at 50–450 Torr and at temperatures from room temperature to $200^\circ C$. But a severe weight reduction was observed at a temperature of more than $300^\circ C$.

(2) A weight increase was observed at room temperature in the H_2 (12.4 Torr) atmosphere, as shown in Figure 1. Although a weight reduction due to buoyancy and elimination of absorbed water was observed when the temperature was raised to $142^\circ C$, the weight soon increased again. Moreover, the weight also increased at room temperature in H_2O (10.0 Torr) + H_2 (82.7 Torr).

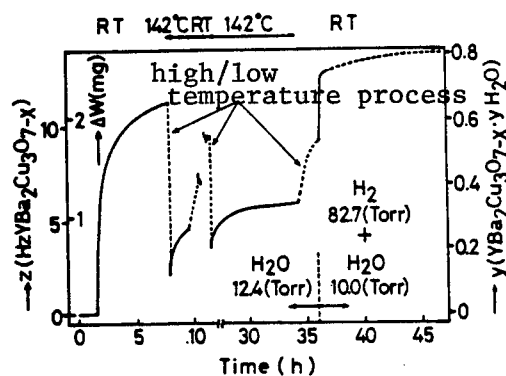


Figure 1. Weight change under H_2 and H_2O treatment of $YBa_2Cu_3O_{7-x}$

Although it has been reported that $YBa_2Cu_3O_{7-x}$ absorbs hydrogen², it can be judged from the results obtained here that water plays an important role, even when reacting with hydrogen. However, on the basis of samples, there have also been cases where almost no water was absorbed. Studies are also under way on the Bi system.

References

1. Masahiro Yoshimura, et al., Phys. Rev., 34, 659–62, 1987.
2. J.J. Reilly, et al., Phys. Rev. B36, 5694–7, 1987.

Electron Microscope Observation of $\text{Ba}_2\text{YCu}_3\text{O}_{7-\delta}$

43067591 Tokyo NIHON FUNMATSU FUNTAI YAKIN KYOKAI in Japanese 16-19 May 88
p 42

[Report by Zenji Hiroi, Mikio Takano, Yasunori Ikeda and Yoshichika Bando, Institute for Chemical Research, Kyoto University; and Ryoji Kanno and Yasuo Takeda, Mie University]

[Text] In a previous presentation, we reported that X-ray observation showed that an intergrowth structure of the tetragonal and orthorhombic systems existed in a sample having an oxygen content of δ 0.1 and an orthorhombic system. The orthorhombic twin structure generally seen was dominant in the sample as a whole, but it is thought that the presence of a tetragonal range cannot be discounted. We believe, based on the results of electron microscope observation and the oxygen array on a Cu (I) surface, that the orthorhombic single phase range is narrow and that a two-phase coexistence with the tetragonal system would be more thermodynamically stable. Moreover, the change from tetragonal to orthorhombic at high temperature is not only an order-disorder transition of the Cu (I) surface oxygen, but it is thought that it is a spinodal decomposing type two-phase separation caused by the fluctuation of oxygen concentration. The process that we have proposed in a simple model based on oxygen order can be explained as follows. As a result of the introduction of oxygen from outside due to a temperature drop and rearray of the internal oxygen accompanying this introduction, the core forming occurs in an orthorhombic range that has a one-dimensional chain order and extends in the (110) direction. The crystal adopts a structure wherein the tetragonal and orthorhombic bands appear alternately, as shown in Figure 1 [photo not reproduced], as a result of the growth of this core. The tetragonal range is reduced with the increase in oxygen content, and changes occur continuously in the lattice constant and the occupying rate of oxygen on the a and b axes. In actually computing the X-ray analysis pattern, if the width of each band is sufficiently small, only a set of peaks appear even when the tetragonal and orthorhombic ranges with respectively fixed different lattice constants coexist. Moreover, the position changes on the basis of the ratio of the tetragonal and orthorhombic band widths, and when the orthorhombic increases, it appears that the entire crystal has gradually changed from tetragonal to orthorhombic. This can be explained by considering that in the two-phase range, the T_c and ball concentrations were not dependent on the oxygen content and did not change in

the range of $0 < \delta \leq 0.2$. In other words, even if the entire oxygen content is changed, the oxygen content in the orthorhombic is always fixed, only the ratio of tetragonal and orthorhombic changes, or the oxygen content in the tetragonal is reduced, and so, it seems to have had no effect on the superconductivity that should occur in the orthorhombic range.

Electrical Resistance, Thermoelectromotive Force in High Temperature of $\text{YBa}_2\text{Cu}_3\text{O}_y$

43067591 Tokyo NIHON FUNMATSU FUNTAI YAKIN KYOKAI in Japanese 16-19 May 88
p 43

[Report by Hiroshi Nagai, Masaru Yokota and Kazuhiko Majima, Faculty of Technology, Osaka University; and Ken Obayashi, graduate student of Osaka University: "Electrical Resistance and Thermoelectromotive Force of $\text{YBa}_2\text{Cu}_3\text{O}_y$ at High Temperature"]

[Text] 1. Objective

It has become clear that the superconducting characteristics of the oxide superconducting material $\text{YBa}_2\text{Cu}_3\text{O}_y$ is affected considerably by the manufacturing conditions, i.e., the heat treatment conditions and atmosphere. However, there are still many unclear points in regard to the phase equilibrium at high temperature that is the basis for these manufacturing conditions. In a previous report, we discussed the possibility of detecting the phase transformation of $\text{YBa}_2\text{Cu}_3\text{O}_y$ at high temperature by electric conductivity measurement¹. In this research, we have continuously studied the effect the addition of Fe exerted on the high-temperature phase equilibrium of $\text{YBa}_2\text{Cu}_3\text{O}_y$ under various oxygen partial pressures.

2. Experiment Method

The materials Y_2O_3 , BaCO_3 , CuO and Fe_2O_3 were used in the sample; blending was accomplished in the proportion $\text{YBa}_2\text{Cu}_3\text{O}_y$ and $\text{YBa}_2(\text{Cu}_{1-x}\text{Fe}_x)_3\text{O}_y$; preliminary sintering was carried out at 900°C for 24 hours, and after being pulverized and sintered (900°C for 24 hours), the sample was cooled in the furnace to room temperature. Using a sample prepared in this way as the starting sample, the high-temperature phase equilibrium under various oxygen partial pressures was studied by electric conductivity measurement, thermoelectromotive force measurement, thermobalance and X-ray diffraction. The atmosphere was oxygen air and Ar/O_2 mixed gas, and the control and measurement of the oxygen partial pressure were conducted using a ZrO_2 solid electrolyte. The electric conductivity at high temperature was obtained by measuring the electromotive force generated at both ends of the sample, which was about 10 mm long, after applying a thermoelectromotive force of about $1\text{K}/\text{mm}$ temperature gradient by the DC four-terminal method. The phase

identification at high temperature was conducted by an X-ray diffractometer on a sample sintered in liquid nitrogen after being maintained at various temperatures for 4-20 hours.

3. Results and Considerations

- (1) The electrical resistance of $\text{YBa}_2(\text{Cu}_{1-x}\text{Fe}_x)_3\text{O}_y$, as in the case of $\text{YBa}_2\text{Cu}_3\text{O}_y$, showed an increasing temperature dependency with the rise in temperature. However, the refraction point accompanying the ortho-tetra transformation became unclear with the increase of X.
- (2) The thermoelectromotive force at high temperature has a negative value in all cases, and the temperature dependency showed a trend resembling very closely that of the electrical resistance.
- (3) The phase transformation temperature of $\text{YBa}_2(\text{Cu}_{1-x}\text{Fe}_x)_3\text{O}_y$ dropped with the increase of X, and it became tetragonal at room temperature when $X = 0.03$.²

References

1. Hiroshi Nagai, et al., Powder and Powder Metallurgy, 34, 607, 1987.
2. Y. Maeno, M. Kato, Y. Aoki, T. Fujita, J.J.A.P. 26 (1987), L. 1982.

Critical Current Density of $\text{GdBa}_2\text{Cu}_3\text{O}_{7-\delta}$ Ceramics

43067591 Tokyo NIHON FUNMATSU FUNTAI YAKIN KYOKAI in Japanese 16-19 May 88 p 44

[Report by Motohide Matsuda, Akira Kikuchi, Yutaka Iwai, Masasuke Takata and Tsutomu Yamashita, Nagoya Institute of Technology; and Mamoru Ishii, Nihon Cement Co., Ltd.]

[Text] 1. Introduction

Expectations are harbored in many fields for putting to practical use high-temperature superconducting ceramics having a superconducting critical temperature of more than 90K. Whereas the critical current density (J_c) required for putting these to practical use is 10^4 - 10^6 A/cm², the present status is that for sintered materials the critical current density is low, about 10 - 10^3 A/cm².

This report will describe the studies conducted on the effect of the method of preparing $\text{GdBa}_2\text{Cu}_3\text{O}_{7-\delta}$ ceramics on J_c .

2. Experiment Method

Gd_2O_3 (purity 99.99 percent), BaCO_3 (purity 99.9 percent) and CuO (purity 99.9 percent) were used as the starting materials. These powders were weighed in the prescribed proportions and wet blended. Then, drying, preliminary sintering, pulverizing and forming into pellet shapes were carried out, and these pellets were subjected to sintering under prescribed sintering conditions. These processes were accomplished in air. Then, oxygen annealing was provided and the furnace cooling method was used. The structure of the samples was observed and evaluated by SEM, EPMA and X-ray diffraction. Measurement of the critical temperature and critical current density was made for the electrical characteristic by the four-terminal method. Au vacuum evaporation film was used for the electrode. Evaluation of magnetic susceptibility was conducted for the magnetic characteristic using a vibration sample type magnetometer (VSM).

3. Experiment Results

Changes in T_c and J_c (values obtained by the four-terminal method) vis-a-vis the sintering conditions are shown in Figure 1. The critical temperature was

not so much affected by the sintering temperature and showed more than 90K. However, the critical current density was greatly dependent on the sintering temperature. A sample sintered at 900°C had an inferior sintering property and J_c was about 200 A/cm², but when the sintering temperature was 930°C, J_c was more than 300 A/cm². Moreover, the value of J_c was inversely reduced when the sintering temperature was raised to the neighborhood of 970°C. There were many Ba in the interface of this sample, and deposition of the second phase with few Gd were observed.

A magnetization characteristic of 77K in a sample prepared at a sintering temperature of 930°C is shown in Figure 2. A diamagnetism has clearly appeared, and it has been ascertained that a positive magnetization has appeared in the magnetic field of about 2.5 kOe.

At another time, we will discuss the correlation between the microstructure and the electrical and magnetic characteristics.

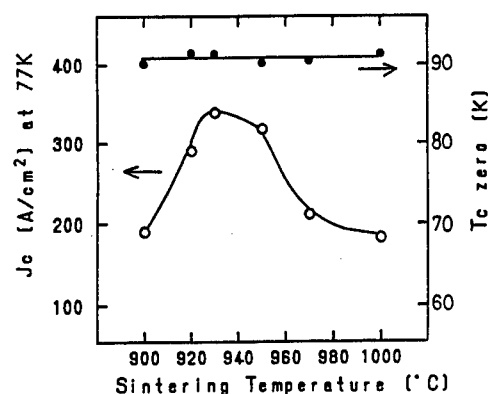


Figure 1. Relationship of sintering temperature and J_c

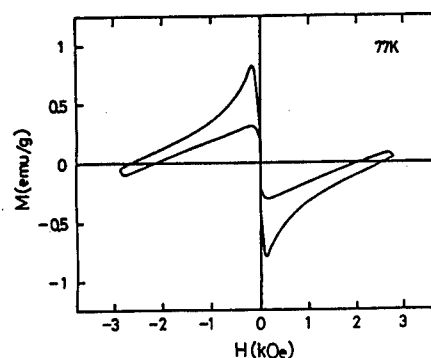


Figure 2. Magnetization characteristic of sample sintered at 930°C

Crystal Structure, Superconductivity Characteristics of $\text{YBa}_{2-x}\text{K}_x\text{Cu}_3\text{O}_{7-\delta}$ System

43067591 Tokyo NIHON FUNMATSU FUNTAI YAKIN KYOKAI in Japanese 16-19 May 88
p 45

[Report by Noboru Ichinose and Shunichi Miyazaki, Faculty of Materials Technology, Science and Engineering Department, Waseda University: "Crystal Structure and Superconducting Characteristics of $\text{YBa}_{2-x}\text{K}_x\text{Cu}_3\text{O}_{7-\delta}$ System"]

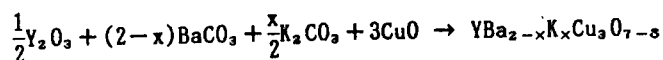
[Text] Objective

Attempts have been made to replace ions in the various sites of the $\text{YBa}_2\text{Cu}_3\text{O}_{7-\delta}$ system for the purpose of developing a high-temperature superconductor. For example, there have been reports on replacing the yttrium with rare earth elements (Sm, Eu, Gd, etc.), replacing the copper ion with bivalent ions (Fe^{2+} , Co^{2+} , Ni^{2+} , etc.) and trivalent ions (Fe^{3+} , Cr^{3+} , Al^{3+} , etc.), and replacing the oxygen ion with a fluorine ion.

In this report, we will describe the results of our studies on the crystal structure and superconducting characteristics of the $\text{YBa}_{2-x}\text{K}_x\text{Cu}_3\text{O}_{7-\delta}$ system, in which the bivalent Ba ion has been replaced by a univalent K ion for the purpose of increasing the essential Cu^{3+} for superconductivity.

Experiment Method

The $\text{YBa}_{2-x}\text{K}_x\text{Cu}_3\text{O}_{7-\delta}$ was prepared by the following process. Barium carbonate (BaCO_3), potassium carbonate (K_2CO_3), yttrium oxide (Y_2O_3) and cupric oxide (CuO) were mixed in a prescribed content according to the reaction formula



These materials were heated and subjected to reaction by an electric furnace.

Preliminary sintering was conducted at 900°C for 3 hours, and sintering was conducted in oxygen for several hours at a temperature of $930^\circ\text{--}970^\circ\text{C}$ in conformity with the composition. Identification of the sample was made by X-ray diffraction, and the temperature characteristic of the electrical resistance was measured by the ordinary four-terminal method.

Experiment Results and Considerations

Since the ion radius of the K^+ ion is close to that of Ba^{2+} , it is expected to melt in over a considerable range. Although our experiment was conducted only up to $x = 0.2$, it appears that it melted in sufficiently in this range, as determined by the X-ray diffraction pattern. Figure 1 shows a partial X-ray diffraction pattern of the orthorhombic systems (013), (103) and (110). The $YBa_2Cu_3O_{7-\delta}$ of $x = 0$, as has been reported, became partially decomposed at a temperature of more than 950°C and deposited Y_2BaCuO_5 . However, when the value of x was great, it did not decompose even at the high temperature of 970°C , and a stable orthorhombic system pattern was observed. In other words, the optimum sintering temperature was shifted to the high temperature side by the introduction of K. Changes of the a and b axes occur more frequently as a result of the introduction of K. Figure 2 shows the sintering temperature dependency of $T_{c\text{off}}$ in the $x = 0.20$ system, relative density (d/d_{th}) and electric resistance (R), indicating good characteristics on the high temperature side. Figure 3 shows T_c and R taken in the optimum sintering condition as the function of x , and T_c become slightly larger as a result of the introduction of K. It was also ascertained that the T_c change in a sample polished in the thickness direction was slight and the dependency in the thickness direction was small, as it was a comparatively fine sample (91.2 percent).

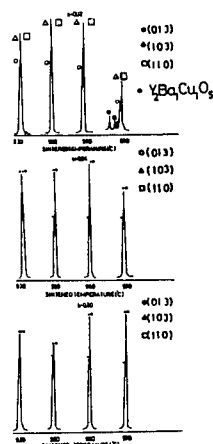


Figure 1. X-ray diffraction pattern of various compositions

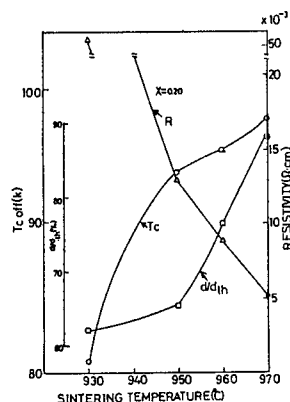


Figure 2. Sintering temperature dependency of T_c , d/d_{th} , R

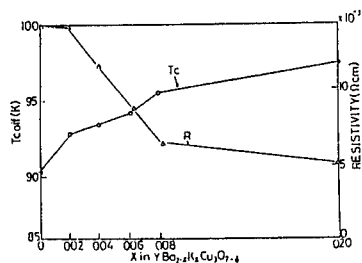


Figure 3. Composition dependency of T_c and R at the optimum sintering temperature

Copper Site Substitution, Oxygen Content of $\text{YBa}_2\text{Cu}_3\text{O}_{7-\delta}$

43067591 Tokyo NIHON FUNMATSU FUNTAI YAKIN KYOKAI in Japanese 16-19 May 88
p 46

[Report by Toshizo Fujita, Yuji Aoki, Terufumi Fujiwara and Yoshiteru Maeno, Faculty of Science, Hiroshima University: "Substitution of Copper Site and Oxygen Content of $\text{YBa}_2\text{Cu}_3\text{O}_{7-\delta}$ "]

[Text] Since there was not a great change in superconductivity even when a one-dimensional chain was disordered in a system in which the Cu of $\text{YBa}_2\text{Cu}_3\text{O}_{7-\delta}$ was replaced by a different kind of element, we previously concluded that the Cu2-O surface mainly contributed to superconductivity. However, the superconducting transition temperature T_c of $\text{YBa}_2(\text{Cu}_{1-x}\text{M}_x)_3\text{O}_{7-\delta}$ [M = Fe, Co] is sensitive to the conditions and process of heat treatment. It is believed that this may be because the way Fe is distributed in Cu sites (Cu 1 and Cu 2) may change, and the oxygen content $7-\delta$ may also change as a result of this distribution change. Measurements of thermogravimetry (TG), electrical resistance, magnetic susceptibility and X-ray diffraction were conducted on the various samples by sintering them at 920°C in air and annealing at 380°C for 33 hours.

It can be reasoned from the oxygen content measuring using TG (Pt crucible used) that about four units of oxygen are excessively coordinated in Fe although it is in a condition that the oxygen has practically escaped from the Cu surroundings in the Cu 1 surface. When estimating the distribution of Fe to the Cu 1 and Cu 2 sites based on this, a result resembling the trend value determined by the Mossbauer effect of ^{57}Fe was obtained. However, it was found later that the measurement result of the oxygen content by TG was dependent on the material used for the crucible, and therefore a problem still existed.

A curvature is observed in low oxygen concentration when the C-axis length change accompanying the temperature change and oxygen content change are plotted (Figure 1). The point of curvature, which is not dependent on the Fe concentration, occurs at about 810°C . It can be considered that this temperature indicates the start of elimination of oxygen other than that on the Cu 1 surface.

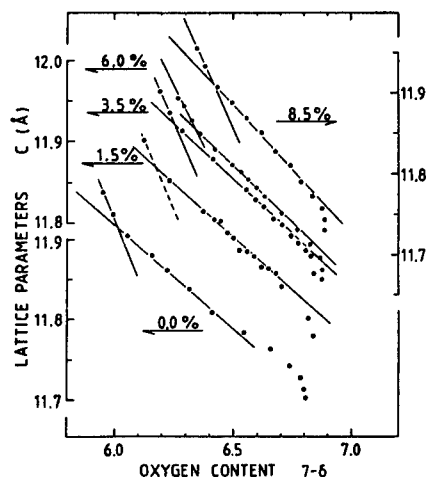


Figure 1. C-axis length change and oxygen content change accompanying temperature change

A crystal structure transition (orthorhombic \rightarrow tetragonal) is seen with the addition of Fe. From the thermodynamical point of view of Fe concentration dependency of this transition temperature (Figure 2), it is possible to explain through the average field model strain energy is taken into consideration. Moreover, a sample with different crystal structures (orthorhombic and tetragonal), despite the oxygen concentration being practically the same, can be obtained by providing a different heat treatment to a sample with the same Fe concentration. The coordination of the nonthermal equilibrium type oxygen, or the transfer of atoms between Cu 1 and Cu 2, can be considered as the cause.

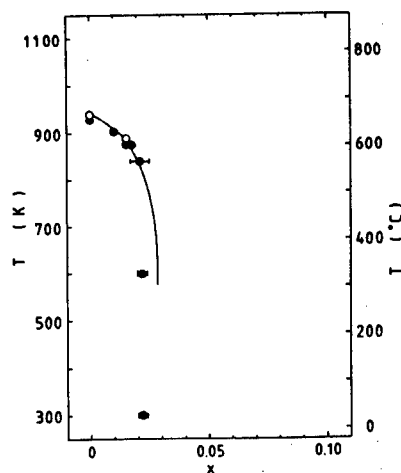


Figure 2. Fe concentration dependency of transient temperature

Electrical, Magnetic Properties of $\text{YBa}_2(\text{Cu}_{1-x}\text{M}_x)\text{O}_{7-y}$

43067591 Tokyo NIHON FUNMATSU FUNTAI YAKIN KYOKAI in Japanese 16-19 May 88
p 47

[Report by Tsukio Otani, Faculty of Science, Okayama Institute of Science:
"Electrical and Magnetic Properties of $\text{YBa}_2(\text{Cu}_{1-x}\text{M}_x)\text{O}_{7-y}$ (M = Fe, Co, Ni)"]

[Text] 1. Introduction

Many reports have been made on the effect exerted on the superconducting characteristics of $\text{YBa}_2\text{Cu}_3\text{O}_{7-y}$ (YBCO) by the addition of a third transition metal. But there are few reports on research into the physical property at high temperatures. In this report, we will describe the results of measuring the magnetization rate and electric resistance from room temperature up to 900°C .

2. Experiment

A sample was obtained by mixing Y_2O_3 , BaCO_3 and CuO with Fe_2O_3 , CoO , and NiO in a prescribed ratio, and after forming into pellets, the pellets were sintered at 930°C (repeated three times) and cooled down to room temperature. After identification by the powder X-ray diffraction method, the magnetization rate was measured by the Faraday magnetic balance and the electric resistance was measured by the DC four-terminal method using gold wire.

3. Results

Fe-doped samples were orthorhombic up to 3 percent. Those of more than 4 percent appeared to be tetragonal, but the pattern differed in accordance with the tetragonal of YBCO. An ordinary tetragonal pattern appeared when a sample was quenched from 900°C . (The lattice constant change vs. the Fe composition is shown in Figure 1.) The high temperature magnetization rate is shown in Figure 2. The magnetic moment increased with the increase of Fe, but an abnormality similar to that of YBCO was seen at a temperature of 550°C - 650°C . On this basis, the possibility is considered great that the low-temperature phase was orthorhombic even at more than 4 percent. Moreover, it was found that the transition point adopted the minimum value in a composition of Fe 3 percent. Figure 3 shows the high-temperature electric resistance of Fe 5 percent. Also, a transition well similar to that of YBCO

was observed. When Co was added, a behavior well was observed that was similar to that appearing with the addition of Fe. When Ni was added, an orthorhombic was maintained up to the addition of 10 percent, and an abnormality was observed at approximately the same high temperature as in YBCO.

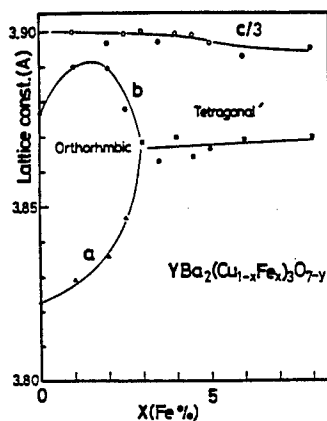


Figure 1. Lattice parameters vs. x in $\text{YBa}_2(\text{Cu}_{1-x}\text{Fe}_x)_3\text{O}_{7-y}$

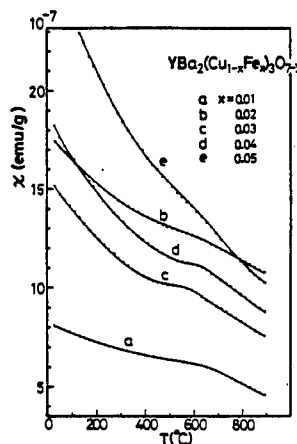


Figure 2. Temperature dependence of magnetic susceptibility of Fe-doped YBCO

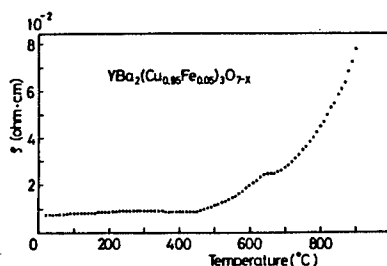


Figure 3. Temperature dependence of electrical resistivity of 5 percent Fe-doped YBCO

Cu-Fe Substitution Effect on Superconductivity

43067591 Tokyo NIHON FUNMATSU FUNTAI YAKIN KYOKAI in Japanese 16-19 May 88
p 48

[Report by Mikio Takano, Zenji Hiroi and Yoshichika Bando, Institute for Chemical Research, Kyoto University; and Yasuo Takeda and Ryoji Kanno, Faculty of Technology, Mie University: "Superconducting Characteristics of $\text{RBa}_2\text{Cu}_3(1-x)\text{Fe}_3\text{xO}_y$ "]

[Text] The superconducting characteristics and structural changes of samples in which the Cu site in the $\text{YBa}_2\text{Cu}_3\text{O}_7$ superconductor has been replaced by Fe, Co, Ni or Zn reflect the properties of impurities and are individual. (Many reports are listed in the Kodansha scientific journal edited by Fueki and Kitazawa on page 232 under the heading "Chemistry of Oxide Superconductors.") In contrast to the X-ray diffraction diagram changing to tetragonal at $x \geq 0.03$ in the case of Fe and Co, it remains orthorhombic in the case of Ni and Zn, and the lowering rate of T_c ($-dT_c/dx$) is on the order of $\text{Zn} > \text{Fe} \approx \text{Co} > \text{Ni}$. We found that when the sample was treated under high oxygen pressure ($10^2 \sim 10^4$ atm), the oxygen content increased and the trend was for T_c to return to its former value in the case of Fe and Co, but both the oxygen content and the T_c showed practically no change in the case of Ni and Zn. Explanations will be given here especially on samples containing Fe.

(i) Changes as a result of high oxygen pressure treatment of T_c : In Figure 1, T_c is plotted against x . When heat treatment with oxygen pressure at 1 atm is compared with that at 100 atm, it is found that the difference in T_c becomes greater as x increases, and it reaches 20K at $x = 0.04$. Moreover, the transition width becomes very narrow with treatment at 100 atm. On the basis of the measurement of complex susceptibility, it appears that the reason the transition becomes narrow is because the intergranular becomes "clean." After all, the difference in oxygen content caused by oxygen pressure becomes greater as x increases. This is related to the x dependency of the microstructure mentioned below.

(ii) Microstructure: TEM observation was carried out to ascertain whether the high oxygen pressure treatment had caused a change in the structure. The structure becomes tetragonal at $x \geq 0.03$ in the XRD, but according to TEM observation, the crystal particles are divided into small domains with an orthorhombic structure, and in neighboring domains the a and b axes are

mutually exchanged. Since the size of the domain is 5-10 nm at $x = 0.04$, it may be that only the average structures have been observed in the XRD. The domain size practically does not change as a result of oxygen pressure. The x dependency of the oxygen content increase may be mainly due to oxygen entering into the domain boundary; the domain size becomes smaller as x increases. An oxygen content increase is similarly seen under high oxygen pressure also in the case of Co adopting a micro domain structure, and the reason why this does not happen in the case of Ni and Zn remaining orthorhombic in the XRD can be understood in this context.

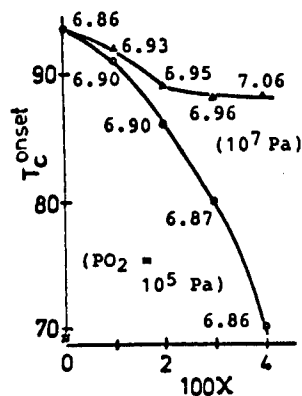


Figure 1. T_{conset} depending upon x and y

(iii) Observation of Fe condition by means of Mossbauer effect: There are four types of Fe conditions in accordance with the Mossbauer effect, and the proportion changes greatly based on the oxygen content. For example, Fe^{4+} is obviously generated under treatment with high oxygen pressure in the case of $x = 0.01$.

The experiment range is presently being expanded to a higher Fe concentration and higher oxygen pressure, and we will present the results on these also.

Y-La Substitution Effect on Superconductivity of $\text{YBa}_2\text{Cu}_3\text{O}_y$

43067591 Tokyo NIHON FUNMATSU FUNTAI YAKIN KYOKAI in Japanese 16-19 May 88
p 49

[Report by Masaru Yokota, Hiroshi Nagai, Kazuhiko Majima, Jiro Kondo and Ken Obayashi, Course of Material Physical Property Technology, Faculty of Technology, Osaka University: "Effect of Y-La Substitution on Superconductivity of $\text{YBa}_2\text{Cu}_3\text{O}_y$ "]

[Text] I. Introduction

Although there is an impression that the superconductivity of $\text{YBa}_2\text{Cu}_3\text{O}_y$ is now entering into the category of classical material, it can be said that research on the superconducting mechanism, development of practical use application, etc., are at a standstill. In a followup to our previous report¹, in which we described research in which La was substituted for Ba in YBa_2Cu_3 , in this report we will provide information on research in which La was substituted for Y.

II. Sample and Test Method

The material powders used in the experiment and the preparation method of the sample were exactly the same as described in a previous report, wherein measurements were made in the range 0-100 mol%. Electric resistance and X-ray diffraction experiments similar to those in the previous report were adopted for the measuring method, and the measurement of magnetic susceptibility was conducted this time using a static magnetic field magnetic balance for further studying the Meissner effect.

III. Experiment Results

(1) The superconducting transition temperature (T_c , K), T_c (onset-offset) and logarithm value of electric resistance (R , ohm, m) at room temperature were computed and are shown in Figure 1. Although these values were measured only up to the liquid nitrogen temperature, T_c did not change up to La approximately 15 mol%, but ΔT_c became minimum at La approximately 10 mol%.

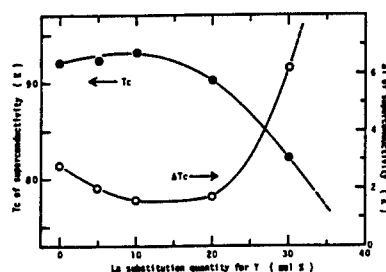


Figure 1. Effect of La substitution for Y on T_c and ΔT_c of superconductivity for $\text{YBa}_2\text{Cu}_3\text{O}_y$ sintered ceramics

(2) On the other hand, the density ratio of $\text{YBa}_2\text{Cu}_3\text{O}_y$, $\text{YBa}_{1.9}\text{La}_{0.1}\text{Cu}_3\text{O}_y$ (reported in previous report) and $\text{Y}_{0.95}\text{La}_{0.05}\text{Ba}_2\text{Cu}_3\text{O}_y$, when sintered under the same condition, becomes 69.5, 64.8 and 78.8, respectively; the density ratio is highest when La is substituted for Y. In the case of the substitution of La for Y, it appeared that the liquid phase sintering progressed well and the sintering density rose, but the correlation with ΔT becoming small is not clear. The point that draws special attention is that the liquid phase generated in the case of the substitution of La for Y did not exert an ill effect on superconductivity. In the future, efforts should be undertaken to make clear the generating liquid phase and the phase diagram of this system.

(3) The effect of the substitution of La for Y on the lattice constant is shown in Figure 2. It is clear from this that an orthorhombic can be maintained even when La is substituted for Y up to 100 mol%.

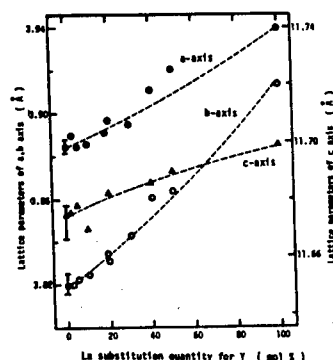


Figure 2. Effect of La substitution for Y on the lattice constants for $\text{YBa}_2\text{Cu}_3\text{O}_y$ sintered ceramics

References

1. Masaru Yokota, Hiroshi Nagai, Kazuhiko Majima, Ken Obayashi, and Jiro Kondo: Powder and Powder Metallurgy, 34, 632, 1987.

Effect of Sn Addition to $\text{YBa}_2\text{Cu}_3\text{O}_y$ Superconducting Oxides

43067591 Tokyo NIHON FUNMATSU FUNTAI YAKIN KYOKAI in Japanese 16-19 May 88
p 50

[Report by Toshihiko Shigematsu, Mariko Ishikawa and Norihiko Nakanishi,
Faculty of Technology, Konan University: "Effect of Addition of Sn to
 $\text{YBa}_2\text{Cu}_3\text{O}_y$ Superconducting Oxides"]

[Text] 1. Interest has been shown in studying the effect exerted on the superconducting characteristics when some of the Y, Ba and Cu that are component elements of $\text{YBa}_2\text{Cu}_3\text{O}_y$ superconducting oxides are replaced by different elements, as a clue to ascertaining how the various component elements are concerned with the appearance of superconductivity. So in this research we studied the effect exerted on the superconducting characteristics when Sn was substituted for Cu or for Ba, using measurements of electric resistance and susceptibility made by XRD and XPS.

2. Preparation of the sample was made by the ordinary solid phase method using Y_2O_3 , BaCO_3 , CuO and SnO_2 as materials. The materials were given preliminary sintering at 900°C in air for 24 hours; after pulverization, mixing and forming, the sample was sintered at 900°C for 24 hours and further sintered at 400°C for 24 hours. The electric resistance was measured by the four-terminal method, and susceptibility was measured in the temperature range of 77-300K by vibration magnetic balance.

3. The results obtained for the sample in which Sn was substituted for Cu are as follows. 1) It was an orthorhombic single phase (composition of $\text{YBa}_2\text{Cu}_{3-x}\text{Sn}_x\text{O}_y$) at $x = 0.33$ by the XRD measurement. 2) The electric resistance was reduced linearly down to just above T_c in all samples, and ΔT_c also returned to the small value of $\sim 1.4\text{K}$. Moreover, the electric resistance value just above T_c was minimum, $0.41\text{m}\Omega\cdot\text{cm}$ ($T = 95\text{K}$), when $x = 0.025$ (Figures 1 and 2). 3) In contrast to T_c not changing as a result of the substitution of Sn, the susceptibility was suddenly reduced with the increase in the Sn substitution content; it leveled off at more than $x = 0.075$ (Figure 3). 4) $\text{Sn}3d_{5/2}$ showed a peak at 485.7 eV . This is because it shifted to the 0.7 eV lower energy side in comparison with 486.4 eV in SnO_2 and SnO .

These results have also been reported together with the results obtained in substituting Sn for Ba in the sample.

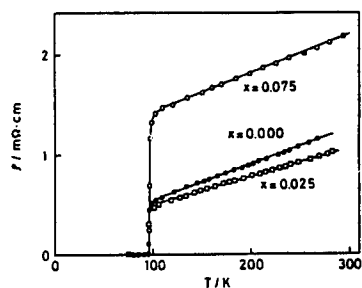


Figure 1. Electric resistance of $\text{YBa}_2\text{Cu}_3-x\text{Sn}_x\text{O}_y$

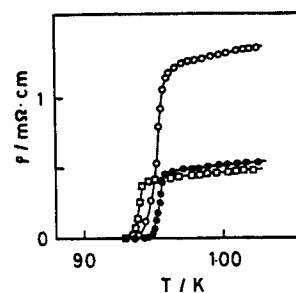


Figure 2. Electric resistance of $\text{YBa}_2\text{Cu}_3-x\text{Sn}_x\text{O}_y$ just above T_c

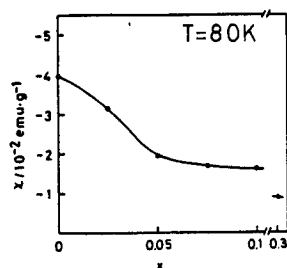


Figure 3. Susceptibility of $\text{YBa}_2\text{Cu}_3-x\text{Sn}_x\text{O}_y$

Composition Control of Bipolar RF Sputtering Y-Ba-Cu-O High-Temperature Superconducting Thin Film

43067591 Tokyo NIHON FUNMATSU FUNTAI YAKIN KYOKAI in Japanese 16-19 May 88
p 51

[Report by Takashi Hase, Hiroshi Kajima, Kozo Nishimura and Yoshio Kawate, Electronic Technology Center, Kobe Steel, Ltd.; and Masahiko Okuda, Mechanical Technology Center, Kobe Steel, Ltd.: "Composition Control of Bipolar RF Sputtering of Y-Ba-Cu-O High-Temperature Superconducting Thin Film"]

[Text] 1. Introduction

In this research, we studied the film forming parameters so as to be able to reproduce the film composition under the same film forming conditions and to exercise film composition control when carrying out film forming of Y-Ba-Cu-O thin film by the bipolar RF sputtering method.

2. Experiment Method

Y-Ba-Cu-O thin film was formed on an SrTiO_3 (100) substrate by means of a bipolar sputtering device using the target of $\text{YBa}_{5.71}\text{Cu}_{6.00}\text{O}_x$ wherein Y_2O_3 , BaCO_3 and CuO powders were mixed and sintered. The substrate temperature was fixed at 300°C . After film forming, composition analysis of metallic elements in the film was conducted using energy distribution EPMA. In this experiment, film forming was conducted by making the oxygen partial pressure, the discharge power density and the distance between the target and the substrate the parameters. After composition analysis, heat treatment was conducted in oxygen temperature, and superconductivity was confirmed by the four-terminal resistance method.

3. Experiment Results

The target using the time dependency of the film composition ratio when conducting film forming under the same conditions is shown in Figure 1. The Cu at%/Y at% ratio and Ba at%/Y at% ratio in the film were reduced together with the elapse of the target use time; an approximately fixed value was exhibited at the point of time after use for more than 40 hours. Upon conducting film forming after cutting and removing about 0.5 mm of the target

surface at the point of time after use for 55 hours, the film composition ratio almost returned to the value it had immediately after the start of target use. The discharge power density dependency of the film composition ratio is shown in Figure 2. As the discharged power density increased, the Cu at%/Ba at% ratio in the film steadily decreased. Figure 3 shows the partial pressure of oxygen dependency on the film composition ratio. The Cu at%/Ba at% ratio in the film was not dependent on the increase in partial pressure and was practically fixed, and the Cu at%/Y at% ratio and the Ba at%/Y at% ratio were reduced at a steady pace with the increase of oxygen partial pressure. It was ascertained from the results shown in Figures 2 and 3 that the procedure should be first to obtain the discharge power density in which the target Cu at%/Ba at% ratio was available, and then to obtain the oxygen partial pressure in which the target Cu at%/Y at% ratio and Ba at%/Y at% ratio were available, and to conduct film forming under these conditions to obtain the target film composition.

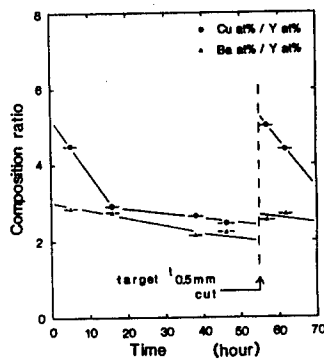


Figure 1. Target using time dependency of film composition ratio

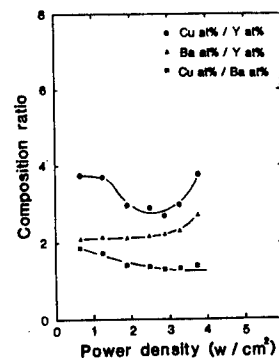


Figure 2. Discharge power density dependency of film composition ratio

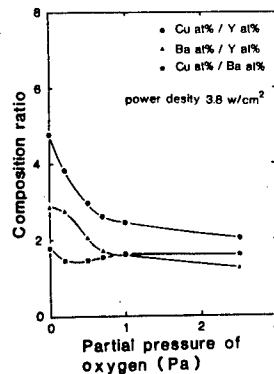


Figure 3. Oxygen partial pressure dependency of film composition ratio

High-Temperature Superconducting Multi Hetero Epitaxial Growth

43067591 Tokyo NIHON FUNMATSU FUNTAI YAKIN KYOKAI in Japanese 16-19 May 88
p 52

[Report by Takeshi Kobayashi, Yuji Yoshisago, Masahiro Iyori and Masayoshi Tonouchi, Faculty of Basic Technology, Handai University: "High-Temperature Superconducting Multi Hetero Epitaxial Growth"]

[Text] 1. Introduction

The introduction of the heterojunction system is effective for further making the most of the characteristics of oxide high-temperature superconductors. The use of this system is linked not only to future applications but also to the appearance of a new superconducting phase that is expected to be generated on a hetero interface. However, the establishment of an ultrathin film epitaxial technology and a technology for evaluating the interface and the surface are necessary for the development of the heterojunction system. This is very interesting research that is profound from the crystal engineering aspect. A heterojunction growth of a lanthanide system (123 phase) was attempted centered on the YBaCuO (123 phase) with the crystal structure well defined and adopting a comparatively simple atomic configuration; as a result, a great deal of new information was obtained. We will report here on research in which an effort was made to obtain Ge (100)-YBaCuO (001) semiconductor/high-temperature superconductor hetero epitaxial growth with good lattice correspondence.

2. Experiment Method and Results

An rf magnetron sputter was used for film forming, and $\text{SrTiO}_3(100)$ and (110) and $\text{MgO}(100)$ surfaces were used for the substrate crystals. Crystal evaluation was made by RHEED observation of the as-grown thin film. Film forming was conducted on YBaCuO, ErBaCuO and NdBaCuO in the range of 1.2-120 nm. First of all, film forming was carried out of YBaCuO and then of NdBaCuO for a total of 120 nm on a (110) SrTiO_3 surface. Hetero epitaxial growth was possible, as shown in Figure 1. An ultrathin film growth was attempted next; completely different results were obtained on an MgO substrate and an SrTiO_3 substrate, as shown in Figure 2. A deformed lattice appeared on the SrTiO_3 substrate on both (100) and (110) surfaces, but a normal crystal structure was restored upon reaching 10 nm thickness growth. Figure 3 shows the growth

of a total of six layers (total thickness 7.2 nm) in which three layers each of YBaCuO and ErBaCuO with a thickness of 1.2 nm were alternately placed on the SrTiO₃(110) surface. It became clear that the deformed YBaCuO crystal structure on the SrTiO₃ substrate was gradually transcribed to the upper layers and epitaxial growth was achieved. As expected, normal crystal was grown in a multi hetero structure with each layer made thicker (60 nm).

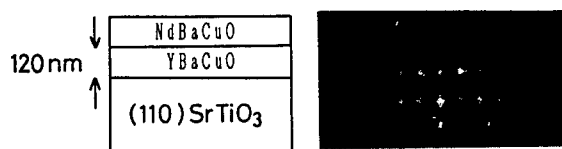


Figure 1. RHEED pattern of NdBaCuO/YBaCuO single hetero epitaxial growth



Figure 2. RHEED pattern of 3 nm thickness YBaCuO (right) MgO(100) substrate, (left) SrTiO₃(110) substrate

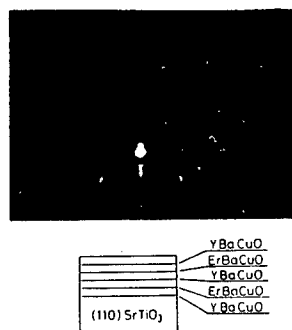


Figure 3. Multi hetero structures on SrTiO₃ substrate. The thickness of various layers is 1.2 nm.

Preparation of High-Temperature Superconducting $\text{Ba}_2\text{Y}_1\text{Cu}_3\text{O}_{7-\delta}$ Thick Film

43067591 Tokyo NIHON FUNMATSU FUNTAI YAKIN KYOKAI in Japanese 16-19 May 88
p 53

[Report by Takashi Yamamoto, Faculty of Electrical Engineering, National Defense Academy; and Tamotsu Ueyama and Kiyoshi Okazaki, Sagami Institute of Technology: "Preparation and Evaluation of High-Temperature Superconducting $\text{Ba}_2\text{Y}_1\text{Cu}_3\text{O}_{7-\delta}$ Thick Film"]

[Text] 1. Introduction

Research has been conducted on thick film in conjunction with ceramics ever since high-temperature superconductivity was confirmed in La-Sr-Cu-O system and Ba-Y-Cu-O system ceramics. This report concerns the results of forming a thick film from $\text{Ba}_2\text{Y}_1\text{Cu}_3\text{O}_{7-\delta}$ + Ag_2O powder.

2. Experiment Method

Superconducting $\text{Ba}_2\text{Y}_1\text{Cu}_3\text{O}_{7-\delta}$ was produced using the partial oxalate method, which combines the chemical method and the conventional method. After powder synthesis, Ag_2O was added at each weight ratio, and a paste was formed by the method shown in Figure 1. This was screen printed at a thickness of 50-150 μm on PSZ, MgO and Al_2O_3 substrates, and sintered at a temperature of 870°-950°C for 30 minutes.

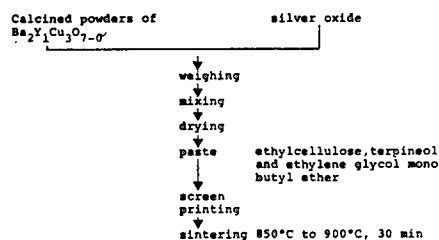


Figure 1. Paste preparation method

3. Experiment Results

The TG and DTA curves of the sample to which Ag_2O was added are shown in Figure 2. The weight change and exothermic reaction seen at 100°-200°C are

not genuine. The sudden weight reduction and endothermic reaction at 400°C are the result of generation according to the following reaction formula.

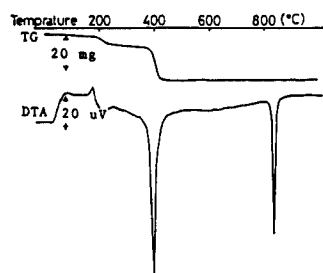
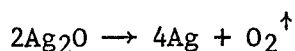


Figure 2. TG-DTA curve of Ag_2O

$\text{Ba}_2\text{Y}_1\text{Cu}_3\text{O}_{7-\delta}$ is easily affected by the oxygen partial pressure. The addition of Ag_2O causes the release of oxygen from within the thick film during the sintering process. The further endothermic reaction at 830°C is caused by the melting of Ag. The chemical reaction of Ag_2O mentioned above does not exert an ill effect on the $\text{Ba}_2\text{Y}_1\text{Cu}_3\text{O}_{7-\delta}$. The Ag melting at 830°C improves the adhesion between the thin ceramic film and the substrate. After synthesis of $\text{Ba}_2\text{Y}_1\text{Cu}_3\text{O}_{7-\delta} \cdot \text{Ag}_2\text{O}$ thick film, studies were conducted by the X-ray diffraction method. The result was that a mixed body of $\text{Ba}_2\text{Y}_1\text{Cu}_3\text{O}_{7-\delta}$ and metal Ag was obtained. An example of the temperature characteristic of resistivity is shown in Figure 3. The characteristic point is that resistivity in the ordinary conducting state (95K>) is low in comparison with a film not containing Ag_2O . The superconducting transition temperature was 85-100K.

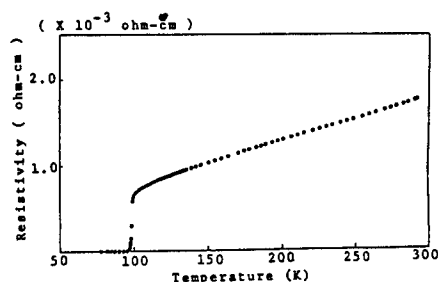


Figure 3. Temperature characteristic of resistivity

Pt/AlO_y/YBa₂Cu₃O_{7-x}/SrTiO₃ Single Crystal Thin Film Tunnel Junction

43067591 Tokyo NIHON FUNMATSU FUNTAI YAKIN KYOKAI in Japanese 16-19 May 88
p 54

[Report by Jun Takada, Kaxunuki Yamamoto and Kenji Iijima, (Foundation) Production Development Scientific Research Institute; Hiromasa Mazaki, National Defense Academy; and Takahito Nakanishi and Yoshichika Bando, Institute for Chemical Research, Kyoto University: "Pt/AlO_y/YBa₂Cu₃O_{7-x}/SrTiO₃ Single Crystal Thin Film Tunnel Junction"]

[Text] The anisotropy of the Cu-O surface in oxide system superconductors is a point that merits attention as characterizing the superconductivity of the material, and research on the junction characteristic of a specified crystal direction is attracting interest from the standpoint of both basic research and application aspects. We previously succeeded in preparing YBa₂Cu₃O_{7-x} (YBCO) system single crystal film of good quality and with a smooth surface by the reaction vacuum evaporation method, and now we have also been able to form two types of quasi-particle tunnels in the parallel and vertical directions on a Cu-O surface containing a junction surface of about 1 mm² using this technology. We will report here on the preparation method and the respective tunnel characteristics.

Two types of single crystal thin films were prepared in which the Cu-O surface of YBCO was parallel and vertical to the substrate surface of single crystal SrTiO₃ with their 100 and 110 planes by allowing the epitaxial growth of YBCO at the substrate temperature of 500°-600°C by means of the activated reactive evaporation. The thickness of these thin films was 1000Å and the in-plane size was 1 x 5 mm². An amorphous aluminum oxide of 60Å thickness was formed on YBCO as an insulating film by evaporating alumina in an oxygen atmosphere of 5 x 10⁻⁴ Torr. Pt 1000Å was formed next as the facing electrode. The substrate was not specially heated during forming of the AlO_y and Pt. Since patterning was conducted using a metal mask during vacuum evaporation, it can be considered that the effect of this process on the film properties was small. Thus, the two types film were obtained to form quasi-particle tunnel junction Pt/AlO_y/YBCO/SrTiO₃, in which the tunneling direction was parallel (CuO ||) and vertical (CuO ⊥) to the Cu-O surface of YBCO (Figure 1).

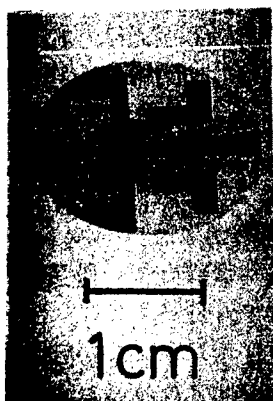


Figure 1. Quasi-particle tunnel junction Pt/AlO_y/YBCO/SrTiO₃

The YBCO on the (100) and (110) surfaces of SrTiO₃ prepared at the same time on the same substrate forming the junction for measuring the four-terminal resistance showed a zero resistance at 82.5K and 73.6K, respectively, and the transition widths (10-90 percent) were 3K and 7K. Although the superconducting characteristics were slightly inferior, two types of YBCO with almost the same degree of quality were available.

Tunnel current I was measured using a constant voltage circuit, and the differential conductance $dI/dV-V$ was obtained by computation (Figure 2). The gap parameter Δ (4.4K) = 11.5 ± 1.5 meV and the coupling constant $2\Delta/kT_c = 3.2 \pm 0.4$ were obtained from the Cu-O surface vertical direction tunneling. Two sets of peaks, ± 5 mV and ± 17 mV, were observed on the Cu-O surface parallel direction, and examinations were made from the standpoint of two-phase superconductivity and proximity effect. Details on the barrier characteristic, etc., will be reported at another time.

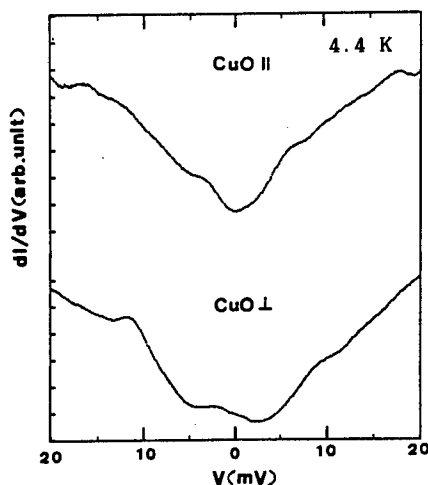


Figure 2. Differential conductance $dI/dV-V$

High-Temperature Superconductivity Generating Mechanism Proposed by New System Physics

43067591 Tokyo NIHON FUNMATSU FUNTAI YAKIN KYOKAI in Japanese 16-19 May 88
p 55

[Report by Shuichi Iida, Teikyo University, emeritus professor of Tokyo University: "Simple Explanation of High-Temperature Superconductivity Generating Mechanism Proposed by New System Physics"]

[Text] After 90K level oxide high-temperature superconductors were discovered in $\text{YBa}_2\text{Cu}_3\text{O}_7$, the presence of 120K level oxides were reported in many similar phase crystals of the BiSrCa and Ti systems, and the point has now been reached at which the thinking on the superconducting mechanism must be changed completely. The so-called BCS theory of Bardeen, Cooper and Schrieffer says that the critical temperature T_c is dependent on the mass of the cation atom at the point that a cooperative interaction is generated among the superconducting electrons with the local lattice vibration (phonon) as the medium, and therefore an isotropic effect is expected, and a coincidence has been observed with the actually measured value on a metallic superconductor. In an oxide superconductor, however, this isotropic effect is practically nil, or it is at least far smaller than the expected value. Therefore, the simple BCS theory does not apply in regard to it. Moreover, the effect of the addition of a magnetic ion is also small. Now, the new system physics, which has been elaborated on the basis of the electron VD model (vortex ring, permanent current ring), has explained almost entirely the mathematical and physical coupling structure of classical physics and quantum physics, which was only vaguely understood conventionally. As a result, it has become possible to analyze problems in physics concerning the deepest aspect of quantum physics from a greatly advanced viewpoint. Thus, first of all, the q-number system, i.e., the system which shows the electrons in the quantum physics system, must be considered as the wave function of the Schrodinger-Dirac flow itself (called electron field); points and permanent current rings (VR electrons) must be considered as having a meaning only in the c-number system; and when it comes to the q-number system, it must be considered that concreteness disappears. A vacuum, according to quantum electrodynamics, is a zero-point energy state which is overflowing with electromagnetic radiant fields (photon fields) that vibrate. Generally, the electron field interacts with the photon field, and the electron energy is slightly lowered (10^{-6}). Although the analysis here involves the problem

of infinite (∞) energy and was not easy by means of conventional quantum physics, this difficulty is eliminated with the new system physics. Based on diagrams provided in various reports, in observing $\text{YBa}_2\text{Cu}_3\text{O}_7$ it appears that insulator layers consisting of Cu^{2+} and O^{2-} , and Ba^{2+} and O^{2-} , and superconducting layers containing Cu^{3+} and La^{3+} have been laminated alternately. Considering that the electron fields and photon fields in the superconducting layers interact by making the layer volume in the insulator layer the resonance cavity, quantum electromagnetic mechanical analysis by means of the new physics predicts that each mode of the standing photon field is excited at a degree of more than 10^7 photon per electron. There is the possibility that this excitation is further amplified by two factors. One factor is the number of electrons taking part, and the number of related electrons becomes 10^7 when the layer width is more than $1 \mu\text{m}$. The other factor is that an amplification can be added by the Q value of the resonance gap as an oxide. According to experiments made by Walther Schleich of West Germany, the spontaneous radiation probability of the microwave from the exciting atom is in proportion to the Q value of its placed cavity, and the probability amplification of $Q = 8 \times 10^8$ has been observed at 2K in the case of an Nb superconducting wall cavity. Although it can be expected that phonon fields of 10A-100A are important for the wavelength, a phonon field is important for example also at an amplification of 10^2 . A coherent coupling vibrator state of the numerous electron fields and photon fields is formed by the vibration of the zero-point electromagnetic field thus amplified. One of the described images of the phase matching state in this complex is the electron field matched with the E vector of the phonon field, and therefore, it is the vibration of the charge density wave. While the conventional analysis does not explain this electron field, the new physics analysis is that even a single electron field has a vibration of the charge density wave. Once the electron field-phonon field composite is excited by this mechanism, it has the possibility of generating a so-called cooperation phenomenon in which the amplitude of the phonon field increases exponentially and functionally. Furthermore, with this excitation there is the possibility of converting to the superconducting layer of Cu^{2+} and $\text{Cu}^{3+} + e^-$ in the initial insulation layer. The simplest described image of Cu^{3+} is a low spin state ion with a zero spin value. Thus, it is considered that a composite has been synthesized in the interior of the superconductor by the excited standing wave photon field and the numerous electron fields that have been modified, and coherently matched by the excited standing wave photon field. The bonding with the thermal phonon field must be small in the forming of this composite. Metallic cation ions are floating in the metallic state electron field in simple metals. This is why they bond easily with the E vector of the phonon field. In intermetallic compounds and oxides, however, a mixed bonding state of ionicity and homopolarity is formed, and this is not easily moved by the E vector; it is an optional mode in which the positive and negative ions move in the reverse direction when they move, and bonding is small with the thermal phonon field, which is the acoustic mode. Thus, the presence of this amplifying mechanism explains why good-quality ordinary superconductors do not become high-temperature superconductors. Since it is accepted that phonon and spin have no correlation with the superconducting amplifying mechanism, it goes without saying that the isotopic effect is small, it does not impede the forming of Cooper pairs and is sensitive to the

presence of magnetic ions. Based on the relationship with the number of electrons of the k-gap of the primary superconducting layer, the thicker the layer thickness, the greater the increase in the number of related electrons, and it is expected that the amplification of electrons will become stronger. This expectation and the possibility of such experiments was put forward last January, and it is considered that the discovery and structural analysis of new high-temperature superconductors verifies the correctness of this proposition. A more detailed analysis in English of the January pronouncement has been distributed in the form of a preprint both domestically and abroad. One of the summaries was published on page 1 of Collection 3 of reports given at the 43d annual meeting (at Koriyama) of the Japan Physical Association in 1988.

Superconducting Oxides With New Structure--Bi-Sr-Cu-O System

43067591 Tokyo NIHON FUNMATSU FUNTAI YAKIN KYOKAI in Japanese 16-19 May 88
p 56

[Report by Jun Akimitsu, Faculty of Science and Technology, Aoyama Gakuin University: "Superconductivity of Superconducting Oxides With a New Structure--Bi-Sr-Cu-O System"]

[Text] Only two types of high-temperature superconducting oxides, $(La_{1-x}M_x)_2CuO_4$ (M: Ba, Sr, Ca) and $LnBa_2Cu_3O_y$ (Ln: Y and lanthanoids), were previously considered high-temperature superconducting oxides, but in recent years, two more superconductors of the Bi system (Bi-Sr-Cu-O system) and Ti system (Ti-Ba-Cu-O system) have been discovered. It may be that these latter two superconductors are materials that belong to the same category in view of the fact that the T_c rises when Ca is added. Therefore, it is important to make clear the points of similarity and difference of the latter two with the aforementioned high-temperature superconducting oxides, and it is also an important problem to clarify why the T_c rises when Ca is added. We discovered the superconductivity of the Bi-Sr-Cu-O system in experiments at our laboratory, and we have studied its physical properties in comparison with those of the Bi-Sr-Ca-Cu-O system. Some of the results obtained can be listed as follows.

- 1) The basic structure of the crystal structure of the Bi-Sr-Cu-O system was established by the Rietveld analysis method. (Figure 1)
- 2) T_c rises in varying degrees when some rare earth elements are substituted in the Bi-Sr-Cu-O system. (Figure 2)
- 3) The energy gap of the superconductor was measured by the point contact method. The results obtained are shown in Figure 3. The value of $2\Delta/kT_c$ obtained under this method was close to 10--considerably greater than the value expected on the basis of the BCS theory.

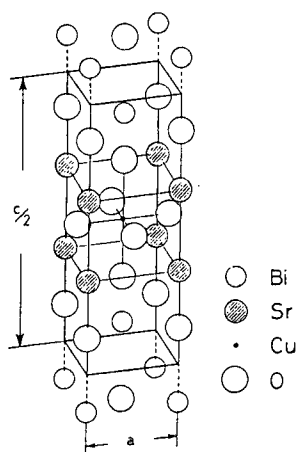


Figure 1. Crystal structure of $\text{Bi}_2\text{Sr}_2\text{CuO}_y$

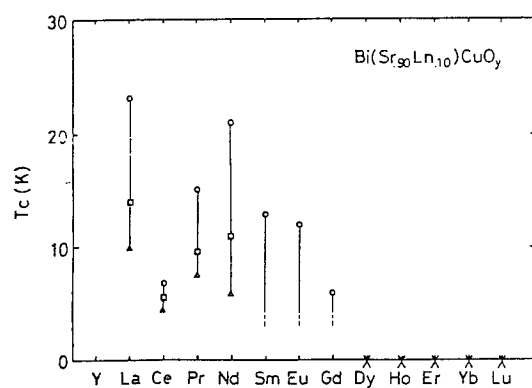


Figure 2. Effect of rare earth element substitution

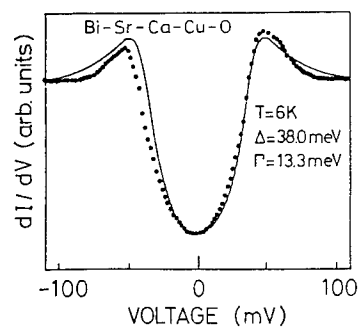


Figure 3. Energy gap of Bi-Sr-Ca-Cu-O system. Solid line shows theoretical values.

Phase Equilibrium of Bi_2O_3 - SrO - CuO System

43067591 Tokyo NIHON FUNMATSU FUNTAI YAKIN KYOKAI in Japanese 16-19 May 88
p 57

[Report by Yasunori Ikeda, Yasushi Ooue, Kazuhisa Inaba, Mikio Takano and Yoshichika Bando, Institute for Chemical Research, Kyoto University]

[Text] C. Michel et al.¹ reported that in the Bi-Sr-Cu-O system a superconductivity of 20K was exhibited in $\text{Bi}_2\text{Sr}_2\text{Cu}_2\text{O}_{7+\delta}$. Although several reports were made subsequently, a definitive report has not been made yet on the phase relationship. The presence of a high-temperature superconductor in a system in which Ca was added has been confirmed recently, but the haploid has not been discovered as yet. We decided first of all to study in detail the Bi-Sr-Cu-O system without the Ca in order to obtain a high-temperature superconductor by the haploid. The experiment method used was the ordinary ceramics method; various compositions and heat treatments were studied with Bi_2O_3 , SrCO_3 and CuO as the materials.

Two new compounds were identified in the Bi_2O_3 - SrO system, and a phase providing five types of different X-ray diffraction diagrams was identified in Bi-Sr-Cu-O system. The result is shown in Figure 1. The Bi_2CuO_4 reported by J.C. Boivin et al.² was formed in the Bi_2O_3 - CuO system; Sr_2CuO_3 , SrCuO_2 and $\text{Sr}_3\text{Cu}_5\text{O}_x$ were formed in the SrO - CuO system; and $\text{Bi}_{1-x}\text{Sr}_x\text{O}_y$ when $x = 0.2\sim 0.3$ s.s., $x = 0.5$, $x = 0.6$ and $x = 0.75$ other than $\text{Sr}_{0.9}\text{Bi}_{1.1}\text{O}_{2.5}$ reported by R. Guillermo et al.³ were formed in the Bi_2O_3 - SrO system. The $\text{Bi}_2\text{Sr}_2\text{Cu}_2\text{O}_{7+\delta}$ phase reported by C. Michel et al. did not exist in the range surrounded by $\text{Bi}_2\text{Sr}_3\text{O}_6$ - $\text{Bi}_2\text{Sr}_2\text{CuO}_y$ - $\text{Sr}_3\text{Cu}_5\text{O}_x$ - SrCuO_2 ; the $\text{Bi}_2\text{Sr}_2\text{CuO}_y$ phase existed along with four types of phases having an X-ray diffraction diagram different from that of the $\text{Bi}_2\text{Sr}_2\text{CuO}_y$ phase. These are all layer compounds having a well resembling long periodicity, and they can be considered as having a profound relationship with the Ca substitution product. Their phase relationship is presently being studied. Figure 2 provides X-ray diffraction diagrams of the almost single-phase: 221(Bi:Sr:Cu), 785 and 776 and of F.4 of the triple-phase.

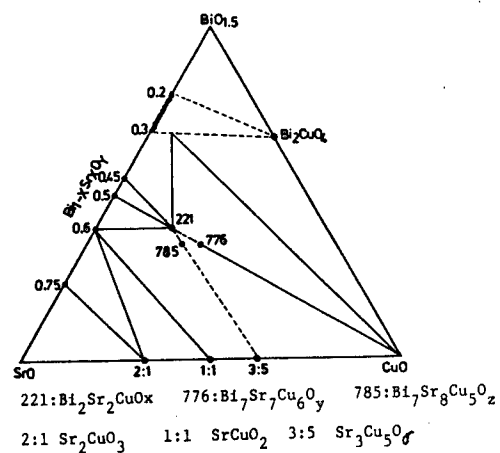


Figure 1. Results of X-ray diffraction diagram

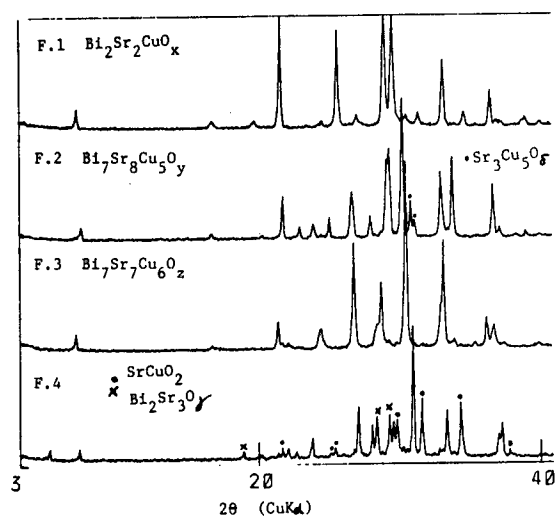


Figure 2. X-ray diffraction diagram of phases

References

1. C. Michel, et al., Z. Phys. B-Condensed Matter 68, 421, 1987.
2. J.C. Boivin, et al., Compt. Rend. 276C, 1107, 1973.
3. R. Guillermo, et al., Rev. Chim. Miner., 15, 153, 1978.

Crystal Phase of $\text{Bi}_2\text{O}_3\text{-SrO-CaO-CuO}$ System

43067591 Tokyo NIHON FUNMATSU FUNTAI YAKIN KYOKAI in Japanese 16-19 May 88
p 58

[Report by Yasunori Ikeda, Yasushi Ooue, Kazuhisa Inaba, Mikio Takano and Yoshichika Bando, Institute for Chemical Research, Kyoto University]

[Text] A quiet development race was instigated with the discovery of Bi-Sr-Ca-Cu-O system high-temperature superconductors. According to the many reports and preprints circulating, the status of the 75K level phase has been virtually established, and it has been almost agreed that the 105K phase is a layer compound having a c-axis period of 37\AA , although a haploid has not been obtained as yet. As we have reported, there are many phases with a long period in the $\text{Bi}_2\text{O}_3\text{-SrO-CuO}$ system, but their relationships have not been made clear. In comparison with simply obtaining the haploid of "123" in the YBC system, the forming condition here is far more difficult; it appears that consistent research on the phase relationship is required. We have studied the entire system in order to identify all of the phases formed by the $\text{Bi}_2\text{O}_3\text{-SrO-CaO-CuO}$ system. We mixed the materials Bi_2O_3 , SrCO_3 , CaCO_3 and CuO in various compositions by the ordinary ceramics method, changed the sintering temperature and time, and studied the formed phases by X-ray diffraction. The result is shown in Figure 1. The diagram is an expansion chart when the $\text{BiO}_{1.5}\text{-SrO-CuO}$ system is made the base and CaO the vertex. Each ternary system shows the phase relationship in the solid phase area ($\approx 840^\circ\text{C}$). The phase diagram shown is at 950°C for the SrO-CaO-CuO system. Although the formed phases in the $\text{BiO}_{1.5}\text{-SrO-CaO-CuO}$ system are not shown in this diagram, the following four phases were identified by X-ray.

- (1) Phase with a slight Ca desolved in the $\text{Bi}_2\text{Sr}_2\text{CuO}_x$ system ($\approx 24\text{\AA}$).
- (2) The 75K superconducting phase $\text{Bi}_2\text{Sr}_2\text{CaCu}_2\text{O}_8$ ($\approx 30\text{\AA}$). We consider that it is a solution up to the 3:2:2:3 neighborhood.
- (3) The 105K superconducting phase ($\approx 37\text{\AA}$) composition is unknown.
- (4) Phase in which the Ca and Cu desolved in the BiSr_2O_y phase (cubic $a = 8.41\text{\AA}$).

A future topic of research will be to make clear the range and phase relationship in which the high-temperature phases can exist stably.

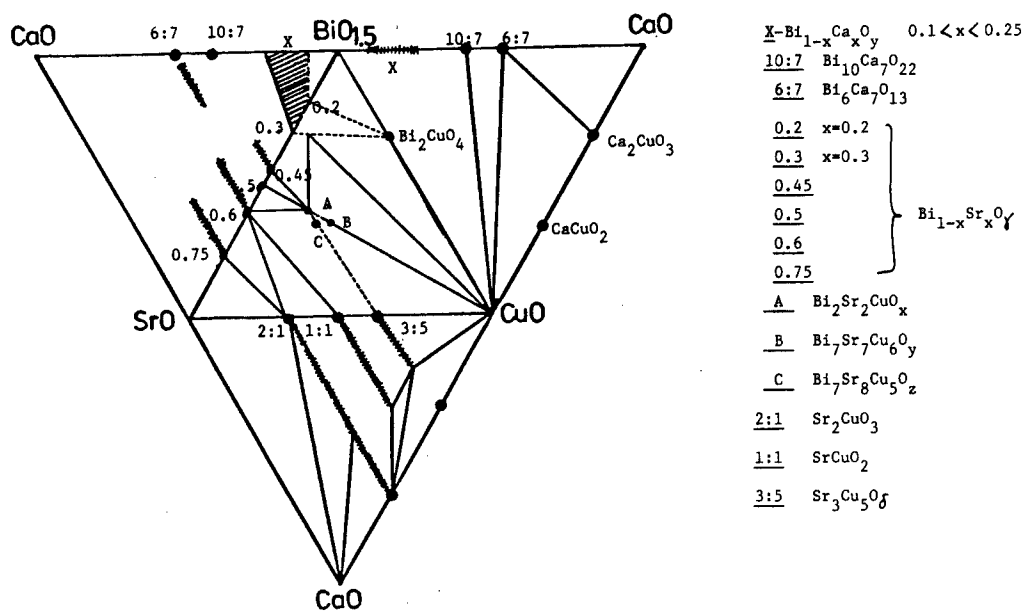


Figure 1. X-ray diffraction diagram of formed phases

Superconductors With Bi-Sr-Cu System Oxides as Base

43067591 Tokyo NIHON FUNMATSU FUNTAI YAKIN KYOKAI in Japanese 16-19 May 88
p 59

[Report by Takayuki Uchida, Masahiro Ito and Yujiro Nagata, Faculty of Science and Technology, Aoyama Gakuin University]

[Text] Objective

An oxide superconductor with a transition temperature exceeding that of $\text{YBa}_2\text{Cu}_3\text{O}_{7-y}$ was discovered recently, and studies have been made on the electrical properties, optimum composition and effect of substitutions in the Bi-Sr-Cu system oxides considered as the basic materials in this research.

Experiment Method

Samples were prepared by mixing the material powders by the conventional ceramics method, pressing and sintering them in air by solid phase reaction. The melting temperature of samples in Bi-Sr-Cu system oxides varied widely according to the composition. Therefore, the sintering temperature for each composition was made $20^\circ\text{--}30^\circ\text{C}$ lower than the melting point, and measurements were conducted on these samples.

Experiment Results

The superconducting phase in the ternary system preparation composition of Bi-Sr-Cu is shown in Figure 1. However, it is difficult to consider the diffraction pattern as a single crystal structure, and it is believed that it is not an example of a haploid. The range of superconductivity extends along the composition of Bi:Sr = 1:1, and the transition temperature showed the maximum value in the Bi:Sr:Cu = 1:1:1 composition. A sample in which La was substituted for Bi in this composition, i.e., $(\text{Bi}_{1-x}\text{La}_x)\text{SrCuO}_y$, was prepared, and its representative electric characteristic is shown in Figure 2. The La content and superconducting transition temperature change are shown in Figure 3. The transition temperature, which rose with the substitution of La, became highest at the composition $x = 0.2$. However, the transition width increased with this. When the substitution content was further increased, the percentage of other phases increased, and superconductivity was not exhibited.

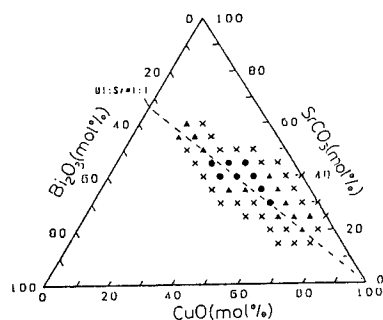


Figure 1. Superconducting composition in the Bi_2O_3 , SrCO_3 , CuO ternary system.
 ● and ▲: superconducting composition (zero resistance observed only at ●), X: semiconductor composition

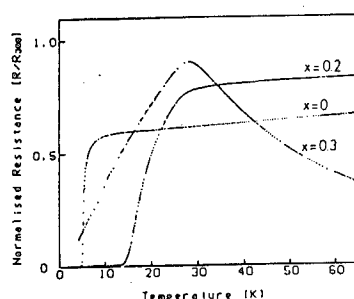


Figure 2. Resistance-temperature characteristic in $(\text{Bi}_{1-x}\text{La}_x)\text{SrCuO}_y$ system

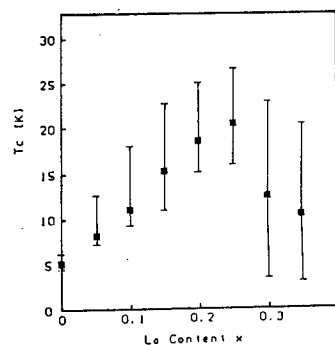


Figure 3. Effect of La content (x) in $(\text{Bi}_{1-x}\text{La}_x)\text{SrCuO}_y$ system exerted on transition temperature

The $(\text{La}_{1-x}\text{Sr}_x)_2\text{CuO}_4$ phase could not be recognized in the X-ray diffraction pattern; it is considered that the superconductivity is basically the same as that of the Bi-Sr-Cu system. We expect also to report on the result of substituting other elements in the Bi-Sr-Cu system. Pioneering research has been conducted by Akimitsu et al. on this system.

References

1. Akimitsu, et al., Jpn. J. Appl. Phys. 26, L2080, 1987.

Complex Magnetization Rate of Bi System Superconductors

43067591 Tokyo NIHON FUNMATSU FUNTAI YAKIN KYOKAI in Japanese 16-19 May 88
p 60

[Report by Hiromasa Mazaki, National Defense Academy; Yasunori Ikeda, Mikio Takano and Yoshichika Bando, Institute for Chemical Research, Kyoto University; and Kichi Oda, Hitoshi Kitaguchi, Jun Takada and Yoshinari Muira, Faculty of Technology, Okayama University]

[Text] The oxide superconductor $\text{BiSrCaCu}_2\text{O}_x$ was prepared by changing the sintering conditions, and the electric resistance and complex magnetization rate were measured. Bi_2O_3 , SrCO_3 , CaCO_3 and CuO with a purity of more than 99.9 percent were mixed at the mol ratio of 3:2:2:3; after pressurizing, they were treated to preliminary sintering at temperatures of 750°C and 800°C for 24 hours. After being pulverized and mixed, they were made into pellets of 10 mm ϕ by means of pressurizing, and after undergoing sintering for 12 hours at a temperature of 820°C - 870°C , the samples were obtained after being cooled in the furnace. The result of powder X-ray diffraction showed that the C-axis was a crystal monophase of about 30 \AA period in samples sintered at less than 830°C , and a small amount of crystals of about 24 \AA existed in samples sintered at 850°C and 870°C . Data on the sample sintered at 870°C are shown in Figure 1.

To obtain samples containing Pb, the starting materials Bi, Pb, Sr, Ca and Cu were weighed, sufficiently pulverized and mixed, and put into an alumina crucible, then sintered at 800°C in air for 12 hours. Next, after being pulverized and mixed again in an agate mortar, the mixture was press molded (20 mm ϕ x 2 mm) at 600 kg/cm², sintered at 845°C in air for 87 hours, and measuring samples were prepared. An example of the measured results of this system is shown in Figure 2.

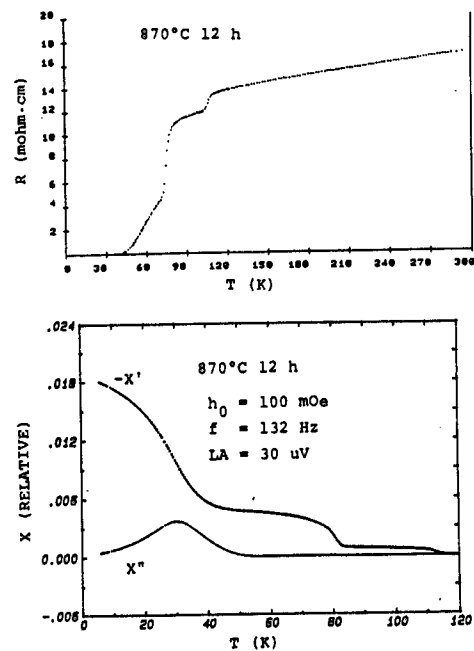


Figure 1. Electric resistance and complex susceptibility of Bi-Sr-Ca-Cu system

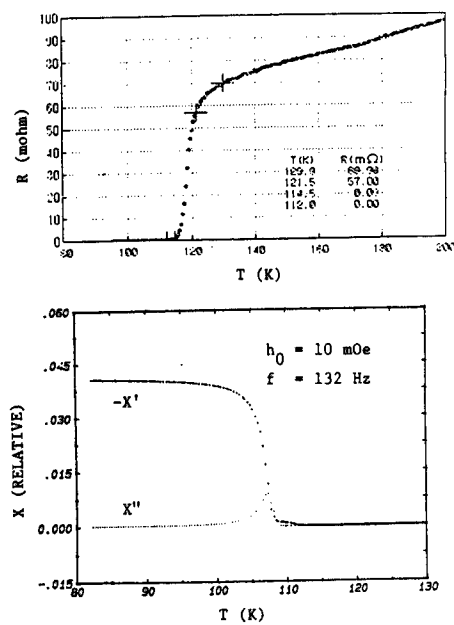


Figure 2. Electric resistance and complex susceptibility of Bi-Pb-Sr-Ca-Cu system

Preparation of $\text{BiSrCaCu}_2\text{O}_{5.5\pm\delta}$, Superconducting Characteristics

43067591 Tokyo NIHON FUNMATSU FUNTAI YAKIN KYOKAI in Japanese 16-19 May 88
p 61

[Report by Hiroki Miyamoto, Kei Miyamoto, Suguru Inamura and Yuzuru Takahashi, Industrial Technology General Laboratory of Osaka Prefecture]

[Text] 1. Objective

It is known that the amount of oxygen deficiency in $\text{Ba}_2\text{YCu}_3\text{O}_{7-\delta}$ changes and the superconducting characteristics change as a result of oxygen partial pressure at sintering. We conducted studies on how the superconducting characteristics of the newly developed high-temperature superconductor $\text{BiSrCaCu}_2\text{O}_{5.5\pm\delta}$ change on the basis of the sample preparation conditions.

2. Experiment Method

After mixing and press molding the material powders Bi_2O_3 (99.999 percent), SrCO_3 (99.99 percent), CaCO_3 (99.9 percent) and CuO (99.99 percent), they were treated to preliminary sintering at 850°C for 10 hours. After pulverizing and molding the material obtained, it was sintered in air for 16 hours at the respective temperatures of 830°C , 850°C , 860°C and 870°C . TG and DTA were measured on these samples. Heat treatment of samples baked at 860°C was conducted in Ar and O_2 ventilating currents at the temperatures of 770°C and 850°C , respectively.

3. Experiment Results

The endothermic peak of DTA measured in Ar flow and O_2 flow appeared at 860°C , as shown in Figure 1. The endothermic peak shifted to the high temperature side, 900°C , in O_2 flow. The weight reduction started at about 760°C in Ar flow, and a great weight reduction accompanied the endothermic reaction. On the other hand, the weight reduction started at about 880°C in O_2 flow, and it became $\delta = 0.64$ at 1050°C . A superconducting phase with an offset temperature of 108K and a phase with an offset temperature of 80K coexisted in samples sintered at 860°C . The resistance reduction rate was 80 percent in the 110K neighborhood. The resistance reduction rate in the 110K neighborhood increased to 86 percent when it was heat treated in O_2 flow at 850°C for 3 hours, as shown in Figure 2. It became $\delta = 0.26$ for the

material heat treated at 770°C in Ar flow, and the resistance reduction rate and transition temperature on the high temperature side dropped together with the oxygen content reduction, as seen in Figure 3.

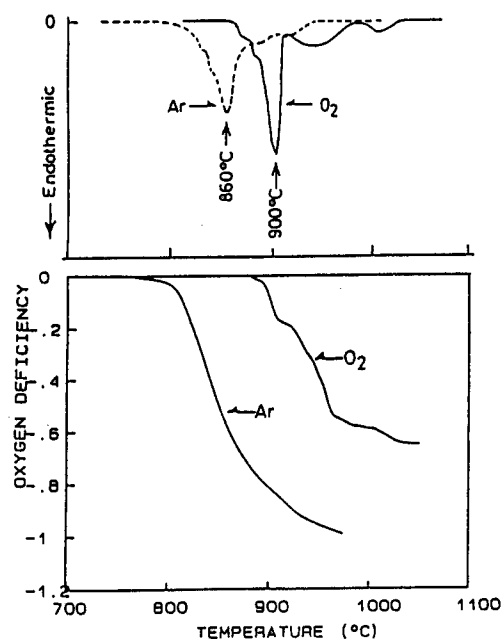


Figure 1. TG and DTA of $\text{BiSrCaCu}_2\text{O}_{5.5\pm\delta}$

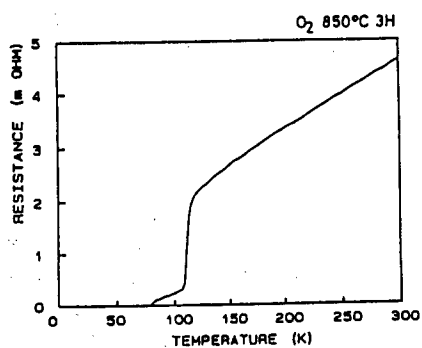


Figure 2. O₂ heat treatment after sintering at 860°C in air

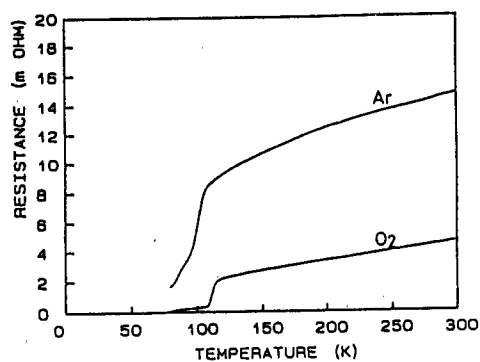


Figure 3. Change in superconducting characteristic brought about by atmospheric heat treatment

Bi System Oxide Superconductors by Oxalate Method, I

43067591 Tokyo NIHON FUNMATSU FUNTAI YAKIN KYOKAI in Japanese 16-19 May 88
p 62

[Report by Naoichi Yamamoto and Yoshio Oka, Faculty of Liberal Arts, Kyoto University; Yoichi Tomii, Faculty of Technology, Kyoto University; Hitoshi Kitaguchi, Kiichi Oda and Jun Takada, Faculty of Technology, Okayama University; and Tsutomu Katamoto and Naomi Horiishi, Toda Institute of Technology]

[Text] 1. Introduction

The presence of a superconducting phase with T_c at about 110K has been reported recently in Bi-Sr-Ca-Cu system oxides. A phase with T_c at about 80K also exists in compounds of this system. The superconducting characteristics are greatly dependent on the composition and heat treatment of samples. In our research, Bi system oxide samples were synthesized using the oxalate coprecipitation method, and the changes in the particle shape and superconducting characteristics brought about by heat treatment were studied.

2. Experiment Method

An oxalate coprecipitation product was obtained by adding ammonium oxalate to the aqueous solution Bi, Sr, Ca and Cu containing the prescribed content of nitrate. The coprecipitation product underwent preliminary sintering at 500°C for 2 hours, and it was then sintered at a temperature of 850°-900°C for 14 hours. Samples of the sintered material were further subjected to heat treatment at varying temperatures and for different periods. The composition of the samples was decided by the ICP method.

3. Experiment Results

The TG-DTA in the pyrolytic process of the coprecipitation product is shown in Figure 1. Thermal decomposition is accomplished by means of exothermic reaction at 260°C, and weight reduction is completed by 500°C. The samples sintered at 850°C for 14 hours mainly consisted of phases with the period between the layer of 30Å (Figure 2). SEM images, shown in Figure 3 [photo not reproduced], indicates that the particle shape of samples sintered at

850°C for 14 hours is a thin piece of about 2 μm , and the particle shape of samples sintered at 876°C for 60 hours becomes a hexagonal plate of about 10 μm . The electric resistance change brought about by heat treatment is shown in Figure 4. A superconducting phase of 80K exists in samples sintered at 900°C for 14 hours, and it has been ascertained that the 110K phase grows when the sample is further heat treated at 878°C for 90 hours.

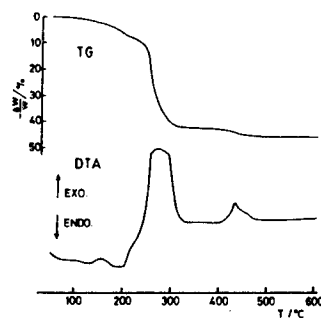


Figure 1. TG-DTA of oxalate coprecipitation product

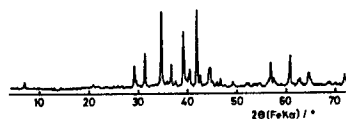


Figure 2. X-ray diagram of sample sintered at 850°C for 14 hours

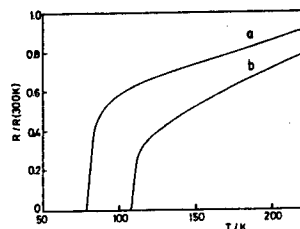


Figure 4. Change in electric resistance brought about by heat treatment. Line a shows the change at heat treatment of 900°C for 14 hours, and line b shows the change at heat treatment of 900°C for 14 hours + 878°C for 90 hours.

Bi System Oxide Superconductors by Oxalate Method, II

43067591 Tokyo NIHON FUNMATSU FUNTAI YAKIN KYOKAI in Japanese 16-19 May 88
p 63

[Report by Kiichi Oda, Hitoshi Kitaguchi, Jun Takada, Akiyoshi Ozaka and Yoshinori Muira, Faculty of Technology, Okayama University; Yasunori Ikeda, Mikio Takano and Yoshichika Bando, Institute for Chemical Research, Kyoto University; and Yasuo Takeda, Faculty of Liberal Arts, Kyoto University]

[Text] 1. Introduction

While the T_c of the oxide high-temperature superconductor $YBa_2Cu_3O_x$ is 90K, a material with a higher T_c is desired for practical use. The Bi-Sr-Ca-Cu-O system superconductor discovered by Maeda et al. (Metal Materials Laboratory) showing a T_c value of 105K harbors possibilities as a future promising material with a T_c value higher than that of the Y-Ba-Cu-O system. However, many problem points remain at present in the synthesis of Bi-Sr-Ca-Cu-O system ceramics containing a great number of high-temperature phases. In our research, ceramics in which part of the Bi was replaced by Pb and the component composition of the Bi-Sr-Ca-Cu-O system compound was changed was synthesized by the oxalate method, and improvements were discovered in the forming amount and electric characteristic of high-temperature phases. This report will describe the results.

2. Experiment Method

Oxalates with various composition ratios were synthesized under precipitation reaction using ammonium oxalate and various nitrates of Bi, Pb, Sr and Ca as the starting materials. After drying the oxalate at 90°C in air for 1 hour and allowing it to react pyrolytically at 500°C for 2 hours, it was pulverized and mixed, and it was given preliminary sintering at 800°C for 12 hours. Then, after pulverizing and mixing it again in an agate mortar, it was press molded (diameter 20 mm, thickness about 2 mm) at 600 kg/cm² and sintered at a temperature of 800°-900°C in air for 10-300 hours. Identification of the crystal phase by X-ray diffraction, measurement of electric resistance by SEM observation and four-terminal method, and measurement of the Meissner effect were conducted on the samples obtained.

3. Experiment Results

The powder X-ray diffraction result of the sintering time effect at a sintering temperature of 835°C is shown in Figure 1 for samples in which the composition ratio of Bi:Pb:Sr:Ca:Cu was 0.7:0.3:1:1:1.8. It was ascertained by means of sintering for 29 hours that high-temperature phases ($a = 5.4$, $b = 27$, $c = 37\text{\AA}$), low-temperature phases ($\text{Bi}_4\text{Sr}_3\text{Ca}_3\text{Cu}_4\text{O}_x$: $a = 5.4$, $b = 27$, $c = 30.6\text{\AA}$), Ca_2PbO_4 and $(\text{Ca,Sr})_3\text{Cu}_5\text{O}_8$ were formed. When sintering was conducted for a long time, however, the forming amount of high-temperature phases was gradually increased, the low-temperature phases were reduced, and the Ca_2PbO_4 was also reduced. It can be estimated from the X-ray diffraction result that about 80 percent of the high-temperature phases existed at 244 hours of sintering. Plate-shaped particles with a particle diameter of 3–5 μm and a thickness of less than 1 μm were recognized on both the fracture and surface of all materials under SEM observation. From the measurement result of electric conductivity and the Meissner effect, the Bi-Pb-Sr-Ca-Cu-O system ceramics synthesized in this research showed that the T_{conset} was $\sim 120\text{K}$ and T_{offset} was $\sim 105\text{K}$, and the Meissner effect was similarly observed. It is clear from these results that the forming amount of high-temperature phases and the electric characteristic were improved by the addition of Pb in the Bi-Sr-Ca-Cu-O system.

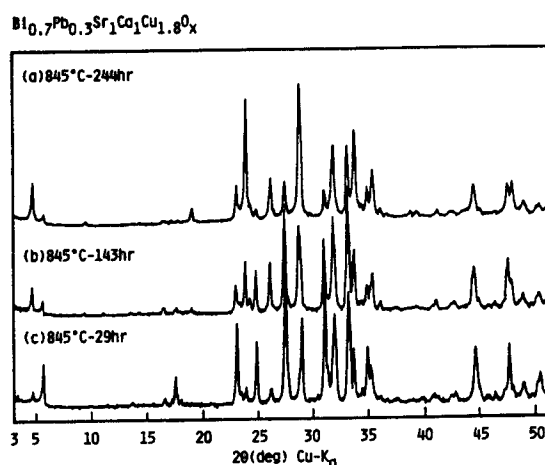


Figure 1. X-ray diffraction diagram

Superconducting Characteristics of Bi-Sr-Ca-Cu-O System Single Crystal

43067591 Tokyo NIHON FUNMATSU FUNTAI YAKIN KYOKAI in Japanese 16-19 May 88
p 64

[Report by Akihiko Yamaji, Makoto Hikata and Yoshizaki Hidaka, NTT Photo-electronic Research Institute]

[Text] 1. Objective

The Bi-Sr-Ca-Cu-O system has been announced as producing high-temperature superconducting oxides that do not contain rare earth elements, and it is attracting great attention as a material with a critical temperature not in excess of 100K. However, it is extremely difficult to obtain a haploid of T_c : 105K in ceramics from this material; only the mixed phase with the T_c phase has been obtained at our laboratory. Therefore, we are studying the means of accomplishing a haploid separation by preparing a single crystal. Although we have not yet obtained a single phase with a T_c of 105K, we will report here on the properties of the low T_c phase single crystal.

2. Experiment Method

Using Bi_2O_3 , SrCO_3 , CaCO_3 and CuO as the materials, a single crystal was prepared by cooling down the fusion liquid in which the Br:Sr:Ca:Cu ratio was variously changed. After being maintained in a platinum crucible at a temperature of 950°C for several hours, it was cooled down to 800°C at the rate of $3^\circ\text{C}/\text{hour}$. Analysis was conducted of the prepared crystal by electron beam and X-ray diffraction. Nondestructive composition analysis was conducted using EPMA.

3. Experiment Results

Three types of crystals with different components were obtained. The composition ratio of these three types of crystals according to EPMA measurement was $\text{Bi}_{4.4}(\text{Sr}_{3.6}\text{Ca}_2)\text{Cu}_4\text{O}_z(\text{C1})$, $\text{Bi}_{4.4}(\text{Sr}_{4.2}\text{Ca}_{1.4})\text{Cu}_4\text{O}_z(\text{C2})$ and $\text{Bi}_{4.6}(\text{Sr}_{2.4}\text{Ca}_1)\text{Cu}_2\text{O}_z(\text{C3})$, indicating that all three types of crystals had a strong cleavage property and that it had a layer structure. It became clear as a result of electron beam diffraction of the C1 crystal that it has a superlattice structure in the b-axis direction. A precession photo of the C1 crystal is shown in Figure 1 [photo not reproduced]. The C1 crystal

lattice constants are $a = 5.403\text{\AA}$, $b = 5.395\text{\AA}$ ($26.98\text{\AA} = 5 \times 5.395\text{\AA}$), $c = 30.70\text{\AA}$, and it has an orthorhombic system crystal lattice. The C2 single crystal shows practically the same lattice constants as the C1 crystal, but the lattice constants of the C3 single crystal are $a = 5.3\text{\AA}$, $b \sim a(b \sim 5a)$, $c = 24.5\text{\AA}$; although the a-axis and b-axis of the C3 single crystal do not differ from those of the C1 and C2 crystals, the c-axis is shorter and it does differ. (The data on the C1 single crystal were obtained by measurement by a four-wheel goniometer, and the data on the C3 single crystal were obtained by means of a Wessenbery photo.) The C1 and C2 single crystals showed superconducting characteristics, but the C3 single crystal did not, even when cooled down to 4.2K. The resistance temperature dependency of the C1 and C2 single crystals is shown in Figure 2.

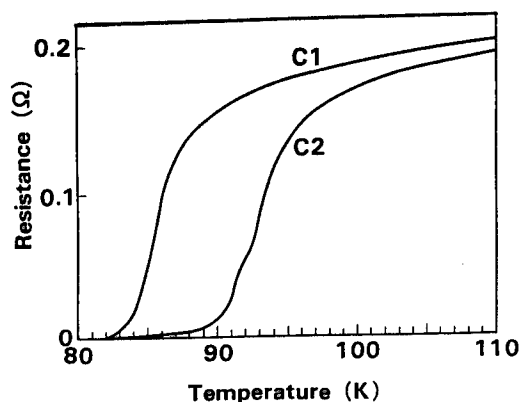


Figure 2. Resistance temperature dependency of C1 and C2 single crystals

Superconducting Characteristics of Ti-Ba-Ca-Cu-O System Superconductors

43067591 Tokyo NIHON FUNMATSU FUNTAI YAKIN KYOKAI in Japanese 16-19 May 88
p 65

[Report by Yuichi Shimakawa, Yoshimi Kubo, Takashi Namako and Hitoshi Igarashi, Basic Research Institute, Nippon Electric Co., Ltd.; and Tetsuro Sato, Environment Technology Research Institute, Nippon Electric Co., Ltd.]

[Text] The Bi-Sr-Ca-Cu-O system and the Ti-Ba-Ca-Cu-O system have recently been reported in succession as superconductors with a transition temperature (T_c) exceeding 100K. In our research, the Ti-Ba-Ca-Cu-O system superconductor was synthesized, and the structure and superconducting characteristics were ascertained by measuring the electric resistance, AC susceptibility, EPMA and X-ray diffraction.

The samples were synthesized by the oxide method. Ti_2O_3 , CaO and oxide obtained by reacting $BaCO_3$ and CuO in advance were used as materials; after mixing and press molding, they were sintered at 900°C in air for 5 minutes. No preliminary sintering was conducted. The temperature change of electric resistance of samples mixed in various ratios is shown in the diagram in Figure 1. The sample that showed the highest transition temperature at $T_{c\text{onset}} \sim 120K$ was the sample mixed at the ratio of Ti:Ba:Ca:Cu = 2:2:2:3, wherein $T_{c\text{end}} = 106K$. Furthermore, diamagnetism was confirmed at a temperature of slightly less than 110K in the AC susceptibility measurement, and it rose in stages in the neighborhood of 100K and 110K. It can be said from these results that the phases $T_c \sim 110K$ and $\sim 100K$ exist in this system. It is clear from EPMA and X-ray diffraction that the phase of $T_c \sim 110K$ is expressed by $Ti_2Ba_2Ca_2Cu_3O_x$ (2223 phase) and is the unit structure of the tetragonal $5.45 \times 5.45 \times 35.6$ (Å), while the phase of $T_c \sim 100K$ is expressed by $Ti_2Ba_2Ca_1Cu_2O_x$ (2212 phase) and is the unit structure of the tetragonal $5.45 \times 5.45 \times 29.3$ (Å). These structures, as shown in Figure 2, can be considered as the BaO, CuO₂ and Ca layers entering between the Tl_2O_2 layers, and it is believed that as proposed in the Bi-Sr-Ca-Cu-O system superconductor, it is a structure with the Cu and Ca layers inserted in the high T_c 2223 phase and the low T_c 2212 phase.

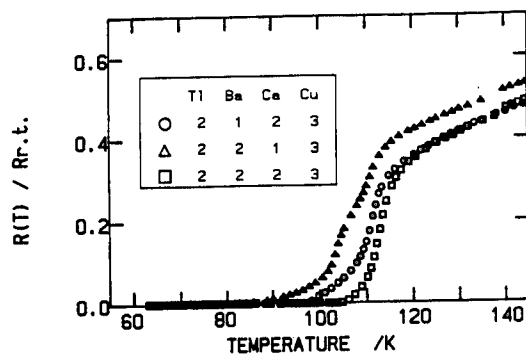


Figure 1. Temperature change of electric resistance

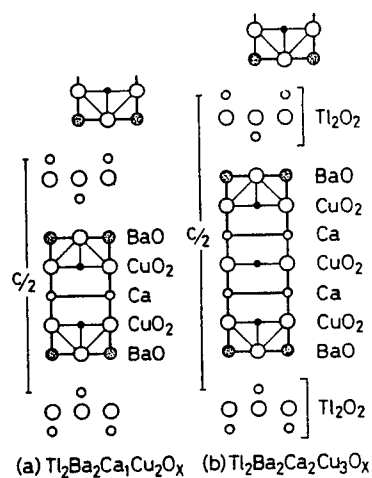


Figure 2. Crystal structure model

Crystal Structure, Superconductivity of $\text{YBa}_2\text{Cu}_3\text{O}_{7-\delta}$

43067591 Tokyo NIHON FUNMATSU FUNTAI YAKIN KYOKAI in Japanese 16-19 May 88
p 66

[Report by Yutaka Ueda and Koji Kosuga, Faculty of Science, Kyoto University]

[Text] Introduction

It is important to ascertain the physical property changes due to the change of δ in the $\text{YBa}_2\text{Cu}_3\text{O}_{7-\delta}$ system in order to elucidate the superconducting mechanism of this material. Many research reports have been made on this, but these reports have varied among the researching members. The method of sample preparation can be considered as one of the reasons for this. Samples having different δ are prepared by quenching at various temperatures utilizing the property that this material causes oxygen deficiency with a rise in temperature under equal oxygen pressure. However, the disordering of oxygen at a position ($\frac{1}{2}00$) and b position ($0\frac{1}{2}0$) occurs simultaneously with oxygen deficiency at temperature rise, the occupancy rate of both positions becomes equal at 650°C in air at $y = 7 - \delta = 6.5$, and it transfers from orthorhombic to tetragonal. Therefore, it is a question of whether or not samples having an order degree of 1 have been available in various oxygen compositions when obtaining samples by quenching. In this research we endeavored to carry out synthesizing of samples in a regulated manner, i.e., the synthesizing of samples with the originally vacant a position left completely vacant and those having various δ with the b position partially occupied, and then we studied the electrical properties. Here are the results.

Experiment and Results

The synthesis of samples was carried out using a specially designed thermal weight balance, and reduction was conducted by N_2 gas or argon gas. The orthorhombic-tetragonal transition at 650°C was confirmed in this case by allowing the scribing of a TG curve in air every time, and the oxygen composition was decided in situ based on the difference between the weight at that point and the final weight. The lattice constant change by oxygen composition is shown in Figure 1. There are points that differ from those that have been reported up to now in the composition changes obtained. As reported in a previous report, a change in the a and b axes near each other is shown in

the case of the temperature change of the lattice constants. This is because the occupancy of oxygen also occurs in a position which was originally vacant (i.e., disordering occurs), and similar changes have also been reported in the case of samples obtained by quenching. In the samples in this research, the a-axis increased linearly together with the δ increase (showing an expansion coefficient practically the same as that of the c-axis) and only the b-axis was reduced, showing a change as if approaching the a-axis. It can be considered from this fact that the target $\text{YBa}_2\text{Cu}_3\text{O}_{7-\delta}$ with the a position completely vacant and the b position with various δ partially occupied by oxygen atoms was synthesized. Moreover, the orthorhombic range was extended up to $y = 7 - \delta = 6.2$ neighborhood in the synthesis method of this research. The electric resistance and the magnetic field dependency of the resistance are most interesting, and we will report on these results at another time.

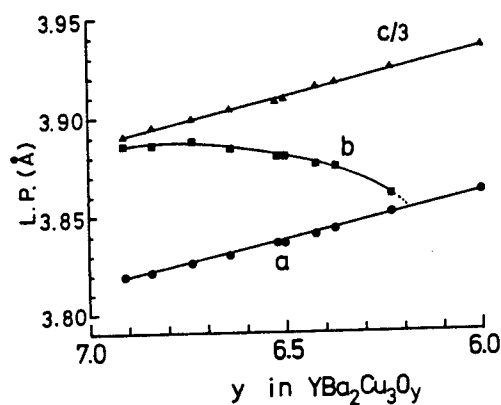


Figure 1. Lattice constant change by oxygen composition

Crystal Structure, Superconductivity of $\text{Sm}_x\text{Ba}_{1-x}\text{CuO}_y$ System

43067591 Tokyo NIHON FUNMATSU FUNTAI YAKIN KYOKAI in Japanese 16-19 May 88
p 67

[Report by Hiroaki Toda, Yutaka Ueda and Koji Kosuge, Faculty of Science,
Kyoto University]

[Text] Introduction

$(\text{R}_E)_{1/3}\text{Ba}_{2/3}\text{CuO}_y$ (R_E : Y and lanthanides elements, $3y = 7$) is a superconductor of $T_c \approx 90\text{K}$. Incidentally, it has been found that it is haploid only in $x = 1/3$ (so-called 123 phase) in the case of $\text{Y}_x\text{Ba}_{1-x}\text{CuO}_y$, and the solution range (x width) is extremely small. In contrast, however, in the case of Y in the $\text{La}_x\text{Ba}_{1-x}\text{CuO}_y$ system, the solution range ($1/3 \leq x \leq 0.5$) existed and the structure¹ of $\text{La}_{0.5}\text{Ba}_{0.5}\text{CuO}_y$ was tetragonal, similar to that of the (123) phase. In our research, the solution range of $\text{R}_E = \text{Sm}$ was examined and the structure and superconducting characteristics were studied.

Experiment Method

Samples were obtained using Sm_2O_3 , BaCO_3 and CuO as materials, and repeating sintering at 900°C in air. Finally, after treatment at 850°C in oxygen atmosphere, the sample was cooled down to room temperature. Electric resistance was measured by the ordinary four-terminal method.

Experiment Results

The $\text{Sm}_x\text{Ba}_{1-x}\text{CuO}_y$ system was a haploid at $1/3 \leq x \leq 0.45$. The lattice constant change is shown in Figure 1. The crystal shape gradually showed the shortening of the length difference of the a and b axes with the increase of x from the orthorhombic of $x = 1/3$; it looked like a tetragonal in the neighborhood of $x = 0.45$, but strictly speaking, it is doubtful that it could be called a tetragonal. The appearance of this change is similar to the temperature change of the lattice constants in the (123) phase. Since the oxygen deficiency and disordering of the ordered array of oxygen in the Cu 1 surface occurs simultaneously in the temperature change of the (123) phase, the change of eliminating the thermal expansion component of the lattice constants corresponds to the change of oxygen occupancy rate in a position ($1/200$) and b position ($0 1/2 0$) of the Cu 1 surface². It can be considered that

the excessive $\text{Sm}(x-1/3)$ enters the Ba position in $\text{Sm}_x\text{Ba}_{1-x}\text{CuO}_y$. The Cu 1 surface is held between the BaO surfaces in this case, and it can be considered that Sm entering the BaO surface may exert an effect on the oxygen concentration and array in the Cu 1 surface. Although it is not clear whether the lattice constant change brought about by the increase of the observed x is caused by the direct lattice change as Sm enters the Ba site or by the secondary effect due to the changing of the oxygen concentration and array in the Cu 1 surface as Sm enters the Ba site, it can be considered as the oxygen content or array of the Cu 1 surface changing as a result of both atoms in the Sm site and Ba site mixing, judging from the similarity with the temperature change of the lattice constants of the (123) phase. Moreover, the electric resistance drops after going through two stages (T_{c1} , T_{c2}). Both T_{c1} and T_{c2} , as shown in Figure 1, become low with the increase of x , and the difference becomes larger. The $T_{\text{c offset}}$ temperature becomes low with the increase of x and it does not show zero resistance even at 4.2K at more than $x \geq 0.43$.

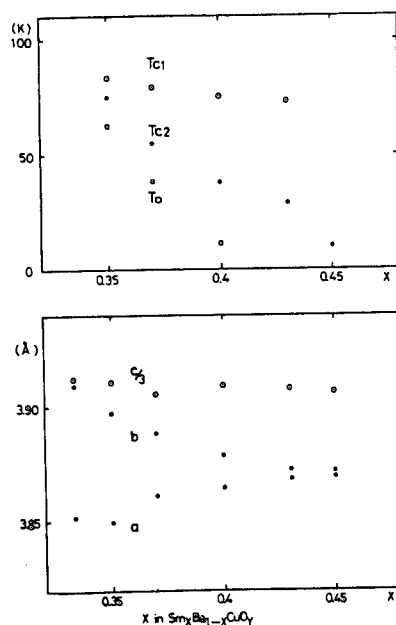


Figure 1. Lattice constant change

References

1. L. Er-Rakho, et al., J. Solid State Chem. 37, 151, 1981.
2. Hiroshi Ueda, et al., Powder and Powder Metallurgy, 34, 636, 1987.

Powder Metallurgy Composite Products Using HIP Method

43067591 Tokyo NIHON FUNMATSU FUNTAI YAKIN KYOKAI in Japanese 16-19 May 88
pp 142-143

[Report by Nobuyasu Kawai and Hiroshi Takigawa, Materials Research Institute of Kobe Steel, Ltd.: "Development of Powder Metallurgy Composite Products Using HIP Method"]

[Text] 1. Introduction

To meet the demand for improved and more complex performance and for advanced qualities of components in the various industries, the manufacture of composite materials based on diffusion connection has been highlighted recently. What has been attracting most attention is a molding method by which powder materials can be solidified based on HIP (hot isostatic processing). This method, whereby powder materials can be solidified and molded based on the HIP method and at the same time joined with dissimilar materials, can be applied to products of complex configuration with ease, covering wide areas of application. Examples of concrete development include a valve body for an oil well, a roll for a cold work mill, and a cylinder for an injection molding machine. In this report, we will discuss the injection molding machine cylinder for plastics engineering, in particular, and report the results of the various properties of the lining alloy produced on the basis of the HIP method aimed at improving the corrosion and abrasion resistance.

2. Method

At Kobe Steel, we produced a Co-based metallurgy powder that is excellent in terms of corrosion and abrasion resistance by means of the Ar gas atomizing method, as illustrated in Figure 1. This powder was filled into the clearance between an SCM 440 steel cylinder and a mild steel capsule in a vacuum state and sealed. Then, HIP processing was carried out at a temperature of 950°C and a pressure of 1000 kg/cm²; machining was performed to remove the internal capsule, and a cylinder lined with a 2 mm thick layer was produced. Tests to confirm the physical properties involved measuring the strength of the connected members, the microscopic organization, mechanical properties, high temperature, corrosion resistance, abrasion resistance, and expansion coefficient of the alloy. As a practical equipment test, an

effort was made to obtain the lifetime of the equipment by molding various kinds of engineering plastics with an injection molding machine. Co-based and Ni-based centrifugal casting materials and nitrided steel, which are very popular, were used as reference materials. Table 1 shows the composition of these alloys.

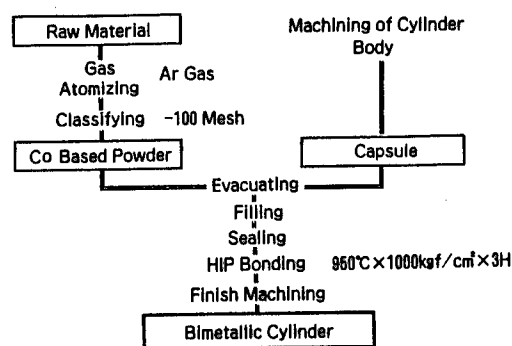


Figure 1. Manufacturing of complex cylinder according to HIP method

Table 1. Composition of HIP-Based Alloy and of Reference Materials

Materials	Symbols	(wt %)							
		Co	Cr	Ni	W	Mo	B	Si	C
HIPed Lining Alloy	HA	Bal	25.0	16.0	10.0	—	3.0	3.0	0.80
Co Based Centrifugal Cast Alloy	CC	Bal	20.0	13.5	15.0	—	3.5	3.5	1.10
Ni Based Centrifugal Cast Alloy	NC	—	16.8	Bal	—	1.8	3.0	5.0	0.60
Nitrided Steel	NS	Fe Bal	1.4	—	—	0.2	Al 0.8	0.2	0.45

3. Results

1) The diffusion layer of the connection member was about 50 μm in thickness; the deposit of an abnormal layer was not observed. The tensile strength in the connection section was found to be 40.9 kg/mm^2 . This value is satisfactory in relation to the calculated values (12 to 24 kg/mm^2) of tensile stress produced under ordinary injection molding conditions in the peripheral direction of the connection member.

2) The abrasion resistance of the HIP alloys evaluated by the Ohgoshi method-based abrasion test exceeded the values of the reference material over the entire sliding speed range, as illustrated in Figure 2. This is considered attributable to the uniform and microscopic distribution of the hard particles of fine B (Cr, W).

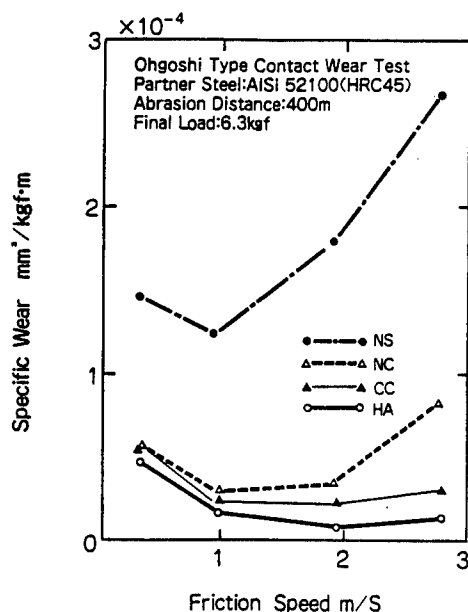


Figure 2. Abrasion test result

3) The result of the practical equipment test, shown in Table 2, indicates that the injection molding of engineering plastics, including 30-45 percent glass fiber, can provide a maximum lifetime exceeding 14 months--a value five to six times that of conventional nitrided steel.

Table 2. Practical Equipment Test Result for Injection and Molding Machine

Compound Resin	Injection Temp. °C	Injection Pressure tsi/csi	Injection Cycle sec	Life	
				HIPed Cylinder	Conventional
PC+G30%	300	1500	30-40	18 months, continue	---
PC+G30%	300	1500	30-40	13 months, 45mm worn, continue	5-6 months (Nitrided)
PBT+G30%	250	800	25-30	17 months, continue	---
POM+G20%	270	1750	25-30	20 months, continue	8 months (Nitrided)
POM+G45%	300	1750	25-30	19 months, continue	15 months (Centrifugal cast)
PES+G30%	350	2700	45	12 months, continue	---
PC+G30%	---	---	---	6310hr, 38mm worn, continue	---

As stated, it has been ascertained that the use of the HIP method is capable of producing the cylinder of an injection molding machine for plastics engineering which is excellent in corrosion resistance and abrasion resistance. Based on these achievements, further attempts are being made to apply the HIP method to the manufacture of a nonmagnetic cylinder for "plamag" [phonetic] using high Mn nonmagnetic steel, a superabrasion resistant cylinder including WC powder, or a bi-axial cylinder which is excellent for kneading. This technology can also be applied to the cylinder of an injection and molding machine for ceramics and metal powder, for which high expectations are harbored for future demand.

Superplasticity Behavior, Mechanical Properties of Superalloy Composites

43067591 Tokyo NIHON FUNMATSU FUNTAI YAKIN KYOKAI in Japanese 16-19 May 88
pp 144-145

[Report by Nobuyasu Kawai, Hiroshi Takigawa, Kenji Iwai and Seiya Furuta,
Engineering Development Head Office of Kobe Steel: "Superplasticity
Behavior and Mechanical Properties of Superalloy Composite Materials Molded
by the HIP Method"]

[Text] 1. Objective

A superalloy that is excellent in terms of high-temperature performance is required in order to develop high-performance gas turbines. In particular, a turbine disk calls for the development of materials that are capable of withstanding high temperature, large centrifugal force and thermal stress. Efforts are being made to apply powder metallurgy technology so as to meet this demand. The aim of this research is to manufacture complex disks that possess superior tensile characteristics, along with the low cycle fatigue characteristics required at the center of the disk and the creep characteristics required of the peripheral parts by using the enhanced complexity of powder metallurgy. In this article, we will report on the result of studying superplasticity behavior and the mechanical properties of a one-piece type complex material which consists of two kinds of superalloy powders solidified by the HIP method.

2. Method

Table 1 shows the chemical composition of four kinds of Ni-based superalloy powders produced by the Ar gas atomizing method. At Kobe Steel, we selected two of these alloy powders, on which we carried out HIP processing two times, thus producing the required composite material; we then endeavored to ascertain the superplasticity characteristics, tensile characteristics and stress rupture characteristics of the material. As a typical example, Figure 1 shows the manufacturing method, the heat treatment and the characteristics evaluation requirements of the material when TMP-3 and Rene 95 powder materials are used.

Table 1. Chemical Organization of Test Samples

Name of material	Chemical composition of material												
	C	Cr	Co	Mo	W	Al	Ti	V	B	Zr	Hf	Nb	Ni
TMP-3	0.07	10.8	6.9	3.1	3.4	3.9	2.8	-	0.01	0.05	-	3.9	bal.
Rene 95	0.05	12.9	8.3	3.5	3.4	3.6	2.5	-	-	0.04	-	3.5	bal.
AF 115	0.05	10.9	14.9	2.8	5.9	3.7	3.8	-	0.018	0.05	0.8	1.9	bal.
Mod. IN 100	0.07	12.4	18.5	3.2	-	4.3	5.0	0.8	0.020	0.06	-	-	bal.

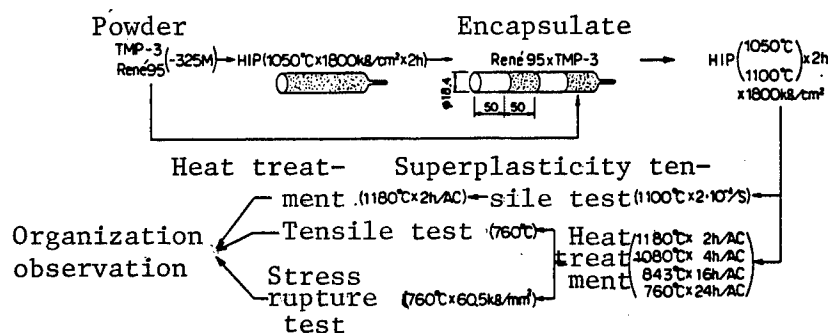


Figure 1. Manufacturing method, heat treatment and characteristic evaluation requirement for composite

3. Result

1) Table 2 shows the superplasticity tensile test result. Based on the combination of TMP-3 and Rene 95, the total elongation of the test material exhibited a low value even when an attempt was made to change the second HIP temperature, which is considered to affect the superplasticity characteristics, and it was subject to rupture at the connected section or the Rene 95 member. On the other hand, the total elongation of the other two composite materials was around 400 percent, and they were not subject to rupture. However, in the case of the latter combination, the elongation of Mod. IN 100 was very small. When superplasticity forging is considered, the combination of TMP-3 and AF 115, both of which show similar elongation, were found to be the most suitable.

2) The high-temperature tensile test result at a temperature of 760°C revealed that only the combination of Mod. IN 100 and AF 115 was subject to rupture at the joint section. In the case of the other combinations, the parent material was subject to rupture on the part of TMP-3.

The greatest values were exhibited by the TMP-3 and AF 115 combination: the tensile strength was 111.6 kg/mm², while the elongation was 5.0 percent.

Table 2. Superplasticity Tensile Test Result for Composites

Material	Second HIP temperature (°C)	Elongation (%)	Rupture position
TMP-3 x Rene 95	1050	TMP-3(56) x Rene 95 (156)	Connection section
TMP-3 x Rene 95	1100	TMP-3(38) x Rene 95 (187)	Rene 95
TMP-3 x AF 115	1075	TMP-3(163) x AF 115 (225)	--
Mod. IN 100 x AF 115	1075	IN 100(13) x AF 115 (400)	--

3) Photo 1 [not reproduced] shows the microscopic organization of Rene 95 at the joint section. No harmful phase was observed at the boundary. The TMP-3 exhibited a fine organization, as it was subjected to solution processing at a temperature lower than the perfect solidification temperature of the r phase. On the other hand, the Rene 95 exhibited a coarse organization--quite opposite to the TMP-3.

4) The stress rupture test result revealed that a combination of Mod. IN 100 and AF 115 was subject to rupture at the joint section similar to that in the high-temperature tensile test. Other combinations were subject to rupture at the section of TMP-3. This is because the TMP-3 exhibited a fine crystal organization. However, the longest rupture life was found when AF 115 was used in the combination.

As reported, the research result of the connection performance, the superplasticity characteristics, and the mechanical properties makes clear that the combination of TMP-3 and AF 115 is the most superior as a superalloy composite.

This research was carried out as part of the "research and development of high-performance crystal control alloys" based on the next-generation industrial basic technology research and development system established by the Agency of Industrial Science and Technology of the Ministry of International Trade and Industry.

Mechanical Properties of Superalloy Compound Disk

43067591 Tokyo NIHON FUNMATSU FUNTAI YAKIN KYOKAI in Japanese 16-19 May 88
pp 146-147

[Report by Nobuyasu Kawai, Hiroshi Takigawa, Tomiharu Matsushita, Kenji Iwai, and Seiya, Engineering Development Head Office of Kobe Steel: "Mechanical Properties of Superplasticity Forged Superalloy Compound Disk"]

[Text] 1. Objective

The manufacture of turbine disks, which are widely used for industrial gas turbines, is undergoing a gradual change from the conventional welding and forging method to the newly developed powder metallurgy method. The aim of using the powder metallurgy method is to meet the demand for improved high alloy disks in order to improve efficiency in view of the rise in inlet temperature of the turbine. In addition, dissimilar characteristics are required for the central parts and the peripheral parts. In the central parts, proper fatigue and tensile strength are required, while in the peripheral parts improved creep strength is needed. In this report, we will describe the results of our study of the manufacture of superalloy compound disks based on the powder metallurgy method, which is capable of satisfying the simultaneous strength requirements along with those of the mechanical properties.

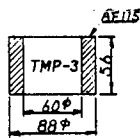
2. Method

Table 1 shows the chemical composition of two kinds of Ni-based superalloy powders obtained by the argon gas atomizing method. At Kobe Steel, we produced a forging preform molded by the HIP method whereby the central parts were comprised of TMP-3 while the peripheral parts were comprised of AF 115 based on the powder combination specified in Table 2. Then, forging was carried out under a superplasticity condition where the temperature was 1080°C while the strain speed was $2 \times 10^{-4}/S$. After the forging operation, an endeavor was made to carry out solidification at 1185°C x 2 hr/AC and the age hardening at 760°C x 16 hr/AC. After the heat treatment, a pancake-shaped test piece was taken from the position indicated in Figure 1, and the test was carried out. Table 3 shows the test requirements.

Table 1. Chemical Composition of Test Piece Materials (Wt%)

Name of material	C	Cr	Co	Mo	W	Al	Ti	B	Zr	Hf	Nb	Ni
TMP-3	0.07	10.8	7.1	3.1	3.4	3.9	2.8	0.01	0.05	-	4.1	bal.
AF 115	0.05	10.9	14.9	2.8	5.9	3.7	3.8	0.02	0.05	0.8	1.9	bal.

Table 2. Manufacturing Requirements for Superplasticity Forging Material

Disk (P: pancake D: disk)	Primary HIP (1080°C x 1800 kg/cm ² x 2h)		Secondary HIP (1100°C x 1800 kg/cm ² x 2h)		Raw material configuration
	Alloy	Grain size	Alloy	Grain size	
P-1	AF 115	-250M	TMP-3	-250M	
P-2	AF 115	-325M	TMP-3	-150/+250M	
P-3	AF 115	-150/+325M	TMP-3	-250M	
D-1	TMP-3	-250M	AF 115	-250M	

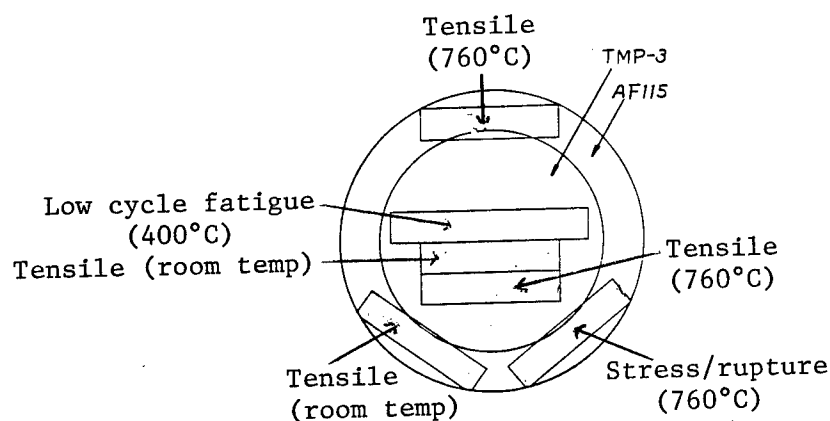


Figure 1. Cutting position of test piece from pancake (P-1)

Table 3. Test Requirements

Tensile	Temperature: room temp, 760°C, strain speed: 0.005 %/min up to 0.2% yield strength
Stress rupture	760°C x 60.5 kg/mm ²
Low cycle fatigue	Load control, R _o = 0, σ_{\max} : 112 kg/mm ² , temperature: 400°C, frequency: 1 Hz

3. Result

The following test results were obtained in the research on superalloy composite disks:

1) No crack or abnormal organization was observed around the joint boundary of the two alloys. An extremely homogeneous organization was presented. No difference in the grain size of the powder sufficient to affect forging was observed within the scope of the experiment. (See Figure 2)

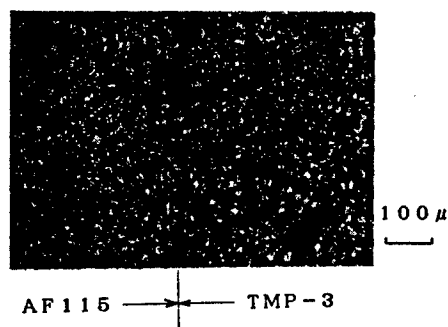


Figure 2. Microscopic organization at joint boundary of P-1 disk

- 2) In practice, no difference was observed in the tensile strength at ambient temperature between the central parts and the peripheral parts. However, a higher characteristic was obtained in the peripheral parts (AF 115) at a high temperature.
- 3) The low cycle fatigue test revealed that a cycle of more than 10^5 was obtained, indicating improvement in the performance due to the enhanced microscopic and homogeneous organization.
- 4) The stress rupture test result showed a rupture lifetime of 203 hours, which is a favorable high-temperature characteristic.
- 5) The metal flow of a 150 mm diameter disk with boss (Figure 3) was found capable of controlling the joining wire with various shapes of raw materials.

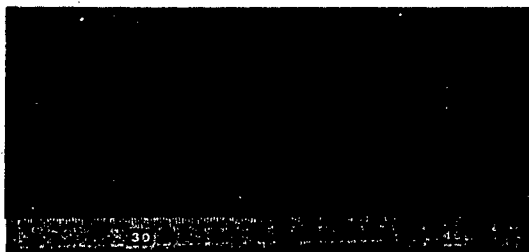


Figure 3. Microscopic organization at cross-section of embossed disk

This research was carried out as part of the "research and development of high-performance crystal control alloys."

Molding Tool Steel Powder by Hydraulic Pressure HIP

43067591 Tokyo NIHON FUNMATSU FUNTAI YAKIN KYOKAI in Japanese 16-19 May 88
pp 148-149

[Report by Nobuyasu Kawai, Tomiharu Matsushita, Tatsuo Yamazaki and Kanji Notomi, Engineering Head Office of Kobe Steel: "Experiment in Molding Tool Steel Powder by the Hydraulic Pressure HIP Method"]

[Text] 1. Objective

Generally, HIP is used for molding gas atomized powder. However, that molding method suffers from the disadvantage that the cycle time requires as long as 3-7 hours, and productivity is quite low, since gas (argon or nitrogen) is used as the pressure medium. To eliminate these disadvantages, at Kobe Steel a hydraulic pressure HIP method (called Quick-HIP or Q-HIP) was developed that is capable of sharply reducing the cycle time, to even a minute unit basis, as grease is used as the pressure medium. Furthermore, it has been confirmed that the characteristics of the molding obtained by the newly developed HIP method are by no means inferior to those of molding obtained by the conventional HIP method. In this report, we will discuss this new HIP method.

2. Method

The three kinds of gas atomized powder given in Table 1 were used as the test powder. The powder was filled into a mild steel capsule and sealed after vacuum heating deaeration to produce preforms for the hydraulic pressure HIP method. These preforms were heated for 2 hours in N_2 at a specified temperature, inserted into a pressure vessel together with heat resisting grease, and then given pressure treatment by the application of a 400 ton press. Figure 1 shows the concept of the HIP processing, while Table 2 shows the hydraulic pressure HIP requirements.

In this experiment, we prepared the gas pressurized HIP molding and SKD11 material specified in Table 2 as a reference material, in addition to the aforesaid hydraulic HIP molding, and carried out the various kinds of heat treatment listed in Table 2. Then, we carried out 1) dimension measurement of the molding; 2) density measurement; 3) microscopic organization observation; 4) tensile testing; and 5) breakdown resistance testing.

Table 1. Compositions of Powders and of Conventional Steel

Alloy	Composition (%)								Remarks
	C	Si	Mn	Cr	Mo	V	W	Co	
Adamite	1.93	0.79	0.91	1.20	0.28	—	—	—	Powder
SKD 11	1.53	0.31	0.31	12.22	1.03	0.38	—	—	Powder
	1.47	0.26	0.41	12.75	0.82	0.28	—	—	Conv. steel
KHA 30	1.29	0.49	—	3.63	5.10	2.91	6.09	7.75	Powder

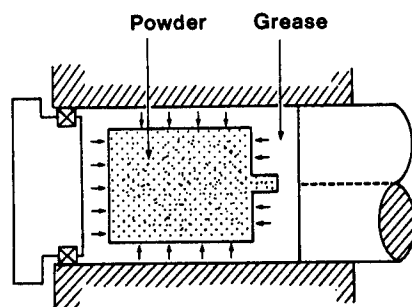


Figure 1. Schematic of Q-HIP

Table 2. Density (Heat Treated Condition) After Hot Compaction

Experiment Number	Alloy Powder	HIP'ing			Heat treatment	Density (% of theoretical)	Remarks
		Temperature(°C)	Pressure(kg/cm ²)	Time(min)			
1	Adamite	1050	1000	1	700°C/3hr, F.C.	99.7	Quick-HIP
2	"	"	5000	1	700°C/3hr, F.C.	100.0	
3	SKD11	1150	5000	1	1020°C/15min, 100, 150, 200, 290°C AC.	100.0	
4	KHA30	"	5000	1	900°C/2hr, F.C.	100.0	
5	Adamite	1050	200	60	700°C/3hr, F.C.	98.8	Conv. HIP
6	"	"	400	60	700°C/3hr, F.C.	100.0	
7	"	"	1000	60	700°C/3hr, F.C.	100.0	
8	SKD11	1100	800	60	1020°C/15min, 100, 150, 200, 290°C AC.	100.0	
9	KHA30	1150	1000	60	900°C/2hr, F.C.	100.0	

3. Result

The following results were obtained with regard to adamite steel powder, SKD11 steel powder and high-speed steel powder in the hydraulic HIP molding experiment:

- 1) The three kinds of powder were molded into a form in which the degree of density is improved by the hydraulic HIP processing, requiring one cycle of around 5 minutes. (See Table 2)
- 2) The contracting state of the preform based on the hydraulic HIP process corresponds to the deformation produced during conventional HIP processing. (Perfect isotropy)
- 3) The pressure required to obtain hydraulic HIP method-based high-density molding is higher than that used in conventional HIP operations.
- 4) The high-density powder material that can be obtained by the hydraulic HIP processing method has a microscopic organization, a breakdown resistance value and a strain characteristic value which are all similar to those of gas pressure-based HIP density materials. (See Figure 2)

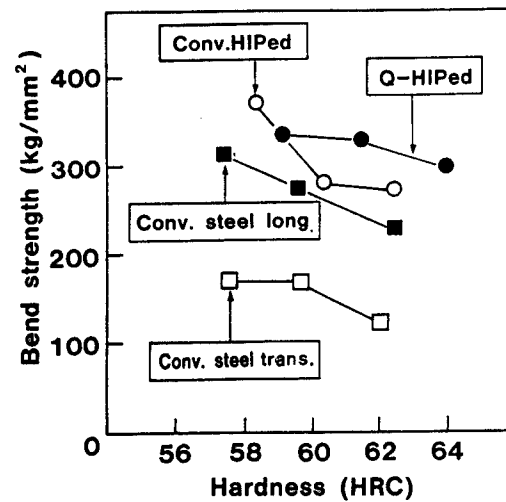


Figure 2. Bend strength (SKD11)

Sintering/Forging of Steel Copper Alloy Powder

43067591 Tokyo NIHON FUNMATSU FUNTAI YAKIN KYOKAI in Japanese 16-19 May 88
pp 150-151

[Report by Hiroshi Hamamoto, Kimio Kondo, Takao Kobayashi, Kazuhiko Ito and Kazuaki Nishini, Toyota Central Research Institute: "Sintering/Forging of Dispersion Reinforced Steel Copper Alloy Powder"]

[Text] 1. Objective

Aluminum dispersion copper alloy, which is excellent in high-temperature strength and conductance¹, is often used for resistance welding electrodes. Usually, this alloy is manufactured according to a method in which the internal oxidized powder is canned, and then the hot-extrusion process is used after vacuum deaeration. However, this manufacturing process involves some disadvantages in regard to the yield of material due to the numerous manufacturing processes. Other manufacturing methods not based on the internal oxidation method³ or the solidification method based on powder roll⁴ have also been reported.

A sintering/forging method is more capable of forming a near net shape than the exclusion method and of reducing the number of processes as well, but it is seldom used for the solidification of aluminum dispersion copper powder. In our research institute, we studied this manufacturing method, which affects the various characteristics of the sintered body of internal oxidized aluminum dispersion copper powder and the forged body of hot coining.

2. Experiment Method

We used Cu-0.33% Al water atomized alloy powder for the raw powder, and CuO powder (-5 μ m, 99.9% purity) as the oxygen supply source for the internal oxidation. The quantity of CuO powder to be added was set at 1.8-3.0, larger than 1.5 where the ratio of O/Al is the stoichiometric composition. The internal oxidation processing of the powder was carried out in a siliconite reactor at a temperature of 900°C for 5 hours after the powder was filled into a copper-lined stainless steel vessel. The processed powder was reduced in a hydrogen atmosphere of 900°C for 1 hour. Furthermore, an "atlighter" [phonetic] (content volume: 5 \pm 10 diameter steel ball adopted)

was used to carry out processing in air. The powder, which was again reduced in hydrogen atmosphere at a temperature of 900°C for 1 hour, was also adjusted. The powder thus obtained was molded at a pressure of 3-8 tons/cm² based on the metallic mold for the tensile test piece based on the standard of the Fine Particle and Powder Metallurgy Association, and was sintered in a nitrogen atmosphere at a temperature of 900°-1000°C for 30 minutes. The forging test piece, which had been preformed at a pressure of 6 tons/cm², was heated in nitrogen atmosphere at a temperature of 600°-1000°C for 15 minutes, then coining-forged into a specified tensile test piece shape at a pressure of 10 tons/cm² with a 250-ton knuckle joint press. We measured the density, the tensile characteristics, the hardness and the conductance of these test pieces and observed their organization and fractures.

3. Experiment Results

3.1. The sintered body of the powder which underwent internal oxidation processing exhibited improvement in its tensile strength in proportion to the increase in the density and sintering temperature. However, we failed to obtain a tensile strength in excess of 40 kg/cm². As illustrated in Figure 1, the forging operation improved the tensile strength: 47 kg/cm² was obtained. The elongation was improved as well; it may reach 4 percent (Figure 1).

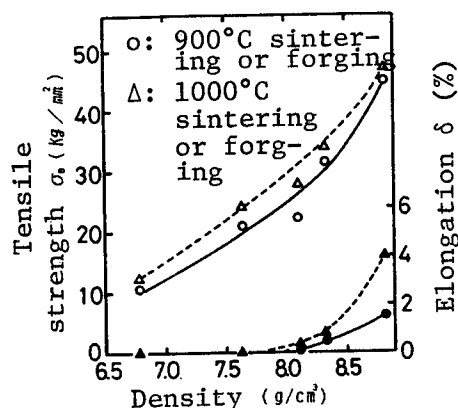


Figure 1. Influence of density

3.2. Satisfactory density was not available at a forging temperature below 800°C, but the test pieces reached the calculated density at a temperature of over 900°C. The tensile strength and elongation were improved in proportion to the increase in the forging temperature. In contrast, the hardness was increased in inverse proportion to the decrease in the forging temperature (Figure 2).

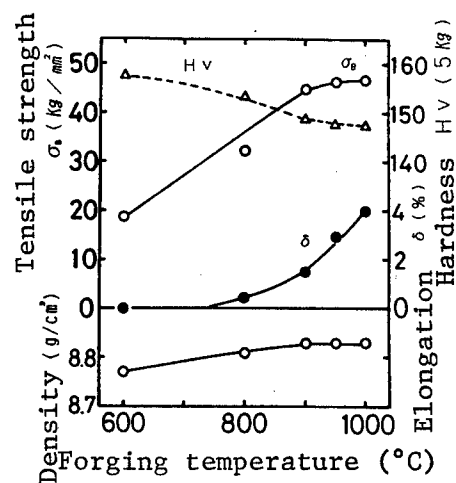
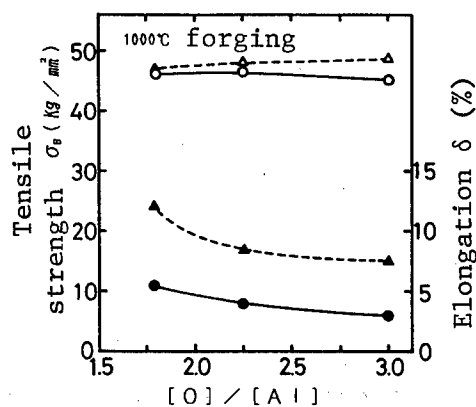


Figure 2. Influence of forging temperature

3.3. When atlighter [phonetic] processing was carried out after internal oxidation, the surface of the powder became smooth and the shape flat. When this powder was sintered or forged, the tensile strength was improved slightly and the elongation was also upgraded by about 200 percent, as shown in Figure 3. The results of fracture observation reveal that the forged body without atlighter [phonetic] processing was often subject to fracture between powder particles, while the forged body of the processed powder was less subject to fracture between particles, producing a fine dimple pattern. It is considered that the processed powder was improved in terms of sintering, thereby increasing the elongation dramatically, since it showed a contracting tendency, bringing about dimensional change at the time of sintering.



o: No atlighter [phonetic] processing
 Δ : Atlighter processing of 3 hours

Figure 3. Effect of atlighter processing

3.4. The greater the addition of CuO powder, which is the oxygen source during internal oxidation, the higher the values exhibited in terms of the tensile strength, the ambient temperature hardness and the annealing softening resistance of the forged body. However, the elongation and the conductance decreased, as indicated in Figure 4.

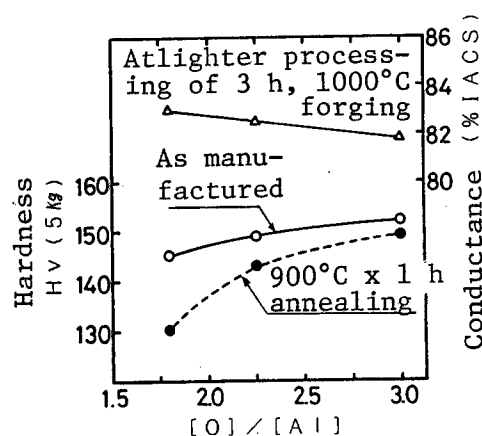


Figure 4. Effect of CuO powder addition

References

1. A.V. Nakarni: "High Conductivity Copper and Aluminum Alloys," E. Ling, P.W. Taubenblatt ed., The Metallurgy Society of AIME, New York, 77, 1984.
2. Yamada and Komatsu: "Academic Review of the Metallurgical Society of Japan," 37, 895, 1973.
3. Shinmi, Kawasaki, and Watanabe: Summary of a collection of reports given at 1985 fall convention of Fine Particles and Powder Metallurgy Association, 176.
4. Hirota, Kawasaki, and Watanabe: Summary of a collection of reports given at 1986 fall convention of Fine Particles and Powder Metallurgy Association, 80.

Relationship Between Processing, Mechanical Properties

43067591 Tokyo NIHON FUNMATSU FUNTAI YAKIN KYOKAI in Japanese 16-19 May 88
pp 152-153

[Report by Shinichiro Kakehashi, Masato Ohtsuki, and Toru Kono, Central Research Institute of Mitsubishi Metal Corp.: "Relationship Between Processing Capacity and Mechanical Properties of Fast Solidified Aluminum Alloy Powder During Forging Operation"]

[Text] 1. Objective

Compared with the HIP and exclusion methods, application of the powder forging method allows the processing of fast solidified aluminum alloy powder at lower cost, reducing the manufacturing process for products that have complex shapes.^{1,2} In this process, the degree of rupture dispersion of oxidized film on the powder surface caused by forging processing is considered to have a great effect on the mechanical properties of the material.³

In the research at our institute, we studied the powder forging materials for Al-Fe-based alloy, which is a heat-resistant alloy, and the influence its forging requirements exert on the various kinds of mechanical properties. The following is a report on our research.

2. Method

We used an air atomizing powder comprised of Al-9Fe-1.5V-1.0Zr to carry out metal molding of the powder, as shown in Figure 1. In an effort to improve the density of the metal mold, we selected an enclosed type and carried out hot coining; we then performed hot forging for the stamp forgings which is designed to fracture the oxidized film of the powder surface based on elasticity deformation, thus changing the draft. Based on this process we produced test pieces. The powder forming was carried out on the basis of a metallic mold produced in Sharpy configuration at a forming pressure of 6 tons/cm², while the forging operation was carried out after the test piece had been heated in Ar gas atmosphere up to the specified forging temperature. Then, a press machine was used to produce the test piece. The hot forging was carried out so that the forged body would extend in only one direction, which was assumed to be a tensile direction. Then, the specified test piece was cut out. Next, we studied the influence of the draft on the tensile

characteristics, observed the optical organization of the forged body, and examined the tensile fracture surfaces by means of a SEM image.

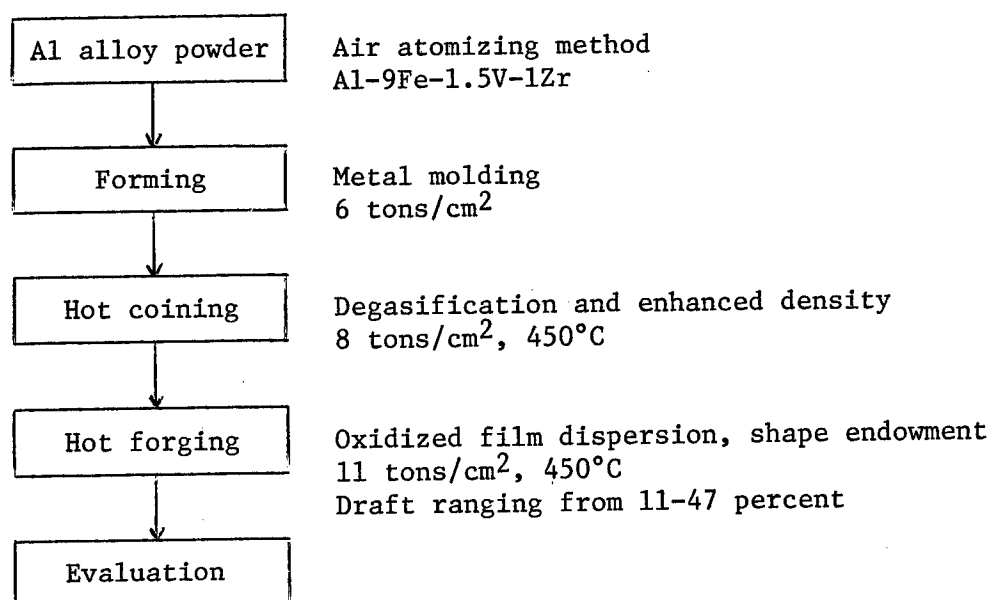


Figure 1. Evaluation process of Al-Fe group alloy powder

For the purpose of comparison, we also evaluated hot-excluded powder materials having the same composition. Furthermore, we carried out evaluation of forged and hot-excluded materials of Al-8Fe alloy powder into which only a trace of alloy elements had been added. The exclusion was carried out at an exclusion rate of 25 and a billet temperature of 450°C in the case of Al-9Fe-1.5V-1Zr and of 400°C in the case of Al-8Fe. The forging of Al-8Fe was also carried out at a temperature of 400°C.

3. Results

Photo 1 [not reproduced] shows the optical organization of the forged materials at each draft. We observed that the powder was subject to a gradual change to a flatter surface.

Figure 2 shows the results of tensile tests for forged and excluded materials at an ambient temperature. It can be seen that the tensile strength and elongation of the forged materials (flat materials and notched materials (shape configuration $a = 2$)) are increased in proportion to the rise in the draft. This phenomenon is believed to be attributable to the fact that the rise in the degree of processing accelerates the rupture dispersion of the dioxide film present on the powder surface, thus increasing the bonding strength. With regard to the excluded materials, the data on them was plotted in terms of exclusion ratio (25) and forging draft (96 percent).

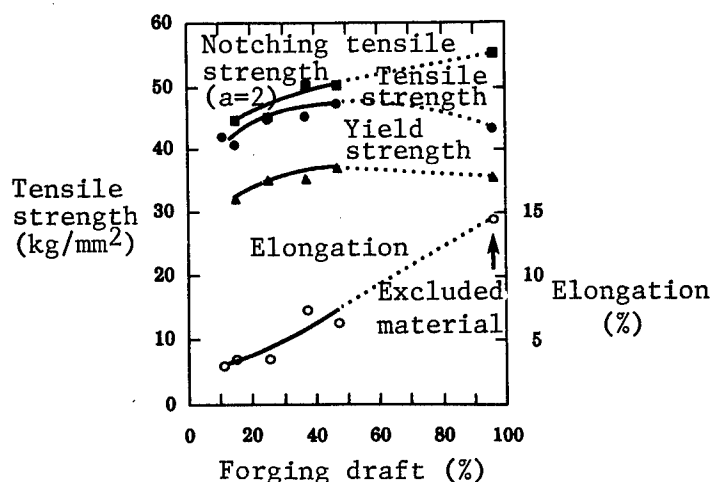


Figure 2. Relationship between forging processing output and mechanical properties

Figure 3 shows the high-temperature tensile properties of two kinds of Al-9Fe-1.5V-1Zr-based forged materials with different drafts (25 percent and 47 percent) and Al-8Fe forged materials with a draft of 25 percent. With regard to the tensile strength, we did not observe any marked difference due to the difference in the processing output. As for the elongation, the Al-9Fe-1.5V-1Zr-based materials exhibited a lower, positive temperature dependence in inverse proportion to the increase in processing output. The temperature dependence of the Al-8Fe-based materials was small even in the case of forged materials having a small processing output. Photo 2 [not reproduced] shows SEM images of the rupture plane in the ambient and hot-temperature tensile tests for the Al-9Fe-1.5V-1Zr forged materials with a draft of 25 percent. It was observed that at the ambient temperature, they are subject to rupture in the powder grain boundary, while a number of dimple patterns, which demonstrate ductile rupture, are present at a high temperature. This is considered attributable to the fact that they are softened within the powder grains at a high temperature, although the processing output is small and the bonding strength in the grain boundary is low, thereby accelerating the transannular rupture and increasing the transannular elongation as well. With regard to the Al-8Fe materials, their transannular strength is relatively low at ambient temperature, which is considered attributable to the low-temperature dependence of the elongation.

At another time we will discuss the influence exerted by the forging direction, the heat treatment and the amount of powder oxygen upon the mechanical properties.

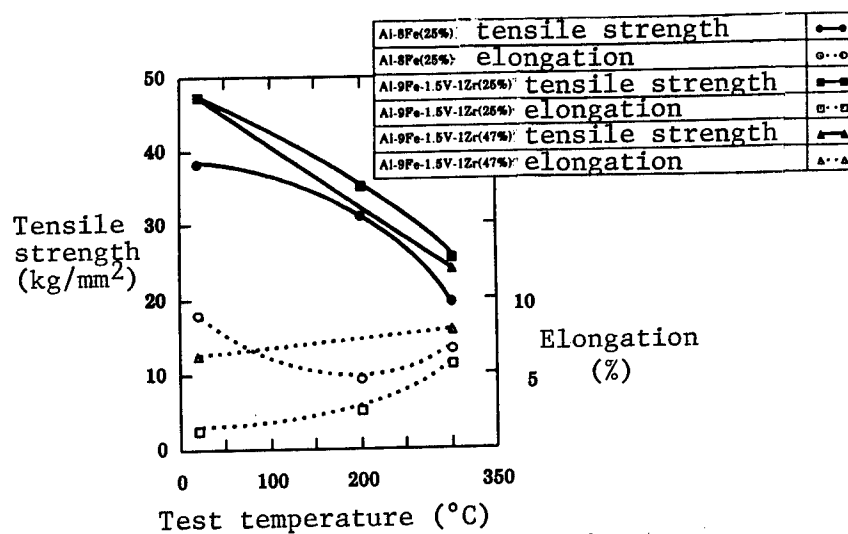


Figure 3. High-temperature characteristics of forged materials and excluded materials

References

1. Mahito Otsuki, Toru Kono, Teruyoshi Tanase and Osamu Mayama: Summary of collection of reports given at 1986 fall convention, 40-41.
2. Kono and Otsuki: Summary of collection of reports given at the 30th symposium of the Light Metals Association, 35, 1987.
3. Young-Wong Kim, W.M. Griffith and F.H. Froes: J. Metals, 37, 27-33, 1985.

WC Content in Cemented Carbide

43067591 Tokyo NIHON FUNMATSU FUNTAI YAKIN KYOKAI in Japanese 16-19 May 88
pp 194-195

[Report by Nobujiro Tsuchiya, Masahide Fukuda and Tsuyoshi Nakai, Fuji Dice Corp.; and Hisashi Suzuki, Engineering Department of Chiba Industrial University: "The Effect of β_t /WC Content Ratio on the Various Characteristics of WC- β_t -Co Alloy"]

[Text] I. Introduction

The cemented carbide based on WC- β_t -Co in the pseudo four-dimensional system to which β_t (SS of WC-TiC-TaC) belongs is one of the important sintered alloys used for cutting tools for steel, etc. The effect of the content of β_t or β (SS of WC-TiC) on the mechanical properties is a very important topic, on which numerous studies have been conducted.¹⁻⁵ According to these studies, the deflective strength (σ_m) drops in proportion to the increase in the β_t or (β) additives. However, there exists some difference in the σ_m among the nonadditive alloys, while some difference is also observed in the drop level of σ_m and the configuration of the strength drop curve. Reports explaining the reason for the drop in strength have been published since 1967. In our research, we studied the mechanical properties of the WC- β_t -16vol%Co alloy by changing the volumetric rates of β_t in various manners.

II. Sample and Experiment Method

We used WC powder (grain size 1.3, 3.0 μm), β_t powder (49/21/30, grain size ~2.0 μm) and Co powder, which are all available on the market, as the raw materials for our experiment. We prepared WC- β_t -16vol%Co alloy having various kinds of compounds on the basis of the standard vacuum sintering method (10^{-2} torr) after wet ball mill, drying, and forming operations. The sintering requirements were specified as (1380° and 1430°C) x 1 hr; then HIP treatment (1350°C x 1 hr) was carried out at in argon at 1000 atm in order to obtain the samples. Our aim was to investigate the respective samples in terms of the σ_m , hardness (Hv), the alloy organization, and the origin of breakage based on JIS-specified test pieces in regard to the β_t content. Using coarse particles mixed in the β_t for our experiment, we studied two cases: one in which the coarse particles were screened using

a 1000 mesh sieve, and the other in which the screened particles were further crushed before the experiment. The β_t that was used without additional treatment has been designated sample A, the β_t that was screened has been designated sample B, and the β_t that was screened and further crushed has been designated sample C.

III. Experiment Result

Figure 1 shows the results of measurement of σ_m in terms of β_t content (mass%) contained in the carbide. The values of each sample are very similar under the specified conditions. Figure 2 shows the dimensional (2a) distribution of the origin of breakage in terms of sample A. Figure 3 shows the distribution of σ_m corresponding to Figure 2. In accordance with Figure 2, the 2a distribution does not vary with the β_t content substantially, but this is not the case with the σ_m distribution. The $\bar{\sigma}_m$ or σ_m (max) drops in proportion to the increase in β_t . Photo 1 [not reproduced] provides an example of the origin of breakage. Each sample is assumed to be an agglomerate of β_t ranging up to about 30 μm . Figure 4 shows the result of Hv measurement. Figures 1 and 4 show the results sintered bodies produced at a temperature of 1430°C.

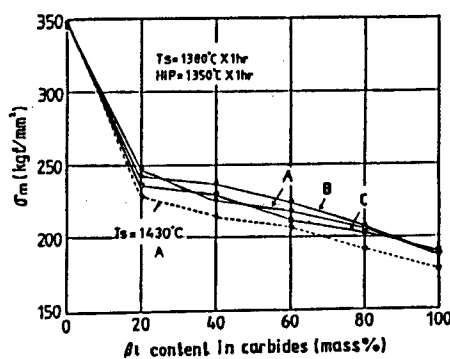


Figure 1. Effect of β_t content on deflection strength of samples A, B and C

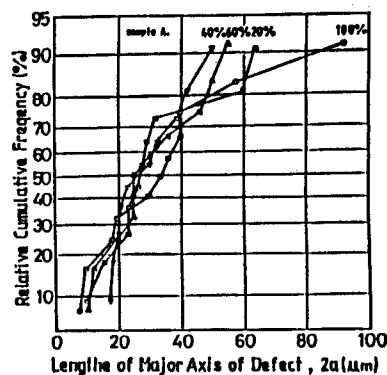


Figure 2. Effect of β_t on distribution of defective (2a) dimensions in sample A

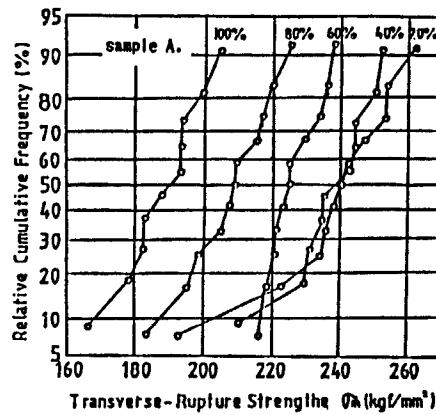


Figure 3. Effect of β_t content on distribution of defective strength of sample A (see Figure 2)

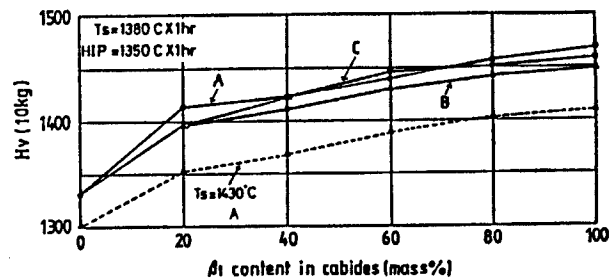


Figure 4. Relationship between β_t content and each sample

References

1. E. Amman and J. Hinnuber: Stahl und Eisen, 71, 1081, 1951.
2. Kubota and Hara: Sumitomo Electricity, No 82, 107, 1963.
3. Suzuki, Hayashi and Kawakatsu: Academic Journal of Japan Metallurgy Association, 31, 1100, 1967.
4. Suzuki and Hayashi: Academic Journal of Japan Metallurgy Association, 34, 491, 1970.
5. Suzuki, Tanase and Nakayama: Fine Particle and Powder Metallurgy, 23, 341, 1976.

Joint of Cemented Carbide by Ni-Group Amorphous Materials

43067591 Tokyo NIHON FUNMATSU FUNTAI YAKIN KYOKAI in Japanese 16-19 May 88
pp 196-197

[Report by Hidenori Kozuki, Kazutoshi Yamada and Yasuo Okuno, Hyogo Prefect Machinery and Metal Industry Guidance Office; and Masaaki Ikebe, Katsuto Ishibashi and Masahiro Iwasaki, Sun Alloy Industry Corp.: "Joint of Cemented Carbides by Ni-Group Amorphous Materials"]

[Text] 1. Introduction

Cemented carbide molds, which are used for manufacturing electronic components, are made up of several sections that are formed, sintered and then jointed. For some applications they are preferred over one-piece molds based on a single sintering operation. Various kinds of connection methods can be considered for the dissimilar cemented carbide used to joint the molds, but the brazed joint may be considered the simplest and most convenient joint method.

When the cemented carbide is to be connected by brazing, the most suitable brazing materials for use as the main components are considered to be Co and Ni, which are most frequently used as binding materials for carbides and nitrides. Before the current improvement, these brazing materials were only available in powder form, and their use was considered very inconvenient. However, the quenching hardening method that was developed recently is capable of providing sheet-shaped amorphous brazing materials which are easy to handle and applicable to brazing in wider areas. These are some of the features of the new brazing materials.

In order to obtain basic information about the brazing of cemented carbide, using Ni-Co group amorphous brazing materials, in our research we aimed at gaining an understanding of the changes in the materials produced in the brazing sections, and in particular at evaluating the strength problems.

2. Experiment Method

The cemented carbide used in our experiment was the most simple WC-Co based alloy. As indicated in Table 1, we varied the Co content and used three different sizes of WC particles. We endeavored to form the cemented carbide

at a pressure of 49-68.6 MPa and to carry out preliminary sintering of the material at 873-1073K and 3.6ks (in H₂). The alloys were produced in a sintering operation at 1653K and 3.6ks (in a vacuum of ~10 Pa) after they were formed into a specified shape.

Table 1. Mean Particle Size of WC and Co Content in Cemented Carbide Used

Specimen	A	B	C	D	E
Co Content (mass%)	5.0	11.0	17.0	10.0	9.0
Mean Particle Size of WC (μm)	2.7	2.7	2.7	0.6	6.0

We used Ni-Co based amorphous brazing materials in the two different compositions indicated in Table 2, which are available on the market. We carried out cemented carbide brazing in combination with materials of the same group (five types) and in combination with dissimilar materials (two types, A-C, and D-E). The brazing operation was carried out in a vacuum (about 7 Pa). The materials were held for 600s at specified brazing temperatures. Table 2 shows the respective brazing temperatures.

Table 2. Chemical Composition and Brazing Temperature of Amorphous Filler Metal Used

Element	(mass%)							Brazing Temperature (K)
	Co	B	Cr	Mo	Fe	Si	Ni	
MBF75	23.0	3.8	10.2	7.0	5.5	—	bal.	1478
MBF90	20.0	2.7	—	—	—	4.0	bal.	1423

We evaluated the strength of the brazing sections based on the three-point bending test and the single-axis tensile test. In addition, we endeavored to study the material changes produced in the brazing sections based on photographic appearance, EPMA, micro-Vickers hardness meter, X-ray diffraction, and SEM.

3. Experiment Result

Various efforts were made to study the brazing of various kinds of cemented carbide using Ni-Co group amorphous brazing materials. The main results obtained in our research are as follows.

- 1) The less the Co content of the brazing materials and the smaller the WC particles, the more easily they are subject to dispersion on the cemented carbide side. We observed the generation of phase in all of the cemented carbide in the areas in which the brazing materials were dispersed.
- 2) Figures 1 and 2 show the effect of the carbon content and WC particle sizes on the deflective strength of the brazing sections under the three-point bending test. These relationships show the same trend as that affecting the deflective strength of cemented carbide.

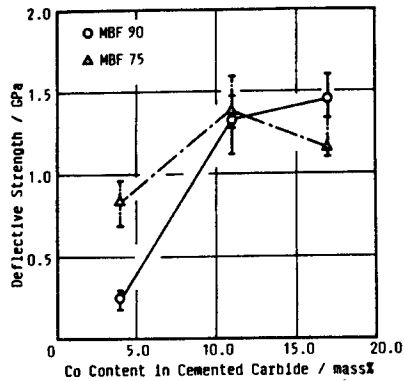


Figure 1. Effect of Co content in cemented carbide on deflective strength of brazed joint

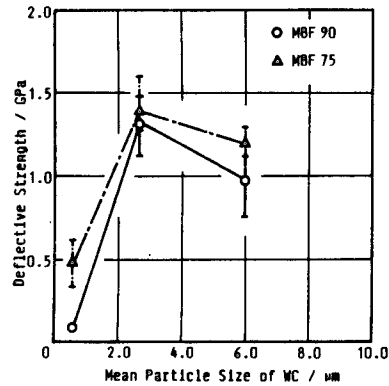


Figure 2. Effect of mean particle size of WC on deflective strength of brazed joint

Since the residual brazing material layer is extremely thin, some 15 μm and under in width, we were unable to identify the correlation between the width of the residual brazing layer and the deflective strength. As clearly indicated in Figure 3, the greater the deflective strength of the cemented carbide, the more enhanced the deflective strength of the brazed joint.

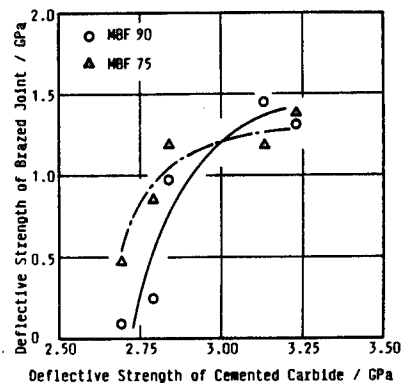


Figure 3. Relationship between deflective strength of brazed joint and that of cemented carbide

The effect of the carbon content and particle size on the tensile strength of the brazed joint showed a trend similar to that of the deflective strength.

3) When cemented carbide is connected with Ni-Co group amorphous brazing materials, the highest brazing strength is obtained in the case of a cemented carbide in which the carbon content is about 10 percent and the WC particle size is about 3 μm .

References

1. Hisashi Suzuki: Cemented Carbide and Sintering Hard Materials, Maruzen, p 120.

Relationship Between Strength, Matrix Organization of CVD Coated Cemented Carbide

43067591 Tokyo NIHON FUNMATSU FUNTAI YAKIN KYOKAI in Japanese 16-19 May 88
pp 198-199

[Report by Atsushi Fukawa, Mitsuo Ueki and Keiichi Kobori, Toshiba Tungalloy Corp.; and Hisashi Suzuki, Chiba Industrial University: "Relationship Between Strength and Matrix Organization of CVD Coated Cemented Carbide"]

[Text] 1. Objective

Compared with noncoated matrix, cemented carbide that is coated with a hard substance such as TiC by the chemical vapor deposition (CVD) method is subject to a drop in strength.¹ The strength of cemented carbides coated by the CVD method is considered to have the relationship $\sigma_o = \sigma_m (1 + 2\sqrt{d/p})$, where σ_o : the strength of the matrix over the interface between the film and the matrix; and d : the thickness of the coated film (without η phase).¹ Thus, the strength of coated alloys is considered to be subject to the effect of the matrix as well as to that of the composition. Therefore, in our research we endeavored to investigate the effect of the alloy organization on σ_m and the cutting performance of the coated alloy due to the presence of coating treatment in terms of the matrix of P30 composition with different particle size of carbide.

2. Method

With regard to the matrix, we used high carbon WC-8mass%TiC-12mass%TaC-8mass%Co alloys (the volumetric rates of β_t and Co are 44.0 and 11.4 percent, respectively), and changed the particle size of the carbide under sintering conditions wherein the temperatures were 1380°, 1420° and 1500°C over 1 hour. With regard to any of the above alloys, we sought to carry out HIP treatment after sintering for σ_m measurement samples and polishing of all surfaces to a satisfactory extent in order to eliminate residual stress after grinding, and thus to prepare a JIS specified test piece.

The goal was to coat these samples with 2 μ m and 6 μ m thick TiC by the CVD method (using a mixed gas of $\text{TiCl}_4 + \text{H}_2 + \text{CH}_4$ at a temperature of 1050°C).

As for the noncoated samples, our aim was to observe their organization and measure the hardness (Hv) and σ_m . Then, we sought to observe the interface organization between the TiC coat and the matrix and to measure the σ_m in order to study the strength of the coated alloys in relation to the organization of the matrix. Finally, we investigated the deflective resistance quality of the coated alloys by means of a cutting test.

3. Result

Photo 1 [not reproduced] shows the SEM organization of each alloy. The grey color-phase represents the β_t while the white-color phase represents the WC. Of course, both β_t and WC have a high sintering temperature. Our research revealed that the higher carbon alloys have the more coarse particle size.

Figure 1 shows the Hv measurement result of each alloy. It shows that the more coarse the particle size and the higher the carbon content of the alloy, the greater the reduction in the Hv and Σl values.

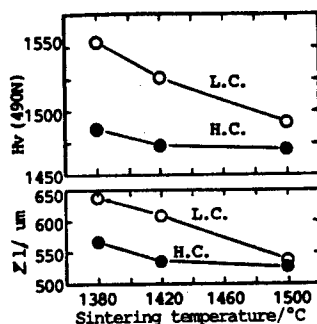


Figure 1. Effects of sintering temperatures on Hv and Σl of substrate

Photo 2 [not reproduced] provides an example of the interface organization between the coated layer and the matrix of a 6 μm thick sample coated with TiC. The low carbon alloy produces an η phase of 1-2 μm on the interface, whereas the high carbon alloy fails to produce an η phase.

Figure 2 shows the average deflective strength (σ_m) of each alloy before and after coating treatment. The σ_m of a noncoated alloy has a lower sintering temperature (smaller particle alloys). In contrast, the slightly lower carbon alloys have a higher sintering temperature. The σ_m of the coated alloys is subject to a drop in strength in proportion to the increase in the coat thickness compared with noncoated alloys. However, in the case of either a 2 μm or a 6 μm thick coating, the degree of drop is reduced in proportion to the increase in the sintering temperature (coarse particle alloy). The σ_m of the low carbon alloy is superior in the case of coarse particle size alloys.

Figure 3 shows the result of our investigation into the deflective resistance quality by means of a cutting test of the coated alloys. The

deflective resistance quality of the coated alloys are found to be excellent irrespective of the carbon content in the matrix, and to be more excellent if higher sintering temperature and more coarse particle size alloys are obtained.

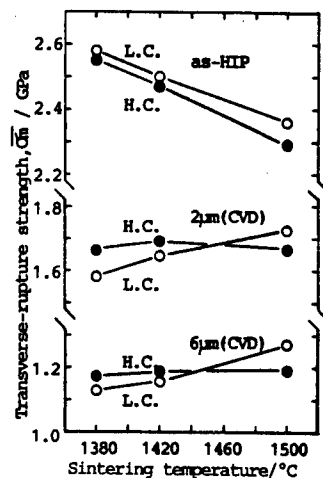


Figure 2. Effects of sintering temperatures on $\bar{\sigma}_m$ of non-coated alloys and TiC coated alloys. Thickness of TiC layer, indicated.

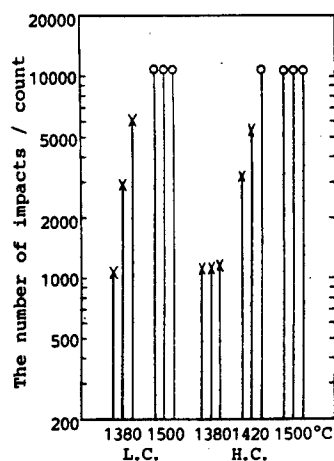


Figure 3. Results of intermittent cutting tests.
 Work: SCM440 (HB=273) $V=1.68\text{m/s}$ (101m/min)
 Insert: SNGN120408 $d=1.5\text{mm}$
 $f=0.149\text{mm/tooth}$

References

1. Suzuki and Hayashi: Fine Particle and Powder Metallurgy, 28, 257, 1981.

Low Ni Layer Produced on TiC-TiN-Mo₂C-Ni Cermet Surface

43067591 Tokyo NIHON FUNMATSU FUNTAI YAKIN KYOKAI in Japanese 16-19 May 88
pp 200-201

[Report by Takeshi Saito, Tsuyoshi Saito and Mitsuo Ueki, Toshiba Tungalloy;
and Hisashi Suzuki, Chiba Industrial University: "Low Ni Layer Produced on
Surface of TiC-TiN-Mo₂C-Ni Cermet"]

[Text] 1. Objective

When nitrogen added cermet (alloy) is vacuum-sintered, it is known that a soft layer whose surface system (SS) has disappeared appears on the surface layer (~10 μm) of the alloy due to the denitrification.¹ On the other hand, when we endeavored to investigate the nitrogen additive cermet that is available on the market, we found that a binder poor region (BPR), which often reaches a depth of 500 μm , was produced on the inner side of the denitrification layer. BPR is considered to affect the characteristics of tools in a manner similar to the SS layer. As we did not encounter any reports on BPR, we decided to investigate the cause of the generation of BPR.

2. Method

We used TiC, TiN, Mo₂C and Ni powders (particle size of 1.2-2.5 μm) which are all available on the market. We prepared various carbon content-based TiC-(0-20)vol%TiN-10vol%Mo₂C-10vol%Ni alloys by vacuum sintering at 1400°C x (5-60) minutes as a JIS-specified test piece for deflection strength measurement. In addition, we endeavored to grind the surface of the test piece after the sintering operation, and we prepared a test piece by resintering the piece under the same conditions. We sought to investigate the changes by means of photographic appearance, SEM organization, and Ni and Mo content (EPMA analysis), thereby identifying the origin of BPR.

3. Result

For reference, Figure 1 shows the concentration distribution of Ni, Mo, and Ti obtained from the surface when a medium carbon (MC) non-nitrogen additive alloy was sintered at a temperature of 1400°C for 60 minutes. (The concentration of each element in the center of the sample is specified as 1 and is

indicated from a depth of 10 μm up to the surface in the center. In the other illustrations, the concentration of non-nitrogen additive alloy in the center is also standardized and specified.) It is clear that no BPR was produced in this case. In addition, we also tried to confirm that non-nitrogen additive alloy does not produce any BPR based on the carbon content. Photo 1 [not reproduced] shows the SEM organization of non-nitrogen additive alloy (MC). The photo shows that a hard layer phase exists on the surface, indicating that the sintering atmosphere is carburizing in nature.² It also clearly indicates that no substantial change was produced on the organization from directly under the hard layer phase up to the central part.

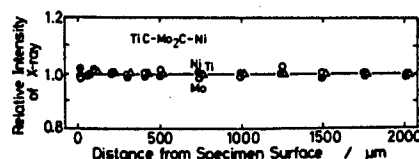


Figure 1. EPMA analyses of Ni, Mo and Ti in TiC-10vol%Mo₂C-10vol%Ni medium carbon (MC) alloy

Figure 2 shows the concentration distribution of 20vol%TiN additive alloy (MC) when it is sintered for the specified time. From the illustration, we can see that a 5-minute sintering operation has already produced BPR, and the thickness of the BPR has been increased with the lapse of time. Photo 2 [not reproduced] shows the SEM organization (30-minute sintering) at that time. A de-SS layer is produced on the surface layer, but the SS is becoming more and more inwardly coarse, thereby increasing the volumetric rate of the carbide and nitride (the volumetric rate of the binder phase is decreased), and this corresponds to the result indicated in Figure 2. Photo 3 [not reproduced] shows the organization of low carbon (LC) alloy sintered for 30 minutes. The presence of a hard phase layer, although slight, can be observed on the surface layer. It is clear that the difference in the organization between the surface layer and the internal layer is minimum. As for the influence of carbon content, the generation of BPR and organic change are generally evident in the case of alloys having higher carbon content. However, no BPR is produced on free carbon included alloys or LC alloys, and no organic change is produced near the surface layer either.

To make sure, we decided to cut the surface layer of the 20vol%TiN additive sample by 1000 μm and to demonstrate the result of resintering after the removal of BPR shown in Figure 3. The phenomenon in this case is virtually identical to that of an ordinary sintering operation.

As discussed above, our research indicates that the generation of BPR is not directly associated with the formation of a de-SS layer or the liquid phase flow in the early stage of condensation; it is considered attributable to the diffusion movement of carbide and nitride forming elements such as Mo and Ti from the inner layer of the alloy to the surface layer during sintering. It

is considered that this phenomenon is associated with denitrification from the surface of the sample during sintering and the sintering atmosphere as well.

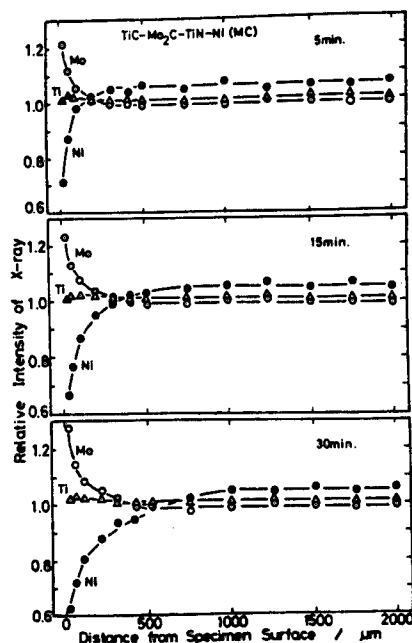


Figure 2. EPMA analyses of each element in TiC-10vol%Mo₂C-20vol%TiN-10vol%Ni MC alloy

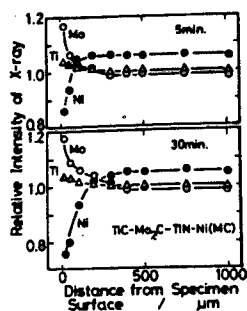


Figure 3. EPMA analyses of each element in TiC-10vol%Mo₂C-20vol%TiN-10vol%Ni MC alloy (resintered)

References

1. Suzuki, Hayashi, and Matsubara: Fine Particle and Powder Metallurgy, 29, 58, 1982.
2. Hayashi, Namiki, and Takashima: Fine Particle and Powder Metallurgy, 29, 159, 1982.

Ni, Carbon Effect on Sintering Mechanism of Mo_2FeB_2 Hard Alloys

43067591 Tokyo NIHON FUNMATSU FUNTAI YAKIN KYOKAI in Japanese 16-19 May 88
pp 202-203

[Report by Tsuneyuki Ide, Kazunori Nakano and Kenichi Takagi, Technological Research Institute of Toyo Steel Plate Corp.: "Effect of Ni and Carbon Content on the Sintering Mechanism of Mo_2FeB_2 Family Hard Alloys"]

[Text] 1. Objective

The authors sought to clarify the Fe-6%B-48%Mo family three-dimensional sintering mechanism and the reinforcing mechanism of the sintered body. The sintering organization is comprised of Mo_2FeB_2 (64vol%) and Fe_2B (8vol%), which are hard particles, while the binding material is comprised of $\alpha\text{-Fe}$. The maximum deflective strength obtained is about 2.0 GPa (hardness HRA88). The liquid-phase sintering of the sintered alloy advances based on two kinds of liquid-phase reactions at a temperature range of 1365-1475K. The reaction formula is expressed by $\gamma\text{-Fe} + \text{Fe}_2\text{B} \rightarrow \text{L}_1$, $\gamma\text{-Fe} + \text{Mo}_2\text{FeB}_2 \rightarrow \text{L}_2$. In a previous report, the authors discussed the effect of the addition of carbon on the liquid-phase sintering mechanism of the alloy family. In this report, we would like to discuss the effect of the addition of Ni and carbon on the liquid-phase mechanism.

2. Method

We used FeB(B:16.0%, C:0.21%), Mo, Fe and graphite powder, the same materials as were used in the previous experiment. We endeavored to add carbonyl Ni powder to the materials, and then to mix the elements so that after sintering the alloy would be composed of extremely low carbon within the range of Fe-6%B-48%Mo-(0~7)%Ni (all expressed by weight %). The carbon content included in the sintered body was set at 0.1% and 0.3% for the study of the effect of the carbon content. Since graphite powder is consumed at a temperature of 1175-1325K on the way to the specified sintering temperature in terms of powder reduction, the carbon content was controlled by adding graphite powder. The mixing fine disintegration, dry treatment of mixed powder, pressed powder forming and vacuum sintering methods were identical to those discussed in our previous report. A sintered deflective strength test piece was obtained for deflection testing after grinding and for measurement of the hardness and density. We sought to study the sintering mechanism using

vacuum-ambient differential thermobalance, and by carrying out heat expansion testing and X-ray diffraction testing, which are all identical to those discussed in the previous report.

3. Result

Figure 1 shows the mechanical properties of the sintering alloy family arranged in terms of Ni and carbon content. In this experiment, the authors adopted the sample values in which the maximum deflective strength was available at the specified temperature from among various sintering temperatures. Figure 1 clearly shows that the deflective strength improved at around 3% Ni content and 0.1% carbon content, in particular. It also shows improvement in the hardness.

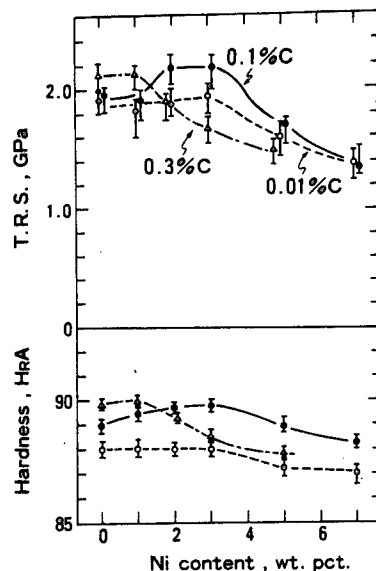


Figure 1. Effects of C and Ni content on transverse rupture strength and hardness of sintered Fe-6%B-48%Mo-Ni-C alloys. Sintering: 1475-1500K, 1.2Ks.

Table 1 shows the main fixing result of sintered alloys comprised of different Ni and carbon contents obtained by X-ray diffraction. The diffraction strength of Mo_2FeB_2 and Fe_2B , which constitute hard particles, is not subject to the influence of Ni or carbon content. In contrast, the binding materials are subject to reduction in $\alpha\text{-Fe}$, while the presence of $\gamma\text{-Fe}$ is observed starting around a content of 5 percent Ni when the carbon content is extremely low, and beginning around a content of 3 percent Ni when the carbon content is 0.1 percent. The Fe may be considered to be a residual austenite stabilized by Ni and C melted solidly within the binding materials.

Table 1. Phases Identified by X-Ray Diffraction in Sintered Fe-6%B-48%Mo-Ni-C Alloys

Ni and C content, wt. %	Mo ₂ FeB ₂	Fe ₂ B	α -Fe	γ -Fe	M ₂₃ C ₆	Fe ₃ C
0Ni-0.01C	VS	W	S	—	—	—
3Ni-0.01C	VS	W	S	—	—	—
3Ni-0.1C	VS	W	S	VW	—	—
3Ni-0.3C	VS	W	W	M	VW	VW
5Ni-0.01C	VS	W	W	M	—	—
7Ni-0.01C	VS	W	VW	S	—	—

S: strong, M: medium, W: weak, (V: very)

Figure 2 shows the measurement result of mixed pressed powder of the sintered alloy family by differential thermobalance (DTA). The measurement shows that when the carbon content is extremely low, along with Ni content, the heat absorption peak ⑤ (L_1 liquid-phase reaction) during a rise in temperature and the heat absorption peak ⑥ (L_2 liquid-phase reaction) move slightly toward the low temperature side, and the exothermic peaks ⑦ and ⑧ accompanied by a solidification reaction during cooling show a similar tendency. In addition, L_1 and L_2 liquid-phase reactions move toward the low temperature side in proportion to the increase in carbon content when their fixed Ni content is 3 percent. At the same time, an L_c liquid-phase reaction can be observed.

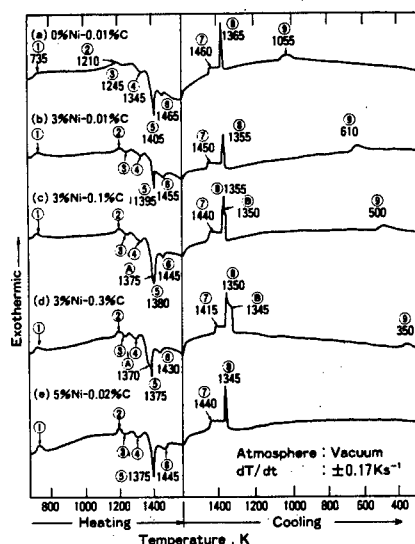


Figure 2. DTA traces for a heating and cooling cycle of Fe-6%B-48%Mo-(0~5)%Ni-(0.01~0.3)%C alloys from the green state

Figure 3 shows the result of heat expansion testing of pressed powder of 3 percent Ni content, 0.1 percent carbon content and no Ni added and

extremely low content of carbon alloys used in the previous test indicated in Figure 2. Pressed powder of 3 percent Ni content and 0.1 percent carbon content produces dramatic contraction within the range of temperature equivalent to the heat absorption peaks (A) and (5) indicated in Figure 2 (c), then produces a second contraction corresponding to the heat absorption peak (6) when the temperature exceeds 1385K.

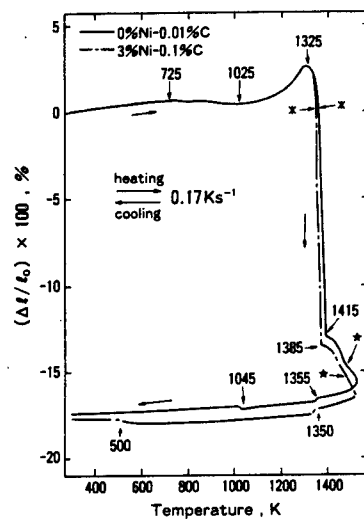


Figure 3. Dilatometric curves for a sintering cycle of Fe-6%B-48%Mo-x%Ni-y%C
(x: liquid formation temperatures,
*: optimum sintering temperatures)

Enhancing Toughness of TiB₂ Sintered Body

43067591 Tokyo NIHON FUNMATSU FUNTAI YAKIN KYOKAI in Japanese 16-19 May 88
pp 204-205

[Report by Tsuneaki Matsudaira, Hideaki Ito and Shigeharu Naka, Engineering Department of Nagoya University; and Hiroshi Hamamoto, Toyota Central Research Institute: "Enhancing Toughness of TiB₂ Family Sintered Body by Application of Hot Press"]

[Text] 1. Introduction

Fine TiB₂ powder of around 1 μ m particle size synthesized in direct solid-phase reaction with TiN and noncrystalloid boron are suitable for the production of a sintered body by the hot press method.^{1,2} When a sample [(TiB₂ + 0.2B) + 0.1 Ti composition] containing free noncrystalloid boron, to which metal titanium powder has been added, is used as raw material, it has been found that a single-phase TiB₂ sintered body having 98 percent relative density can be produced.^{2,3} In this research, we tried to clarify the nature of the TiB₂-based compound sintered body by hot pressing a sample to which excess metal titanium had been added with regard to the proportional composition of TiB₂ in order to enhance the toughness of the TiB₂ sintered body by the coexistence of the metal titanium.

2. Method

(1) Powder Synthesis^{1,2}

We sought to deaerate TiN powder (particle size: 0.5~3 μ m) and noncrystalloid boron powder (particle size: 0.5~3 μ m) separately in a vacuum at a temperature of 600°C for 60 minutes. After mixing based on blended molar refraction where B/TiN = 2.2, the two types of powder were subjected to heat treatment in argon flow at a temperature of 1400°C for 360 minutes, and TiB₂ powder (TiB₂ + 0.2B) containing 20 mol% of free noncrystalloid boron was synthesized.

(2) Sintering and Evaluation

A sample wherein 0~27 mol% metal titanium powder (particle size: 5~10 μ m) was mixed with the synthesized powder was formed at pressure of 20 MPa. The

sample thus mixed was processed in argon atmosphere at a pressure of 20 MPa and a temperature of 1800°C for 30 minutes in order to produce a TiB_2 -Ti family compound sintered body including 0~20 mol% metal titanium by the application of hot pressing. After the sintered body was produced, we endeavored to obtain the contraction curves of each sample during the hot press operation. With regard to the sintered body, the density was measured while the Vickers microhardness was obtained under a drop of 200 g load. The value of fracture toughness K_{IC} was measured based on the denting method (under a load of 10 kg), while the bending strength was measured by carrying out the three-point test. Also, the fractured surface was measured by scanning electron microscope (SEM).

3. Result

Figure 1 shows the contraction curves obtained when three types of samples were hot-pressed. The curved lines on the left side of the broken line represent the heating process, while those on the right side represent the temperature maintenance process. In the case of synthesized powder (a), the effort to increase the density of the sample was found to be insufficient even when it was maintained at 1800°C for 30 minutes. On the other hand, the authors found a marked contraction of the sample during an increase in temperature with regard to sample (b) with a proportional composition of TiB_2 produced by the addition of 10 mol% titanium. The relative density of the sample reached 98.2 percent, thereby producing a single-phase sintered body of TiB_2 .^{2,3} The contraction of sample (c) with titanium excess composition was slightly greater than that of sample (b) with a proportional composition. The relative density reached 99.5 percent, thus producing a sintered body of TiB_2 - 15mol%Ti. It is thought that the marked contraction of sample (c) was produced by the effect of the liquid-phase sintering brought about by the excess molten titanium, along with the reaction sintering effect brought about by the free noncrystalloid boron and additive titanium contained in the synthesized powder in the case of sample (b).

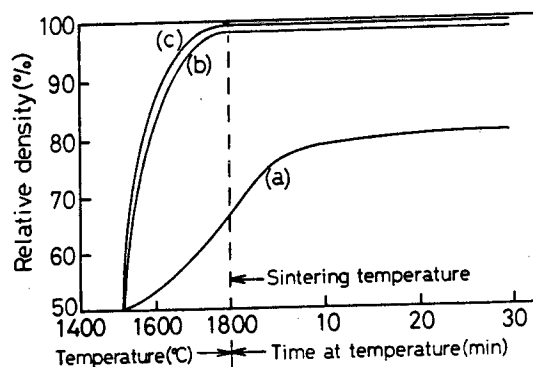


Figure 1. Contraction curves (1800°C, 30 minutes)
 (a) $\text{TiB}_2 + 0.2 \text{ B}$
 (b) $\text{TiB}_2 + 0.2 \text{ B} + 0.1 \text{ Ti}$
 (c) $\text{TiB}_2 + 0.2 \text{ B} + 0.23 \text{ Ti}$

Figure 2 shows the relationship between the relative density, microhardness, bending strength, fracture toughness of various kinds of TiB_2 - Ti family sintered bodies prepared by hot pressing and the titanium content of the sintered bodies. The relative density tended to increase slightly in proportion to the titanium content up to a saturation point of just over 15 mol%.

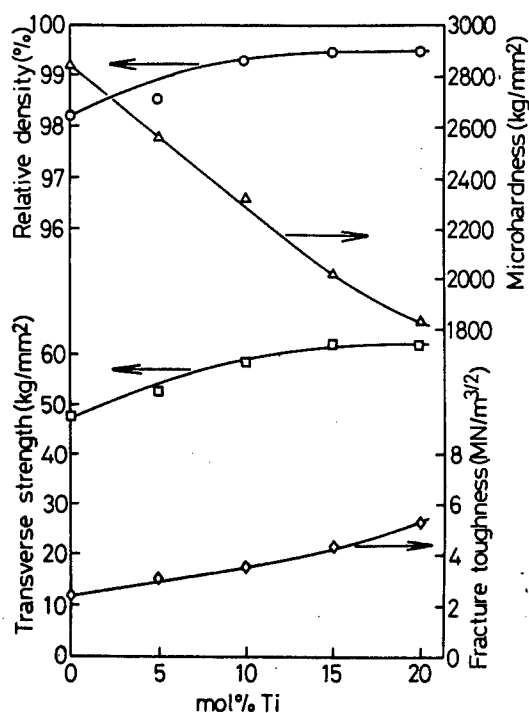


Figure 2. Relationship between Ti content and nature of sintered body

The microhardness of the TiB_2 single-phase sintered body exhibited a value of 2850 kg/mm^2 .^{2,3} The hardness decreased linearly with the content of titanium, reaching the small value such as 1820 kg/mm^2 . On the other hand, the bending strength and the fracture toughness value increased with the titanium content; the bending strength was 62 kg/mm^2 at a composition of 15 mol%Ti, while the fracture toughness was $5.3 \text{ MN/m}^{3/2}$ at a composition of 20 mol%Ti. As stated, the toughness effect on the sintered body of the coexistent titanium was evident.

Figure 3 [not reproduced] shows the fractured surface of the sintered body of TiB_2 - 15 mol%Ti. In contrast to the square-shaped particles of the TiB_2 single-phase sintered body, these particles were round.

References

1. Matsudaira, Ito, Hamomoto, Obayashi, S. Naka, H. Hamamoto, and Obayashi: Collection of reports given during the 1986 fall convention of the Powder Metallurgy Association, 152.

2. T. Matsudaira, H. Itoh, S. Naka, H. Hamamoto and H. Obayashi, Proc. 9th Intern. Sympo. on Boron, Borides and Related Compounds, Duisburg, FRG, p 436, 1987.
3. Matsudaira, Itoh, Naka, Hamamoto, Obayashi: Collection of reports given during 1987 spring convention of the Powder Metallurgy Association, 28.

Reactivity of Al_2O_3 -SiC Ceramics With Ni

43067591 Tokyo NIHON FUNMATSU FUNTAI YAKIN KYOKAI in Japanese 16-19 May 88
pp 206-207

[Report by Yuji Katsumura, Maskai Kobayashi and Keiichi Kobori, Toshiba Tungalloy Corp.; and Hisashi Suzuki, Chiba Industrial University:
"Reactivity of Al_2O_3 -SiC Ceramics With Ni"]

[Text] I. Objective

The authors have carried out a series of researches on Al_2O_3 -SiC powder ceramics.^{1,2,3} According to the latest research in the series³, the cutting performance of a cutting tool of this ceramic material stands midway between the Al_2O_3 -TiC ceramic tool and the Al_2O_3 -SiC whisker ceramic tool (designated SiC(p), TiC, and SiC(w) additive tools, respectively). For example, it was found that the SiC(p) additive tool is consistently superior to the SiC(w) additive tool in terms of flank wear, while the TiC additive tool is even more superior. The authors have sought to ascertain why a difference exists in the flank wear occurring in the SiC(p) and SiC(w) additive tools. For this purpose, the authors sought to pinpoint the cause of the change with specific attention to the difference in the interface reaction between the materials to be cut and the ceramics.

II. Experiment Method

In this experiment, the authors prepared mixed powder comprised of Al_2O_3 -SiC(p) and Al_2O_3 -SiC(w) with a wet ball mill, using about 0.3 μm particle size Al_2O_3 powder, SiC powder (SiC(p)) and 0.4 x 20 μm SiC whiskers (SiC(w)). After being dried, the powder was hot-pressed at a temperature of 2123K and a pressure of 49MPa so as to obtain sheet material of 35 x 35 x 6 mm³. The SiC content was specified as 25 vol% in each case. A test piece having the specified dimensions was cut from each of the two types of hot-pressed sheets. The surface normal to the test surface (parallel to the direction of hot pressing) was mirror-polished. A pure Ni sheet was bonded with this mirror-polished surface by diffusion. The bonding requirements specified were: (1173 to 1573)K x 3.6ks in argon flow at pressure of 33 MPa. A quick bonding operation was also carried out, as necessary. In this research, the authors used a pure Ni sheet as a mating

material for convenience. We assume that we would be able to obtain similar results in the case of an Fe sheet. With regard to various diffusions, we endeavored to investigate the interface organization around the bonded areas in particular. The investigation result reveals that the Si was slightly diffused on the Ni side, while a clear reaction layer (diffusion layer) was produced on the ceramics side. With this result, we investigated the thickness of the reaction layer, the organization and the origin by means of photographic appearance, SEM and X-ray diffraction.

III. Result

Photo 1 [not reproduced] shows the organization of the fracture surface of the ceramics sample supplied for the experiment. Figure 1 shows the relationship between the thickness of the reaction layer and the bonding temperature when both ceramics were bonded with Ni.

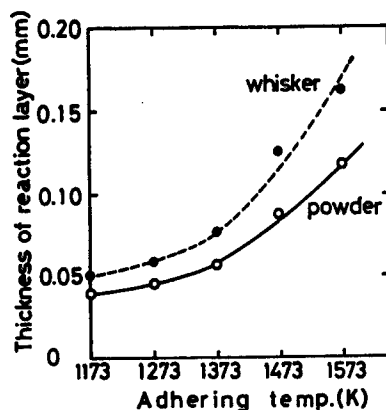


Figure 1. Relationship between thickness of reaction layer and adhering temperature. Adhering time 3.6ks.

Figure 2 (a, b) shows the X-ray diffraction result of the reaction layer corresponding to that in Photo 2 [not reproduced]. Photo 3 [not reproduced] shows the SEM organization of the reaction layer and Ni characteristics X-ray image corresponding to Photo 2 (a).

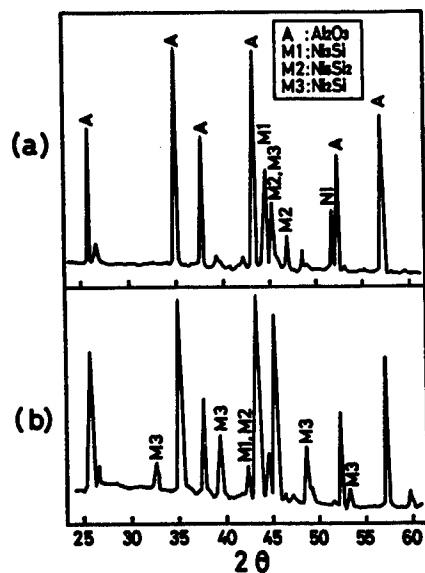


Figure 2. Graph of X-ray diffraction of reaction layer corresponding to Photo 2 (a).

- (a) In the vicinity of the interface,
 (b) 30 μm depth

References

1. Yuji Katsumura, Keiichi Kobori and Hisashi Suzuki: Fine Particle and Powder Metallurgy, 34, 522, 1987.
2. Yuji Katsumura, Keiichi Kobori and Hisashi Suzuki: Fine Particle and Powder Metallurgy, 35, 1988, contributed to the journal.
3. Yuji Katsumura, Keiichi Kobori and Hisashi Suzuki: Fine Particle and Powder Metallurgy, 35, 1988, contributed to the journal.

Mechanical Properties of SiC Whisker Reinforced Al₂O₃ Ceramics

43067591 Tokyo NIHON FUNMATSU FUNTAI YAKIN KYOKAI in Japanese 16-19 May 88
pp 208-209

[Report by Tsutomu Yamamoto and Makoto Asano, Dijet Industrial Co., Ltd.;
and Nobuyuki Tamari, Osaka Industry Laboratory: "Mechanical Properties of
SiC Whisker Reinforced Al₂O₃ Ceramics"]

[Text] 1. Introduction

Recently, various ceramics reinforcement methods have been put forward to eliminate the fragility of Al₂O₃ ceramics. They include fiber reinforcement, particle dispersion reinforcement, and the microstructure method, for example.¹ In our research, we endeavored to investigate the effect of the various factors on the mechanical properties of composite sintered bodies obtained by adding various kinds of SiC whiskers (SiCw) to the Al₂O₃ matrix in order to improve the toughness of the ceramics.

2. Experiment Method

Figure 1 shows the manufacturing process of the Al₂O₃ matrix/SiCw composite sintered body studied in this research. With regard to the raw materials, we used ordinary Al₂O₃ (average particle size: 0.2 μ m) and SiCw (0.5 μ m diam x 50 μ m^l) available on the market. Before mixing, the SiCw was either given no pretreatment, or else it received filtration treatment or ultrasonic treatment. After mixing, the materials were hot press sintered through dry and refined particles at a temperature of 1973~2173K, a pressure of about 40 MPa, and a holding time of 3.6ks.

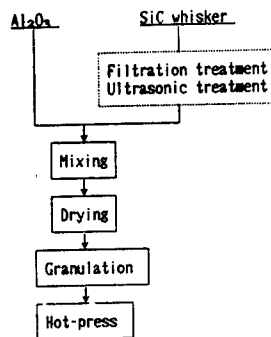


Figure 1. Manufacturing process of Al₂O₃/SiCw composite

The sintered body obtained thus was measured with regard to density (Archimedes method) three-point bending strength (JIS R1601-1981), K_{Ic} (IM method) and Vickers hardness (load: 2.94N). Some test pieces were subjected to SEM observation and X-ray diffraction. As illustrated in Figure 2, the mechanical properties were measured with specific attention to the surface vertical (1) to the direction of the hot press, as well as to the parallel surface (2) as necessary.

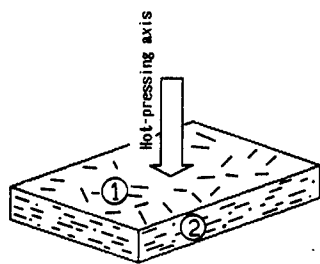


Figure 2. Schematic drawing of hot-pressed $Al_2O_3/SiCw$ composite

3. Result and Examination

Figure 3 shows the result of performing Weibull plots in terms of the bending strength of the $Al_2O_3/30wt\% SiCw$ composite sintered body obtained depending on the pretreatment discussed previously. The Weibull coefficient shows that the strength average values of the sintered bodies that received either filtration treatment or ultrasonic treatment were dramatically increased in comparison with those not treated.

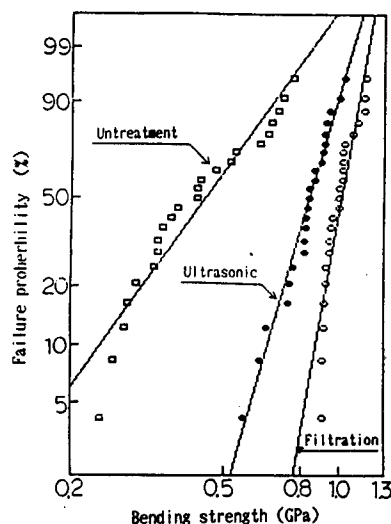


Figure 3. Weibull plots of bending strength for $Al_2O_3/30wt\%SiCw$ composite manufacturing by various processes

Figure 4 shows Weibull plots of the bending strength measured in terms of the vertical and parallel planes to the direction of the hot press, which are the planes of tensile force. It was found that the bending strength on the vertical plane was greater than that of the parallel plane. With regard to the hot-pressed sintered body, the two-dimensional orientation of the SiC whiskers was observed. In addition, the orientation capacity was observed in the case of other mechanical properties.

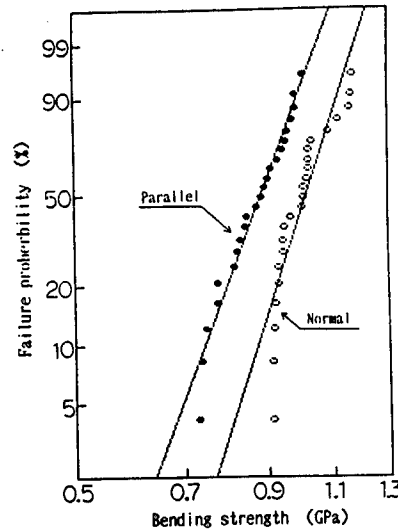


Figure 4. Weibull plots of bending strength for $\text{Al}_2\text{O}_3/30\text{wt}\%\text{SiCw}$ with bending surface normal and parallel to hot-pressing axis

Figures 5 to 8 show the effect of the amount of SiCw content on the sintering temperature, bending strength, fracture toughness and Vickers hardness. The mechanical properties of the composite sintered body were improved with the increase in the amount of SiCw additive. From the observation of the organization, we thought that the crack deflection effect based on the SiCw is good in terms of the toughening mechanism while the load transfer effect is good for a high strengthening mechanism.

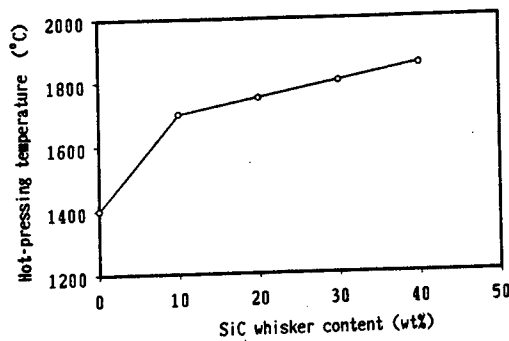


Figure 5. Effect of SiCw content on densification temperature of $\text{Al}_2\text{O}_3/\text{SiCw}$ composites

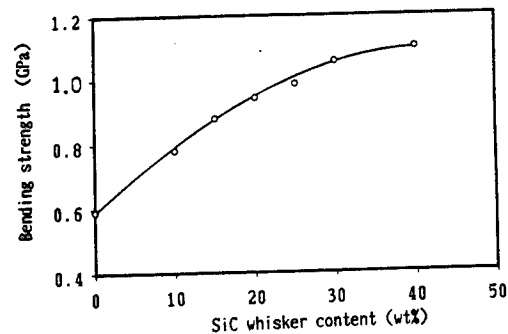


Figure 6. Effect of SiCw content on three-point bending strength of $\text{Al}_2\text{O}_3/\text{SiCw}$ composites

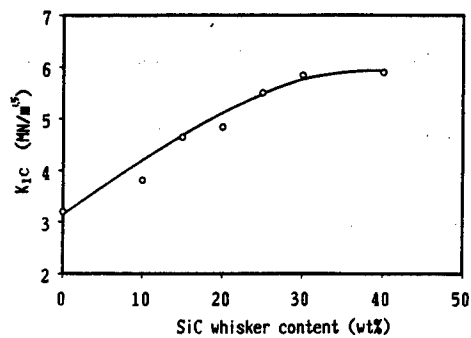


Figure 7. Effect of SiCw content on fracture toughness of $Al_2O_3/SiCw$ composites

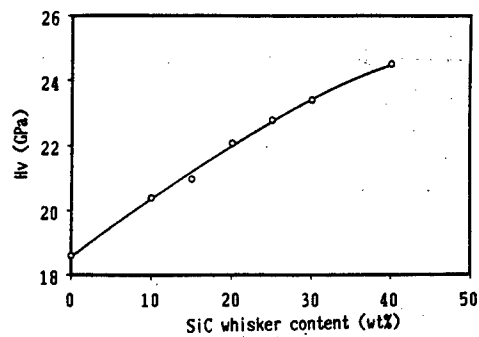


Figure 8. Effect of SiCw content on Vickers hardness of $Al_2O_3/SiCw$ composites

References

1. Nihara et al.: Ceramics, 21, 581, 1986.

Preparation of Composite Ceramics

43067591 Tokyo NIHON FUNMATSU FUNTAI YAKIN KYOKAI in Japanese 16-19 May 88
pp 210-211

[Report by Akifumi Onodera, Hiroyuki Yashihara, Norikazu Takahashi, Hiroyuki Nakae, Yukio Matura and Toshi Hirai, Osaka University Basic Engineering New Technology Development Corp.]

[Text] 1. Introduction

Our research was aimed at producing a cubic crystalloid zinc blended structure boron nitride (zBN) group composite ceramic sintered body using non-crystalloid B-N-X (X = Si, Al and Ti, for example) as raw materials synthesized by the chemical vapor deposition (CVD) method, and then processing these synthesized materials under high pressure and temperature.

Since zBN has the highest hardness and thermal heat conductivity next to diamonds, along with much lower affinity with iron than diamonds, it is regarded as the most important material to play a role complementary to that of diamonds.

The zBN used for cutting and grinding is a sintered body that can be thermodynamically processed under stable high temperature and pressure. Two methods are available for sintering zBN: one with a binder added and the other without. In the former method, a mixture of BN (zBN, gBN (graphite type) wBN (wurtzite)) and an agent for a nitride or boride is used as a starting sample. In the latter, a reaction sinter is produced simultaneously with noncatalytic conversion from the gBN, wBN or amorphous phase (aBN) to zBN. In this report, the authors will discuss a new zBN-related sintered body production process. This process is quite different from the former process, as the new system is intended to produce coexistence with a third element (X), although it is intended to generate zBN without a catalyst and to produce a sintered body simultaneously in a manner similar to the former process. This new system is different from the former process in that the starting material is not simply a mixture of BN and an agent.

2. Experiment Method

The amorphous B-N-X starting samples were synthesized by the CVD method using a mixed gas of the ($\text{BCL}_3 + \text{NH}_3 + \text{H}_2$) family + SiCl_4 or (AlCl_3 , TiCl_4) under the condition of 10~30 torr and 1400°-1600°C.¹ We also endeavored to confirm that the samples were noncrystalloid in nature by means of X-ray diffraction measurement. With regard to the content of X (wt%), we obtained the following data respectively: Si = 2, 6 and 30 and Al = 2, Ti = 1.4. These samples were subjected to high temperature and pressure treatment by means of a regular octahedron type high-pressure generation unit.²

3. Results and Examination

Figure 1 shows the high temperature and pressure treatment conditions and the products available when B-N-Si (Si = 30 percent) was used for the starting samples. The species and quantities of powder were determined by the powder X-ray diffraction method. The starting materials were in a state similar to the amorphous phase up to 1500°C. When the temperature exceeded 1800°C, zBN was produced. And when pressure of 6 GPa was exerted at the same time, gBN was also produced.

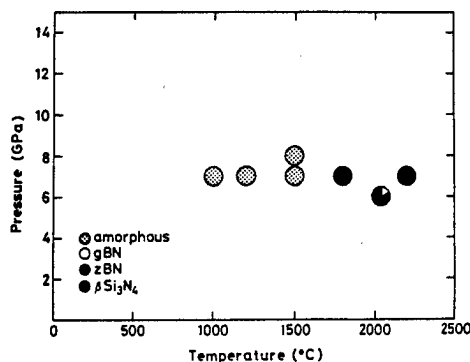


Figure 1. Products resulting from high pressure and temperature conditions using B-N-Si (Si = 30 percent)

Figure 2 shows the X-ray diffraction patterns of the same samples under a pressure of 7 GPa at various temperatures. Whenever zBN appears, the presence of $\beta\text{Si}_3\text{N}_4$ can be recognized without fail. This means that these amorphous B-N-Si samples are subject to dissolution and crystallization simultaneously under high temperature and pressure. However, the temperature at which zBN is generated is about 1000°C higher than that of crystallization from aBN.

Figure 3 (a) and (b) are images of the fracture surface of samples obtained under a pressure of 7 GPa at the respective temperatures of 1800°C and 2200°C shown in Figure 1. The samples are comprised of large and small particles and exhibit a relatively refined organization.

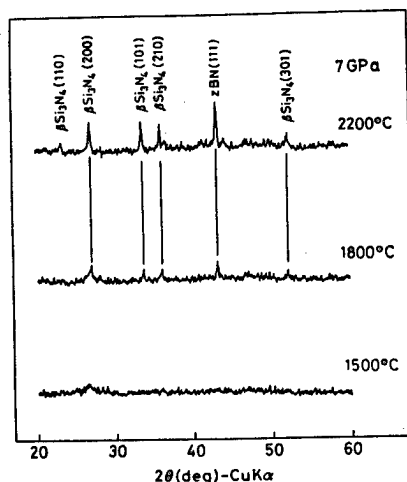


Figure 2. X-ray diffraction patterns with processing of B-N-Si (Si = 30 percent) under 7 GPa



Figure 3. Fractured surface of sintered body of B-N-Si under 7 GPa at (a) 1800°C, (b) 2200°C

Figure 4 is an image showing Vickers dents. Figure 5 (a) provides an enlarged view of these dents. The EPMA in Figure 5 (b) and (c) indicates that the dark portions of Figure 4 correspond to the zBN. The zBN is dispersed into $\beta\text{Si}_3\text{N}_4$, forming high dimensional structures which are mutually related, not single particles.



Figure 4. Image of Vickers pressure dent of sintered body



Figure 5. (a) SEM image and EPMA images ((b) Si, (c) B) of sintered body

References

1. T. Matsuda, N. Uno, H. Nakae and T. Hirai: J. Mater. Sci., 21, 649, 1986.
2. N. Kawai, M. Togata and A. Onodera: Proc. Jpn. Acad., 49, 623, 1973.
3. H. Sumiya, T. Iseki and A. Onodera: Mater. Res. Bull., 18, 1203, 1983.

Seed Effect on c-BN Reaction Sintering

43067591 Tokyo NIHON FUNMATSU FUNTAI YAKIN KYOKAI in Japanese 16-19 May 88
pp 212-213

[Report by Hideaki Ito, Tsuneaki Matsudaira, Katsuya Inoue, Hideki Katoh and Shigeharu Naka, Engineering Department of Nagoya University: "Seed Effect Exerted on c-BN Reaction Sintering"]

[Text] Introduction

A reaction sintering method which is designed to prompt sintering in parallel with inducing a transition reaction from b-BN to c-BN by the addition of c-BN to b-BN is one in which a c-BN sintered body of high purity can be produced.¹ Atmospheric pretreatment of the raw mixed powder has a great effect on the reaction sintering of c-BN. The pretreatment cleans the surface of the b-BN and c-BN particles in H_2-N_2 current at a temperature of $1000^\circ C$ and promotes the orientation growth of the b-BN, which is converted to c-BN, along with the sintering. In this research, the authors investigated how the particle size of the added c-BN seed crystal and the additive affect the behavior of the reaction sintering. In addition, we endeavored to evaluate the organization and hardness of the c-BN single-phase sintered body thus produced.

Experiment Method

Blended samples comprised of b-BN powder of more than 99.9 percent purity (particle size: 1-5 μm) and c-BN powder (average particle size: 0.5, 8, 25 and 42 μm) were subjected to deaeration processing in a vacuum at a temperature of $600^\circ C$ for 60 minutes. Next, atmospheric pretreatment was carried out in H_2-N_2 family flow at a temperature of $1000^\circ C$ for 60 minutes. Then, 1 wt% ammonium nitride was added to the pretreated samples as a volatile catalyst, and the sample was subjected to treatment at a pressure of 6.5-7 GPa and a temperature of $1700^\circ C$ for a period of 30-60 minutes.

The generation phase of the sintered body was identified by means of X-ray diffraction, and the content of c-BN in the sintered body (weight% to the total weight of additive c-BN + conversion c-BN) was obtained. The density of the sintered body was measured by the Archimedes method, while the Vickers microhardness (Hv) was measured under 1000 g load. The grinding surface and the fracture surface of the sintered body were observed by an optical magnifier and a scanning electron microscope (SEM).

Result and Examination

In Figure 1, the influence of the average particle size of the added c-BN seed on the c-BN content of the sintered body is observed. The pretreatment atmosphere was $H_2/N_2 = 1/1$, at a pressure and temperature of 7 GPa and 1700°C for 30 minutes. The added c-BN content was 30 wt% and 70 wt%, respectively. Since the conversion rate from b-BN to c-BN was high irrespective of the added content when the average particle size was 0.5 μm , a high c-BN content was indicated and a sintered body was obtained. The c-BN content was inclined to decrease slightly in inverse proportion to the increase in the average particle size. However, when the c-BN added content was 30 wt%, the smaller amount, the content dropped below 80 percent and a sintered body would not be obtained. On the other hand, when the c-BN added content was 70 percent, a relatively high content was obtained, in excess of 90 percent. Therefore, it could be sintered when the average particle sizes were 8 and 25 μm . However, when an attempt was made to use c-BN seed crystal of an average particle size of 42 μm , it was observed that the bonding power between the particles was weak, and thus the specified sintered body was not obtained.

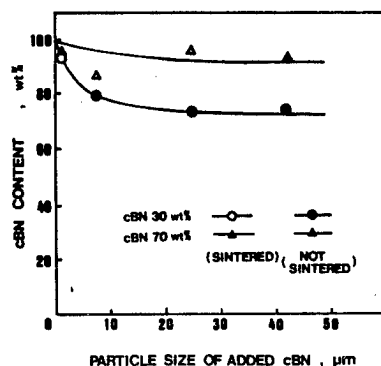


Figure 1. Effect of particle size of c-BN seed (7 GPa, 1700°C, 30 min)

Figure 2 shows the relationship between c-BN seed additive of various particle sizes and the c-BN content. The pretreatment conditions and the high pressure and temperature treatment conditions of the samples were identical to those indicated in Figure 1. The diagonal from the starting point to the 100 percent point indicates the c-BN content of the raw powder. The distance from this straight line to the respective plot points corresponds to the net amount of conversion from b-BN to c-BN. When the particle size was 0.5 μm , a c-BN sintered body having almost 100 percent conversion rate was available by the addition of a relatively slight amount (10 wt%) of c-BN seed. When an effort was made to increase the amount of additive, the c-BN content in the sintered body was maintained at substantially 100 percent. When the particle size was 5-10 μm , a powder was formed in which the c-BN content was 80 percent if the amount of additive was 30 wt%. However, if the amount of additive exceeded 60 wt%, the content was improved so that a sintered body could be obtained. Figure 3 shows a photograph of

the sintered body that could be obtained by the addition of 60 wt% c-BN seed whose average particle size was 8 μm . The sample was subjected to boiling treatment in an atmosphere of 2N-NaOH whereby the nonreacting b-BN was eliminated. The particle size distribution of the c-BN in the sintered body was uniform and it was similar to that of the seed crystal. At the same time, direct bonding was observed between particles. Even when the particle size of the added c-BN seed was 20-30 μm and 36-54 μm , the c-BN content increased in proportion to the increase in the amount of additive. On the other hand, however, the bonding between the c-BN particles was weak, thereby inhibiting the progress of the sintering operation. When an effort was made to prolong the treatment time to 60 minutes, no marked change in the conversion rate or organization of the sintered body was observed.

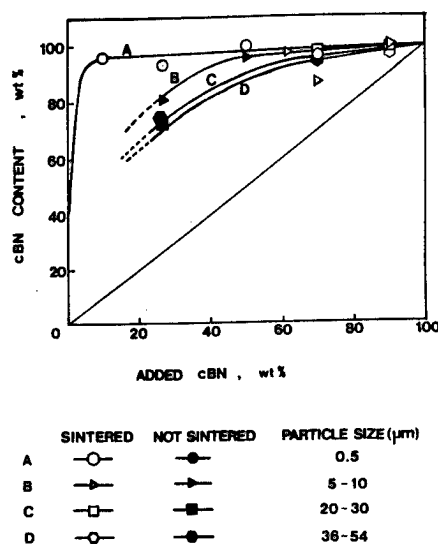


Figure 2. Effect of added c-BN seed content (7 GPa, 1700°C, 30 min)

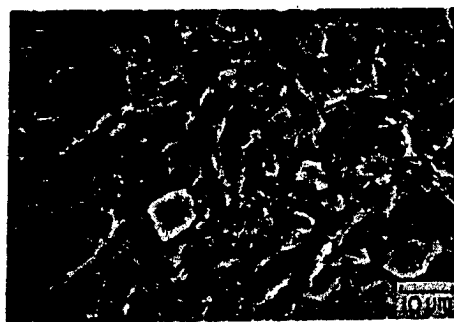


Figure 3. SEM photograph of c-BN sintered body

Particle size of c-BN seed: 8 μm
Amount of added c-BN seed: 60 wt%
Treatment condition: 7 GPa, 1700°C, 30 min

When an effort was made to investigate the effect of the particle size of the c-BN seed and the amount of additive on the microhardness of the sintered body, it was found that $H_v = 5100 \text{ kg/mm}^2$, and the highest value was observed when the average particle size was $0.5 \mu\text{m}$ and the amount of additive was 30 wt%. However, it was observed that the microhardness was inclined to decrease in inverse proportion to the increase in the particle size and the amount of additive.

As stated above, it is apparent that formation of direct bonding between c-BN particles is required to improve the mechanical strength of a c-BN sintered body. An attempt to control the orientation growth of c-BN which is converted to c-BN seed crystal is very important in terms of the reaction sintering accompanied by the conversion from b-BN to c-BN. When the particle size of the c-BN seed crystal to be added is small, the conversion rate is high even if the amount of additive is small, since the reaction surface area of the seed crystal surface is large. Most importantly, a sintered body which is directly bonded can be produced.

References

1. Itoh, Matsudaira, Asano, Inoue, Naka: Fine Particle and Powder Metallurgy, 35 (4), 1984.

Ceramic Particle Dispersed Alloy Powder

43067591 Tokyo NIHON FUNMATSU FUNTAI YAKIN KYOKAI in Japanese 16-19 May 88
pp 214-215

[Report by Hiroshi Asanuma and Mitsuji Hirohashi, Chiba University; and Koji Hayashi, Tokyo University: "Manufacturing Method of Ceramic Particle Dispersed Alloy Powder According to a Solidification Method"]

[Text] Objective

In a previous report¹ on the solidification method, which is a method of producing ceramic dispersed alloy or alloy powder by solidifying ceramic powder well mixed in hot solution, the authors indicated two important points in order to obtain uniform dispersion of the ceramic particles within the alloy. They are that 1) the density of the hot solution must be identical to that of the ceramic; and 2) the cooling speed of the hot solution must be accelerated, while the particle size of the matrix (SiC) powder must be reduced. In that report, the particle size of the ceramic (SiC) powder was specified as 3 μm while the volumetric rate was given as 10 percent, both of which were classified as Class 1. In the present research, the authors endeavored to investigate the influence of the ceramic particle size and the volumetric rate on the dispersed state of the ceramic particles in terms of the alloy organization and cooling speed of the ceramic.

Method

In this experiment, the authors used SiC powder (produced by Fujimi Grinding Material Industry Corp.), which was the same material as that discussed in the previous report.¹ In addition to the 3 μm particle size, in this experiment we adopted 10 μm and 80 μm particle size as well. The Al powder and the Cu powder that were used as a matrix powder were 100-mesh atomized powder produced by Toyo Aluminium Corp. and Fukuda Metal Foil Powder Industry Corp., respectively. Al-(10-50) mass%Cu was selected as the blending composition of the matrix alloy. The volumetric rate of the SiC was mainly specified as 10 percent. In the case of Al-20 mass%Cu, the authors endeavored to study what increased the volumetric rates in terms of the particle sizes of the SiC powder. The experiment methods used in the mixing of the powder, the pressurized powder of the mixed powder, the dissolution of the matrix alloy within the pressurized powder, the agitation of the hot solution, the cooling

and solidification operations adopted in the current research were identical to those used in the previous report.¹

Result

First, the authors endeavored to investigate the effect of the alloy composition (density of hot solution) on the sedimentation and floating of the SiC ceramic particles of each particle size within the alloy solution at a temperature of 1023K. It was found that when the particles were air-cooled from that temperature after agitation, substantially no uneven distribution was observed in the total range of 10~50 mass%Cu in terms of particles of 3 μm and 10 μm size. However, particles of 80 μm size, whose viscosity resistance was considered to be low compared to the specific gravity and the buoyancy, as shown in Figure 1 [photo not reproduced], drop (a) at 10 mass%Cu and float at 33~50 mass%Cu (c), so that the transfer or uneven distribution of the particles were controlled only at about 20 mass%Cu (b), which is between (a) and (b). Specifically, it was found that the SiC particles and their density could be almost identical, and transfer between the particles (specific gravity separation) could be prevented by setting the alloy composition of the alloy solution at about 20 mass%Cu.

Second, the authors endeavored to investigate the effect of the cooling speed (air-cooling and quenching on copper plate) on the dispersed state of the particles within the alloy in terms of ceramic powder (of 3 μm and 80 μm size, respectively), when the composition of the matrix alloy was fixed at 20 mass%Cu and the volumetric rate of the ceramic particles was fixed at 10 percent as well. Figure 2 (a and b) [photo not reproduced] shows the results of the investigation. Figure 2 (a) shows the cross-section organization of the particles (already corroded by hydrofluoric acid aqueous solution) in the case of the 3 μm particle size. It shows that the ceramic particles were unevenly distributed in the crystal grain boundary section in the matrix at either (air-cooling or quenching on copper plate) cooling speed. In addition, when quenching was carried out on copper plate, for example, it was found that the particle size of the first crystal α phase was as large as about 20 μm . However, this crystal particle size was larger than the particle-to-particle distance under the assumption that all of the particles were uniformly dispersed. Therefore, it can be assumed that the ceramic particles uniformly dispersed in the solution were subject to uneven distribution as a result of the rejection of the first crystal in the growth process of the first crystal in the matrix, no matter what the cooling speed. In fact, ceramic particles of 80 μm size (b) were uniformly dispersed even in the case of quenching. This is considered attributable to the fact that the particle size of the first crystal α phase was smaller than the particle-to-particle distance.

Our experiment based on this method indicated that the maximum limit of the volumetric rate (V_f) of the ceramic particles that could be composited with ease was 10~15 percent in the case of 3 μm size particles and 30~35 percent in the case of 80 μm size particles. Beyond these values, the viscosity of the solution for the ceramic composite alloy is increased dramatically, so the flowability of the solution deteriorates to a greater extent. When the

particle size is 80 μm , the particle-to-particle distance is virtually identical to the particle size of the first crystal α phase, even if the volumetric rate of the ceramic reaches $V_f = 30$ percent. So they are not unevenly dispersed.

Figure 3 [photo not reproduced] shows the cross-section organization of thin film that can be obtained by quenching on a rotary disk with regard to the ceramic particles of the respective specified particle size when the matrix composition is specified as Al-20 mass%Cu. Based on our experiment, by this method it is possible to obtain alloy thin film wherein the ceramic particles are relatively uniformly dispersed irrespective of the size of the ceramic particles. It was also found that they can be powdered by a ball mill.

References

1. Hara, Asanuma, Hirohashi, Hayashi: Collection of reports given at 1987 spring convention of Fine Particle and Powder Metallurgy Association, p 192.

- END -

10

This is a U.S. Government publication. Its contents in no way represent the policies, views, or attitudes of the U.S. Government. Users of this publication may cite FBIS or JPRS provided they do so in a manner clearly identifying them as the secondary source.

Foreign Broadcast Information Service (FBIS) and Joint Publications Research Service (JPRS) publications contain political, economic, military, and sociological news, commentary, and other information, as well as scientific and technical data and reports. All information has been obtained from foreign radio and television broadcasts, news agency transmissions, newspapers, books, and periodicals. Items generally are processed from the first or best available source; it should not be inferred that they have been disseminated only in the medium, in the language, or to the area indicated. Items from foreign language sources are translated; those from English-language sources are transcribed, with personal and place names rendered in accordance with FBIS transliteration style.

Headlines, editorial reports, and material enclosed in brackets [] are supplied by FBIS/JPRS. Processing indicators such as [Text] or [Excerpts] in the first line of each item indicate how the information was processed from the original. Unfamiliar names rendered phonetically are enclosed in parentheses. Words or names preceded by a question mark and enclosed in parentheses were not clear from the original source but have been supplied as appropriate to the context. Other unattributed parenthetical notes within the body of an item originate with the source. Times within items are as given by the source. Passages in boldface or italics are as published.

SUBSCRIPTION/PROCUREMENT INFORMATION

The FBIS DAILY REPORT contains current news and information and is published Monday through Friday in eight volumes: China, East Europe, Soviet Union, East Asia, Near East & South Asia, Sub-Saharan Africa, Latin America, and West Europe. Supplements to the DAILY REPORTs may also be available periodically and will be distributed to regular DAILY REPORT subscribers. JPRS publications, which include approximately 50 regional, worldwide, and topical reports, generally contain less time-sensitive information and are published periodically.

Current DAILY REPORTs and JPRS publications are listed in *Government Reports Announcements* issued semimonthly by the National Technical Information Service (NTIS), 5285 Port Royal Road, Springfield, Virginia 22161 and the *Monthly Catalog of U.S. Government Publications* issued by the Superintendent of Documents, U.S. Government Printing Office, Washington, D.C. 20402.

The public may subscribe to either hardcover or microfiche versions of the DAILY REPORTs and JPRS publications through NTIS at the above address or by calling (703) 487-4630. Subscription rates will be

provided by NTIS upon request. Subscriptions are available outside the United States from NTIS or appointed foreign dealers. New subscribers should expect a 30-day delay in receipt of the first issue.

U.S. Government offices may obtain subscriptions to the DAILY REPORTs or JPRS publications (hardcover or microfiche) at no charge through their sponsoring organizations. For additional information or assistance, call FBIS, (202) 338-6735, or write to P.O. Box 2604, Washington, D.C. 20013. Department of Defense consumers are required to submit requests through appropriate command validation channels to DIA, RTS-2C, Washington, D.C. 20301. (Telephone: (202) 373-3771, Autovon: 243-3771.)

Back issues or single copies of the DAILY REPORTs and JPRS publications are not available. Both the DAILY REPORTs and the JPRS publications are on file for public reference at the Library of Congress and at many Federal Depository Libraries. Reference copies may also be seen at many public and university libraries throughout the United States.